

General Disclaimer

One or more of the Following Statements may affect this Document

- This document has been reproduced from the best copy furnished by the organizational source. It is being released in the interest of making available as much information as possible.
- This document may contain data, which exceeds the sheet parameters. It was furnished in this condition by the organizational source and is the best copy available.
- This document may contain tone-on-tone or color graphs, charts and/or pictures, which have been reproduced in black and white.
- This document is paginated as submitted by the original source.
- Portions of this document are not fully legible due to the historical nature of some of the material. However, it is the best reproduction available from the original submission.

Contract
EC-77-C

CONS/5081-1
NASA CR 159397

ENERGY

NOIHKRKHON

OF
THERMAL ENERGY STORAGE
TO PROCESS HEAT AND WASTE HEAT
RECOVERY IN THE
IRON AND STEEL INDUSTRY

FINAL REPORT FOR THE
PERIOD SEPTEMBER 1977 - SEPTEMBER 1978

Lincoln B. Katter
Daniel J. Peterson



Date Published - October 1978

Work Performed Under Contract No. EC-77-C-01-5081

ROCKET RESEARCH COMPANY
YORK CENTER
REDMOND, WA 98052



U. S. DEPARTMENT OF ENERGY

Division of Energy Storage Systems

(NASA-CR-159397) APPLICATIONS OF THERMAL
ENERGY STORAGE TO PROCESS HEAT AND WASTE
HEAT RECOVERY IN THE IRON AND STEEL INDUSTRY
Final Report, Sep. 1977 - Sep. 1978 (Rocket
Research Corp.) 136 p HC A07/MF A01

N79-11473

Unclas
33928

G3/44

CONS/5081-1
NASA CR 159397

APPLICATIONS OF
THERMAL ENERGY STORAGE
TO PROCESS HEAT AND WASTE HEAT
RECOVERY IN THE
IRON AND STEEL INDUSTRY

FINAL REPORT FOR THE
PERIOD SEPTEMBER 1977 – SEPTEMBER 1978

Lincoln B. Katter
Daniel J. Peterson

ROCKET RESEARCH COMPANY
YORK CENTER
REDMOND, WA 98052

Date Published – October 1978

U. S. DEPARTMENT OF ENERGY
Division of Energy Storage Systems

Work Performed Under Contract No. EC-77-C-01-5081

1. Report No. NASA CR 159397	2. Government Accession No.	3. Recipient's Catalog No.	
4. Title and Subtitle Applications of Thermal Energy Storage to Process Heat and Waste Heat Recovery in the Iron and Steel Industry		5. Report Date October 1978	6. Performing Organization Code
7. Author(s) I. B. Katter and D. J. Peterson		8. Performing Organization Report No. RRC-78-R-607	10. Work Unit No.
9. Performing Organization Name and Address Rocket Research Company York Center Redmond, Washington 98082		11. Contract or Grant No. FC-77-C-01-5081	13. Type of Report and Period Covered Contractor Report
12. Sponsoring Agency Name and Address U. S. Department of Energy Division of Energy Storage Systems Washington, D. C. 20545		14. Sponsoring Agency Code CONS/5081-1	
15. Supplementary Notes Final report prepared under Interagency Agreement FC-77-A-31-1034 Project Manager, R. A. Duscha, Power Generation and Storage Division, NASA Lewis Research Center, Cleveland, OH 44138			
16. Abstract <p>This document presents the results obtained and conclusions drawn during the performance of a study entitled, "Application of Thermal Energy Storage Techniques to Process Heat and Waste Heat Recovery in the Iron and Steel Industry". The study was performed by Rocket Research Company, with support from team members: Bethlehem Steel Company (Seattle plant) and the Lighting Department of the City of Seattle (Seattle City Light).</p> <p>The system identified in this study operates from the primary arc furnace evacuation system as a heat source. Energy from the fume stream is stored as sensible energy in a solid medium (packed bed). A steam-driven turbine is arranged to generate power for peak shaving (either internal company load peaks or utility area demand peaks can be smoothed with the system). A parametric design approach is presented since the overall system design, at optimum payback, is strongly dependent upon the nature of the electric pricing structure. Since utility rates are currently in a state of flux, this work was felt to have a greater future value if that variable could be chosen for each specific case.</p> <p>The scope of the project was limited to consideration of currently available technology so that industry-wide application could be achieved by 1985. Slight additional scope limitations were found from the additional criterion that concepts and equipment must be compatible with the heavy industrial environment.</p> <p>A search of the literature, coupled with interviews with representatives of major steel producers, served as the means whereby the techniques and technologies indicated for the specific site are extrapolated to the industry as a whole and to the 1985 time frame. The conclusion of the study is that by 1985, a national yearly savings of 1.9 million barrels of oil could be realized through recovery of waste heat from primary arc furnace fume gases on an industry-wide basis.</p> <p>Economic studies indicate that the proposed system has a plant payback time of approximately 5 years. Due to the favorable economic and technical results in the program, additional work leading to a full-scale demonstration is recommended. This program would be carried out in five phases to prove the overall feasibility of the concept and provide industry with the necessary data for nationwide implementation.</p>			
17. Key Words (Suggested by Author(s)) Energy Storage, Energy Conservation, Arc Furnace, Steel Industry, Electric Power, Cogeneration, Peak Shaving		18. Distribution Statement Unclassified Unlimited STAR Category 04 DOE Category UC-94a	
19. Security Classif. (of this report) Unclassified	20. Security Classif. (of this page) Unclassified	21. No. of Pages 134	22. Price*

* For sale by the National Technical Information Service, Springfield, Virginia 22161

TABLE OF CONTENTS

Section	Page
ABSTRACT	vii
1.0 INTRODUCTION	1
2.0 INDUSTRY SURVEY	3
2.1 Iron and Steel Making Processes	3
2.2 Techno-Economic Environment in the Steel Industry	8
2.3 Slag ¹ - Suitability as a Sensible Storage Medium	9
2.4 Selected Process for Waste Energy Recovery	9
3.0 SYSTEM SELECTION	10
3.1 Energy Source Selection	19
3.2 Choice of Energy End Use	20
3.3 Energy Storage Means	21
3.4 System Flow Arrangement	23
4.0 INTERFACE REQUIREMENTS	29
4.1 System Location	29
4.2 Procedural Interface	32
5.0 SIZING AND PERFORMANCE ANALYSIS	33
5.1 System Description and Operation	33
5.2 Waste Heat System Sizing and Performance Computer Codes	35
5.3 Results of Sizing and Performance Analysis	37
5.4 Correction of System Design for Transient Storage Bed Effects	39
5.5 Overall System Predictions	44
5.6 Estimated National Energy Savings	52
6.0 SYSTEM DESIGN AND COST	53
6.1 Preliminary Design	53
6.2 System Economics	56
7.0 SYSTEM ASSESSMENT AND PLAN FOR RECOVERABLE REJECT ENERGY	67
7.1 Phase II - Technology Development	68
7.2 Phase III - Pilot Plant Design	72
7.3 Phase IV - Fabrication, Assembly, and Test of Pilot Plant	74
7.4 Phase V - Full-Scale System Design	75
7.5 Phase VI - Fabrication, Assembly, and Test of Demonstration System	75
7.6 Overall Program Schedule	75
8.0 SUMMARY AND CONCLUSIONS	77

TABLE OF CONTENTS (Concluded)

- APPENDIX A – Glossary of Terms
- APPENDIX B – System Design Model
- APPENDIX C – Thermal Storage Bed Computer Program
- APPENDIX D – Operational Data Collection
- APPENDIX E – References

PRECEDING PAGE BLANK NOT FILMED.

2

LIST OF FIGURES

Figures	Page
1 Raw Steel Production by Process Type	4
2 Electric Furnace Steelmaking	6
3 Fume Temperature Record Before Water Quench	11
4 "C" Battery, Soaking Pit No. 10	15
5 "C" Battery Stack Gas Temperature After Recuperation	16
6 Walking Ramp Temperature Measurements	17
7 Evolution of System Flow Arrangement	24
8 Melt Shop Section	30
9 Melt Shop Building and Surrounding Area Plan	31
10 Steel Arc Furnace Energy Recovery System	34
11 Logic Diagram: System Optimization Process	38
12 Optimum Storage Discharge Temperature	40
13 Charge Time Vs. Capital Cost Factor	41
14 Peaking Store Charging and Discharging Percent Heat Loss Versus Percent Increase in Bed Length	45
15 Peaking Store Effect of Increased Storage Bed Length Upon Storage Bed Heat Loss	46
16 Peaking Store Effect of Increased Storage Bed Length on System Parasitic Power – Bed Material – Scrap Iron	47
17 Peaking Store Capital Cost Factor Optimization Versus % Bed Length Increase, Material – Scrap Iron	48
18 Effect of Discharge Time and Storage Material on System Net Power Output	49
19 Optimized and Corrected Overall System Capital Cost Versus Discharge Time	50
20 Component Capital Cost Comparison for Scrap Iron System	51
21 Existing Seattle Bethlehem Plant Evacuation System	54
22 Proposed Energy Recovery System Installed in Bethlehem Seattle Plan	55
23 Cost of Electric Power to Industrial Users	57
24 Example of Time of Day Price Schedule	58
25 Implementation Plan for Utilization of Reject Heat From Iron and Steel Processing	69
26 Program Schedule	76

LIST OF TABLES

Table	Page
1	Average Temperature and Duration Estimates of Ray (Before Quench) Furnace . . . 12
2	Soak Pit Data 13
3	Reheat Furnace Data 18
4	Energy Source Selection Evaluation 19
5	State-of-The-Art Storage Materials 22
6	Economic Analysis Example Case 59
7	Pretax Net Present Value (\$1000) Comparison for Various θ_C/θ_D and Economic Life 60
8	Pre-Tax Net Present Value Analysis for Baseline Case 61
9	Pretax Internal Rate of Return Analysis for Baseline Case 62
10	Pretax IROR Comparison for Various θ_C/θ_D and Energy Cost (For 15-Year Plant Economic Life) 62
11	ROI Analysis (as Operation Return) 64
12	Economic Analysis Baseline 64
13	Payback Period Analysis 65

ABSTRACT

This document presents the results obtained and conclusions drawn during the performance of a study entitled, "Application of Thermal Energy Storage Techniques to Process Heat and Waste Heat Recovery in the Iron and Steel Industry". The study was performed by Rocket Research Company, with support from team members: Bethlehem Steel Company (Seattle plant) and the Lighting Department of the City of Seattle (Seattle City Light).

The system identified in this study operates from the primary arc furnace evacuation system as a heat source. Energy from the fume stream is stored as sensible energy in a solid medium (packed bed). A steam-driven turbine is arranged to generate power for peak shaving (either internal company load peaks or utility area demand peaks can be smoothed with the system). A parametric design approach is presented since the overall system design, at optimum payback, is strongly dependent upon the nature of the electric pricing structure. Since utility rates are currently in a state of flux, this work was felt to have a greater future value if that variable could be chosen for each specific case.

The scope of the project was limited to consideration of currently available technology so that industry-wide application could be achieved by 1985. Slight additional scope limitations were found from the additional criterion that concepts and equipment must be compatible with the heavy industrial environment.

A search of the literature, coupled with interviews with representatives of major steel producers, served as the means whereby the techniques and technologies indicated for the specific site are extrapolated to the industry as a whole and to the 1985 time frame. The conclusion of the study is that by 1985, a national yearly savings of 1.9 million barrels of oil could be realized through recovery of waste heat from primary arc furnace fume gases on an industry-wide basis.

Economic studies indicate that the proposed system has a plant payback time of approximately 5 years. Due to the favorable economic and technical results in the program, additional work leading to a full-scale demonstration is recommended. This program would be carried out in five phases to prove the overall feasibility of the concept and provide industry with the necessary data for nationwide implementation.

1.0 INTRODUCTION

Traditional sources of inexpensive electric power are currently exploited to nearly the fullest extent possible. Additional growth in electric power production may be accommodated through operation of gas turbine systems to carry the peak loads, with the existing thermal plants and hydroelectric facilities supplying the baseload generation capability. This high dependence upon petroleum products for peak power production is undesirable in the current and future economic climate. In some instances, industrial waste heat is of sufficiently high grade to serve as a source for a peaking turbogenerator system, directly displacing fossil fuel.

Currently, electric energy is priced in a manner to share the cost of expensive peak power over the entire baseload. Pricing structures which charge the user more nearly what the utility must pay for its power (i.e., where baseload power is inexpensive and peak power is substantially more expensive) are under consideration in many areas of the country. The details of how such a pricing structure finally becomes implemented will have a significant effect upon the cost and payback analyses of generation systems installed to supplant the purchase of peak power.

The iron and steel industry is a likely field in which to search for opportunities to generate electric power from waste energy. Two major factors contribute to this state:

1. The steel melting and forming processes occur over a high temperature range; hence, the waste energy streams are of relatively high grade.
2. Electric generation on-site is a relatively common practice in this industry.

The purpose of the study reported herein is to investigate the application of energy storage techniques to enhance the potential utilization of waste energy in the iron and steel industry as a means for generating peaking power. Energy storage plays a vital role in allowing the time of power generation to coincide with the time of maximum demand. Only currently available technology compatible with the heavy industrial environment is considered, so that national implementation by the year 1985 is feasible.

During the conduct of the study, the Bethlehem Steel Corporation scrap metal refining plant in the Seattle area served as a specific site about which detailed analysis was conducted. This plant is typical of electric arc furnace installations throughout the United States, allowing the results of this site-specific study to be extrapolated to a national basis. Bethlehem Steel also participated in measurements to quantify various waste energy sources and in analysis of plant impact and interface requirements for the waste heat recovery system. Seattle City Light, the energy supplier for Bethlehem Steel, participated in the program by providing data on local and nationwide energy costs and the estimated escalation rates for energy in the future.

The project proceeded in seven tasks. A survey of the published literature, coupled with interviews with selected representatives from the industry, provided the baseline information from which the overall effort proceeded. In the second task, a number of waste energy streams and storage concepts were evaluated. The third task involved the measurement of selected data of the industrial partner's site to more accurately assess the magnitude and availability of the waste energy streams. Based upon the results of the first three tasks, the most promising concept was selected; the interface between this system and the existing site/operations was defined during the fourth task. The major project effort went into the fifth task, sizing and performance analysis. A computer model of the proposed system was developed by which the numerous system tradeoffs could be analyzed and an optimum approach selected from both technical and economic considerations. A preliminary design for the application at the partner's site was developed during the sixth task. During the seventh task, a plan was developed leading toward a future demonstration.

2.0 INDUSTRY SURVEY

The initial task of the program involved a survey of published literature in three areas in the iron and steel industry: the basic iron and steel making processes, the technical and economic climate in the industry, and the use of steel slag as a thermal bed storage material. A list of the references consulted is presented in Appendix E. Interviews with selected representatives in the steel industry served to expand upon and update the information derived from the literature. This task of the program basically shaped the overall study efforts of the program as the waste energy source to be utilized was selected as a result of work in this task. The following sections present the results of the literature search and the industrial process and waste energy source selected for further study.

2.1 IRON AND STEEL MAKING PROCESSES

2.1.1 Iron Making

Iron ore is reduced to cast iron in a blast furnace. The furnace is charged with iron ore, limestone, and coke; and combustion is supported by a blast of hot air. Each ton of iron produced requires approximately 2 tons of iron ore, 1 ton of coke, 0.5 ton of limestone, and approximately 3 tons of air. Gases which exit the blast furnace are combustible, with almost all blast furnace top gases being used in a "blast furnace stove" (Reference 1). The blast furnace stove is similar to an ordinary recuperator in function, but with the additional feature that the hot gas is burned with ambient air. The resulting energy is then utilized to preheat the air utilized in the blast furnace. In the case of larger, high pressure (20 to 35 psig) blast furnaces, the mechanical energy of the compressed gas is recovered directly through an expansion turbine. Since this direct means for recovery of energy contained in the blast furnace top gas is already proven in its fossil fuel displacement capability, the application of an indirect means (incorporating storage) can approach the current savings only if there are no energy losses in the storage system.

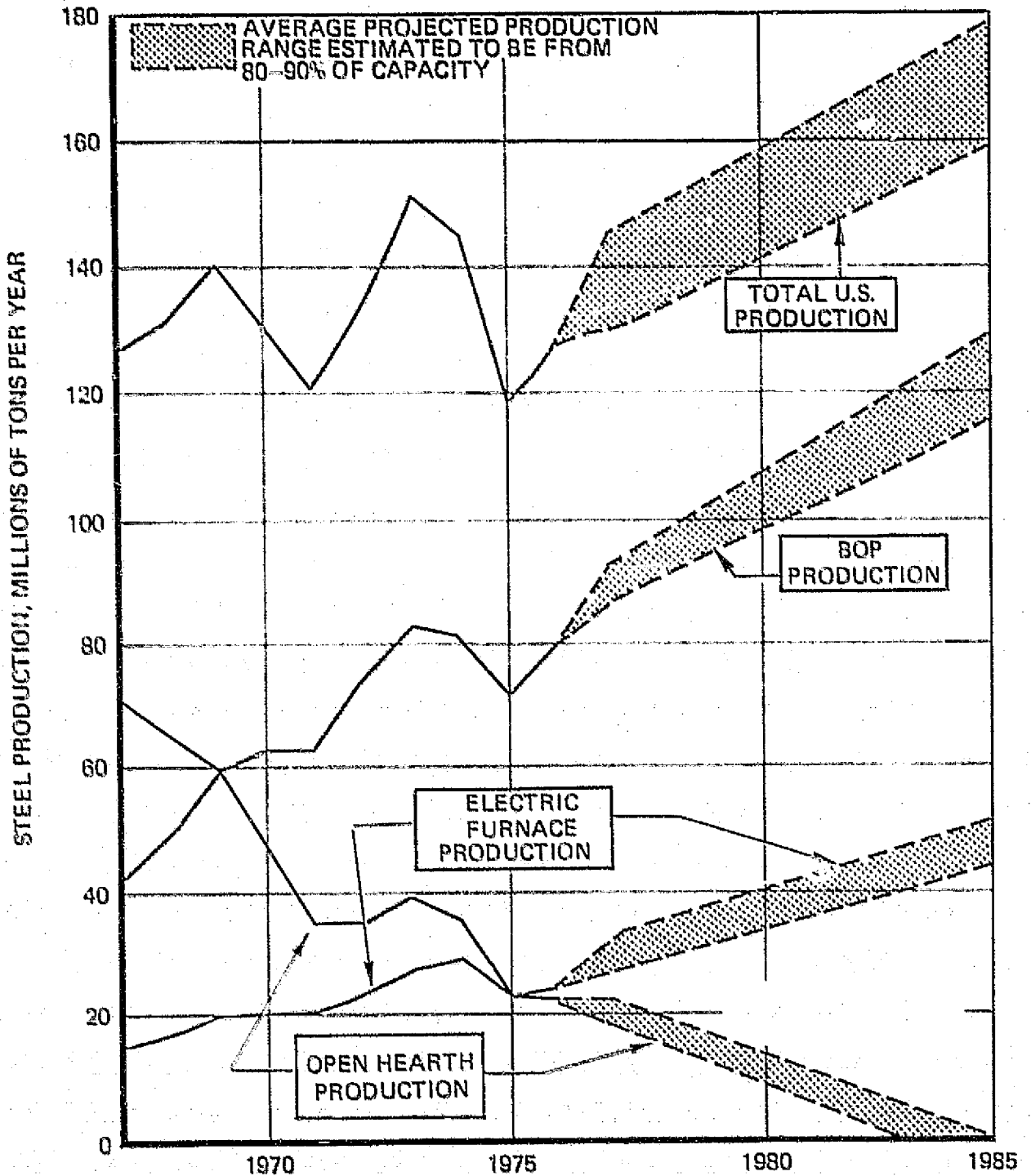
2.1.2 Steel Making

Three types of furnaces exist for the making of steel. These are:

1. Basic oxygen furnace (BOF)
2. Open hearth furnace (OH)
3. Electric arc furnace (EF).

In Figure 1, the annual steel production in the United States is plotted versus time since 1967, with projections shown to 1985. In the late 1960's, open hearth steel production accounted for over 50% of the national production, with the basic oxygen process contributing one-third of the total and electric arc furnaces supplying the remaining 10 to 15%. In recent years, open hearth steel production has been steadily phased out in favor of

RAW STEEL PRODUCTION BY PROCESS TYPE



SOURCE: AISI. for 1967 to 1976 including ADL estimates 1977-1985.

ORIGINAL PAGE IS OF POOR QUALITY

the more modern electric arc and basic oxygen processes. By 1985, the national steel production will be shared between basic oxygen furnaces (72%) and electric arc furnaces (28%). Since the open hearth process is being phased out, only the BOF and EF processes are investigated in this study.

Basic Oxygen Process – In the basic oxygen process of steel manufacture, the charge consists of 70% molten iron and 30% cold scrap. Oxygen is forced through the mixture, burning carbon dissolved in the iron, to provide the energy to heat and melt the scrap. The gases which exit from the furnace in the BOF process contain a high percentage of carbon monoxide which has the potential to be utilized as a fuel. There are a number of problems concerning the handling of the potentially explosive gas mixture which are currently under investigation. To date, these problems have prevented utilization of carbon monoxide as a fuel in the United States, although it is expected that these problems will be solved in the future since the technology is very similar to that already in use in the handling of top gas from blast furnaces in iron production. It is economically more attractive to utilize the gases from the BOF process as a fuel in a direct recuperation process than to store the energy for subsequent use. As a result, the waste energy contained in BOF top gas was eliminated from further consideration in the study.

Electric Arc Furnaces – The charge for an electric arc furnace is 100% cold (nonmolten) scrap. The energy requirements to produce steel from scrap are significantly less than those required to produce steel from iron ore when all the energy required to produce the intermediate molten iron is accounted for. As a result, the estimates presented in Figure 1 for future electric arc steel production may be conservative as escalating energy costs will tend to make the electric arc process relatively more attractive.

In the electric arc furnace process, shown in Figure 2, an electric arc is struck from the carbon anodes directly to the scrap charge with the resistance of the metal generating sufficient heat to bring it to the molten state. Various trace elements are added in order to produce a desired grade of steel. Oxygen blows (1 to 5 minutes each) are used. While these are similar in principle to the oxygen blow in the BOF process, these are of a reduced quantity, resulting in a low fuel value of the gases coming off the electric arc furnace.

In all electric arc furnaces above approximately 40-ton capacity, the furnace is hooded to remove hot gases resulting from the process. These gases, at an average temperature of approximately 1,300°F, must be quenched and routed to baghouses where particulate matter is removed prior to exhausting to the atmosphere. The gases exiting the electric arc furnace represent a good potential waste energy source.

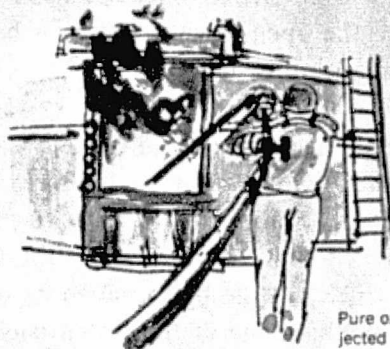
2.1.3 Coke Making Process

The removal of hydrogen-bearing volatiles from coal to produce a smokeless carbon product for the iron making and foundry industries is one of the largest energy users in the iron and steel industry. The volatiles driven off are captured and used as fuel in the process itself.

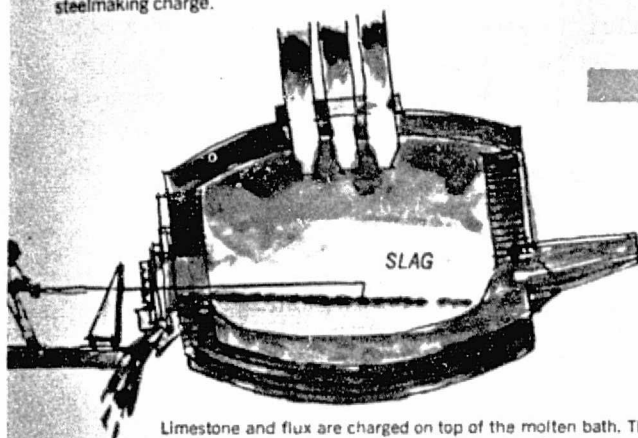
ELECTRIC FURNACE STEELMAKING

A long-deserved reputation for producing alloy, stainless, tool, and other specialty steels belongs to America's electric furnaces. Operators have also learned to make larger heats of carbon steels in these furnaces; this development helps account for the record tonnage outputs of recent years.

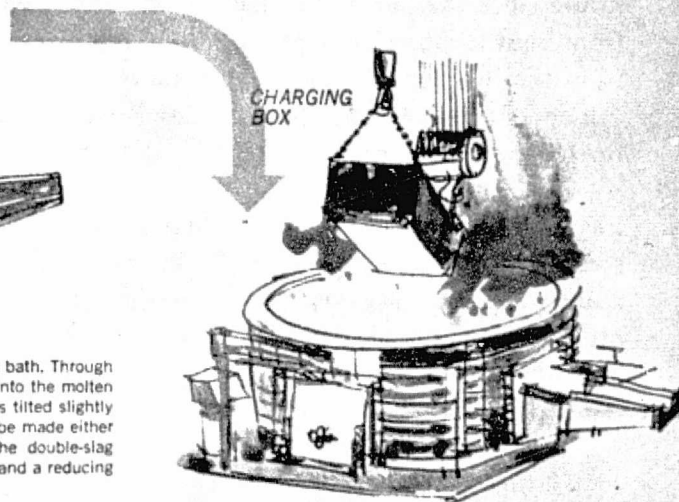
The heat within the electric furnace is intense and rigidly controlled. Modern electric furnaces have top sections that can be moved away so that special containers can charge scrap into them from above. Sometimes pig iron is also charged and pre-reduced iron ore, in various forms, is rich enough in iron to be used as an electric furnace steelmaking charge.



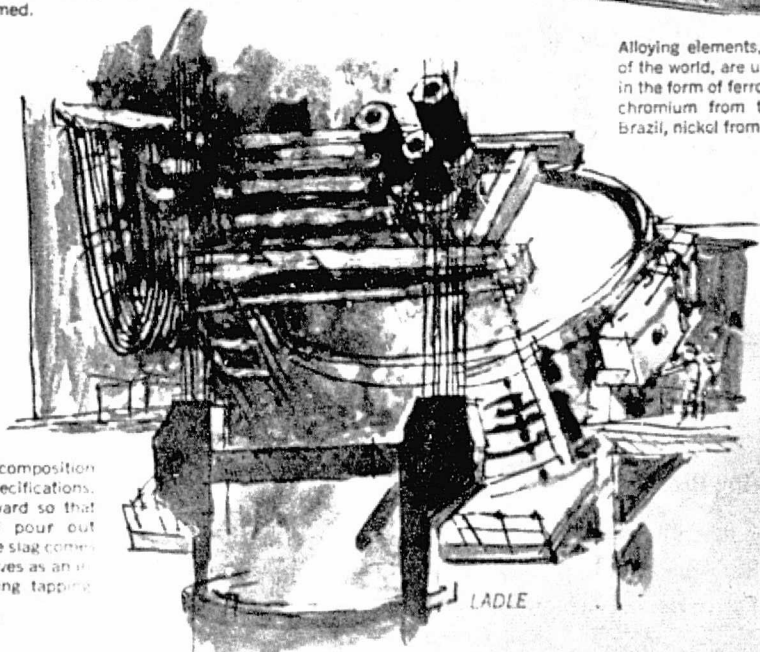
Pure oxygen may be injected to speed up carbon removal from the molten metal.



Limestone and flux are charged on top of the molten bath. Through a chemical interaction, impurities in the steel rise into the molten slag, which floats on top of the metal. The furnace is tilted slightly and the slag is raked off. Electric furnace steel can be made either with a single-slag or a double-slag practice. In the double-slag method, an oxidizing slag is first formed, raked off, and a reducing slag formed.



Alloying elements, which come from many parts of the world, are usually added to the molten steel in the form of ferroalloys. Typical elements include chromium from the Philippines, tungsten from Brazil, nickel from Canada, and cobalt from Africa.



When the chemical composition of the steel meets specifications, the furnace tilts forward so that molten metal may pour out through the spout. The slag comes after the steel and serves as an insulating blanket during tapping.

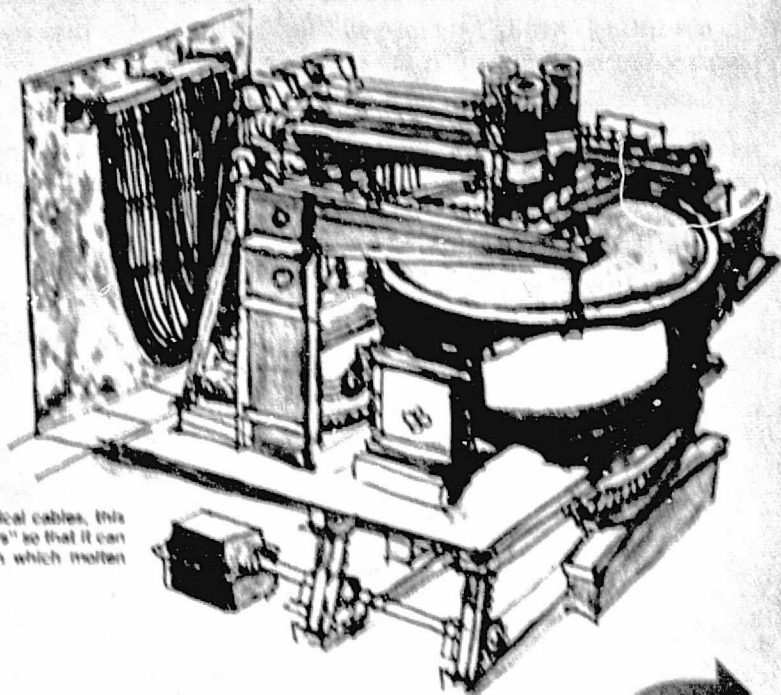
AMERICAN IRON AND STEEL INSTITUTE PUBLICATION: "STEEL MAKING FLOW CHARTS"



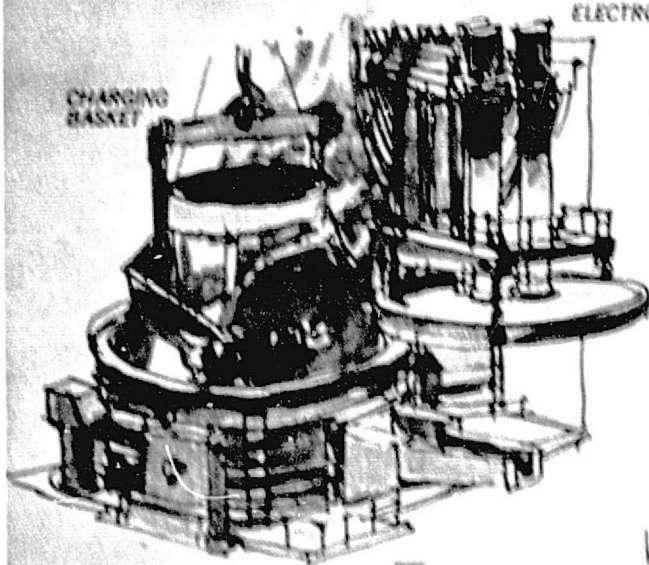
ELECTROMAGNET

STEEL SCRAP

Steel scrap may vary widely in quality. It is carefully sorted and weighed before it goes to the electric furnace.



With its carbon electrodes attached to electrical cables, this electric furnace is shown mounted on "rockers" so that it can be tilted toward the tapping spout, through which molten steel emerges.



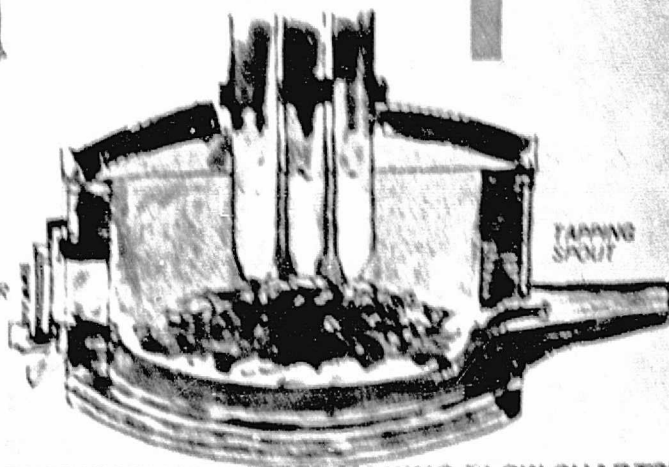
CHARGING BASKET

ELECTRODES

The electrodes are lowered through the roof of the furnace and the electric power is turned on. The current in an electric furnace arcs from one electrode to the metallic charge and from the charge to the next electrode.

The entire top of an electric furnace may swing to the side, electrodes and all, so that a charging basket of steel scrap may be lowered into the furnace. The bottom of the basket is curved, thus charging the furnace.

DOOR



TAPPING SPOUT

However, a very large energy loss is associated with quenching the finished product. The coke quenching process is recognized as the largest energy loss in the industry; hence, considerable effort at improvement is under way. Technology incorporating an oxygen-free gas forced through the hot (1,700°F) coke until it is cooled below the point where it will support combustion in air (300°F) is termed "dry quenching". Such means are in use in Europe, especially the U.S.S.R. Quoting from Reference 1*, "... starting with a pilot plant in 1960, the Soviet Union now has over 50 dry quenching installations in operation. In Russia, such facilities are now mandatory for all new coke oven batteries . . .". If the dry quench process is developed in the United States, the best use for the hot gases will be for direct preheating of the coal. Energy storage based systems using this source will not be competitive.

2.1.4 Rolling and Finishing

The product flow path from molten steel to finished steel has several options and branches. In the conventional method, the molten steel is cast into ingots, reheated in soaking pits to uniform internal temperature, rolled to an intermediate shape (bloom, billet, or slab), cooled to room temperature, inspected for surface defects, processed to remove surface defects if necessary, reheated in a reheat furnace, rolled to the desired shape, cooled again to room temperature, and shipped. At the other end of the energy efficiency spectrum, molten steel is continuously cast, transferred directly to the finishing mill, rolled to the desired shape, cooled to ambient and shipped. Intermediate between these two cases are conditions where intermediate shapes transfer directly from the blooming mill to a finishing mill, and cases where continuously cast forms require reheating before the finishing mill due to delays enroute. Energy utilization varies by about a factor of three from least to most energy efficient process. Since the more energy-efficient processes are proven working processes in Japan and Europe, it seems likely that progressively more U.S. plants will convert to this technology as the price of energy rises to approach that in Japan and Europe.

The large number of options in product flow processing tends to make each steel making plant require a separate analysis when considering energy savings in the rolling and finishing processes, thereby preventing the development of a waste energy collection system applicable to the total industry.

2.2 TECHNO-ECONOMIC ENVIRONMENT IN THE STEEL INDUSTRY

2.2.1 Role of Internally Generated Power

On-site generation of electric power is a widespread practice in the industry; hence, the presence of the skills required for operation and maintenance of power generation systems is presumed. In many cases, the air compressors for the blast furnaces are also turbine driven. Topping cycle generators are installed in many plants which have a large requirement for

*All references consulted are listed in Appendix E.

low pressure steam. Minimum difficulty is expected in incorporation of a thermal storage, peak shaving system with existing processes.

2.2.2 Capitalization Practice in the Steel Industry

Traditionally, in the steel industry, opportunities for investment which show a payback not exceeding 5 years are considered attractive. In recent years, mandatory expenditures for pollution controls have depleted the supply of capital to the point where even a 1-year payback may not receive funding. Although the price of energy to the steel industry has increased in recent years and now represents approximately 17% of the product sales price, the effect has not been as dramatic as the capital depletion effect. Hence, expenditures for energy conservation, although showing some leverage over competing demands for capital, are not apt to be made spontaneously in sufficient quantity to allow for significant national energy savings within the near future.

2.3 SLAG – SUITABILITY AS A SENSIBLE STORAGE MEDIUM

Slag, a by-product of steel manufacture, is composed of various metal oxides and silicates. In some cases, sufficient steel inclusions are present to justify crushing, screening and magnetic separation of the higher metallic bearing fragments. Rejects are land filled or sold as a road surfacing material.

The chemical nature of slag from electric furnaces is different from BOF-produced slag. BOF slag is frequently used as a road surfacing constituent. Electric furnace-produced slag may not be such a good material for this application. One instance of roadway use of electric arc furnace slag buckled and broke up. The fault was attributed to poor dimensional stability of the slag. Occasionally, electric furnace-produced slag will be introduced into a BOF, resulting in an extra heavy slag layer, to meet road surfacing demands. Although a particle of slag covered with asphalt and otherwise exposed to the elements has a significantly different environment than one contained within a thermal storage bed, an indication of unstable dimensions in one case must be taken as a warning signal for the other until the process is totally understood.

No measurements or estimates of the thermal properties of slag (thermal conductivity, thermal expansion, specific heat) were located. Thermal expansion is of considerable interest as it effects the wall stress required of the storage bed containment and the propagation of existing stress cracks within a given slag mass (or granule). As a result of the lack of data on the thermal properties of slag, measurements were made during this study and are discussed in Appendix D.

2.4 SELECTED PROCESS FOR WASTE ENERGY RECOVERY

As a result of the discussion and conclusions in the previous sections, the electric arc furnace process was selected for detail study under the program. In the other iron and steel processes, direct energy utilization (in lieu of storage) appears more economically attractive; thus those processes were eliminated from further consideration.

The following sections describe measurements of waste energy sources made within the Bethlehem Steel plant. Five waste energy streams were identified within the Bethlehem Steel plant as follows:

1. Primary fume stream
2. Soak pit stack gases
3. 32-inch mill output shapes
4. Mill furnace stack gases
5. Smaller mill output shapes.

Temperatures and flow rates were measured for each of these, allowing accurate calculation of the energy content.

2.4.1 Primary Arc Furnace Fume Stream

At the Bethlehem/Seattle Recycling Plant, primary fume exits the furnace through a port in the removable furnace hood and is turned 90 degrees in the top fume elbow to proceed downward in a refractory lined spray chamber. A series of water jets is arranged in the spray chamber to quench the primary fume to approximately 550°F. During furnace tapping operations, the furnace, furnace hood, top elbow and spray chamber rotate as a unit. A flexible elbow connects the spray chamber and the stationary downstream ductwork. Considerable additional fume cooling occurs through mixing with ambient air, drawn in through gaps between the flexible elbow structural members.

Cooling primary fume through water spray is not a common technique in the steel industry. More commonly, the entire cooling effect is achieved through ambient air dilution. In an efficient waste energy recovery system, the fume temperature must be kept as high as possible; hence, both quenching means will be eliminated. Therefore, the existence of an atypical quenching means at the specific example site will not influence the applicability of the resultant techniques to the industry as a whole.

The example site was instrumented to measure primary fume temperature at the top fume elbow, fume quench water flow rate, mix gas temperature at the bottom (flexible) elbow, and mixed gas total and static pressure (downstream).

Prequench fume temperature shows somewhat more variation with time than was expected. Figure 3 is an example of the raw data. Five full heats occur on the circular graph. Many spikes to 3,000°F are in evidence as well as many "negative spikes" to 100°F. Table 1 presents estimates of average temperatures for each heat during the monitoring period. The final system must cope with a supply temperature which (when averaged through a 3-hour period) may be as high as 1,750°F or as low as 850°F, as well as periodic excursions from room temperature to 3,000°F of 1 to 5 minutes' duration. The average temperature of this stream is 1,300°F.

ORIGINAL PAGE IS
OF POOR QUALITY

FUME TEMPERATURE RECORD BEFORE WATER QUENCH

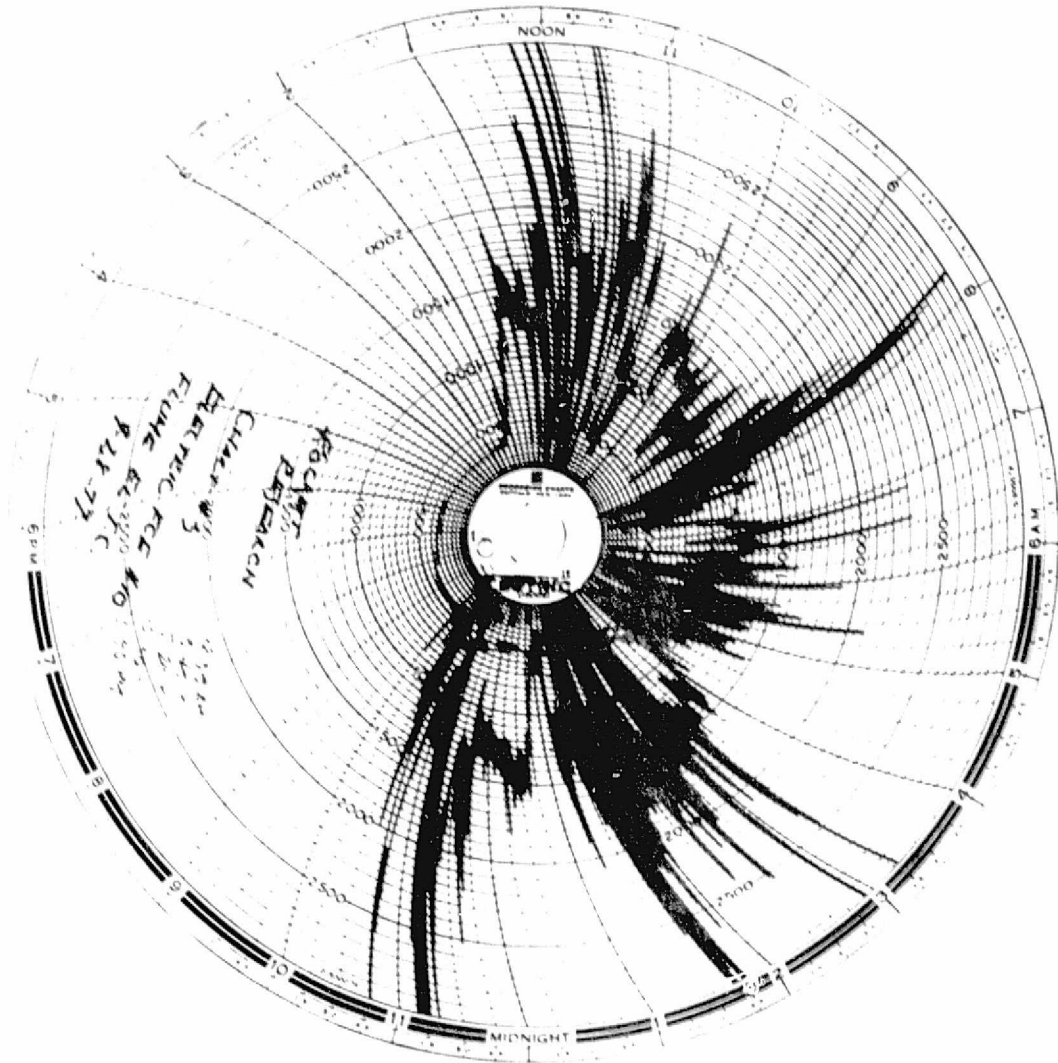


Table 1
**AVERAGE TEMPERATURE AND DURATION ESTIMATES
 OF RAW (BEFORE QUENCH) FUME**

<u>Date</u>	<u>Furnace</u>	<u>Heat</u>	<u>Heat Time</u>	<u>Pour Time</u>	<u>Average Heat Temp.</u>	
9/26/77	#10	1	3 hr/05 min.	10	1,050	
		2	2 hr/45 min.	?	1,550	
		3	Thermocouple burnout during pour (??)			
		4	Thermocouple replaced after start #4			
		5	3 hr/10 min.	?	1,200	
9/27/77	#10	1	2 hr/55 min.	10	1,350	
		2	3 hr/45 min.	14	1,750	
		3	3 hr/15 min.	15	1,050	
		4	Thermocouple burnout			
		5	Thermocouple burnout			
9/28/77	#10	1	2 hr/07 min.	30	1,450	
		2	2 hr/52 min.	15	1,500	
		3	2 hr/50 min.	32	1,100	
		4	2 hr/50 min.	20	1,200	
		5	2 hr/30 min.	?	1,450	
9/29/77	#10	1	3 hr/05 min.	38	975	
		2	2 hr/45 min.	22	1,150	
		3	*	*	850	
		4	*	?	950	
		5	Thermocouple burnout			
Time-weighted average temp.					1,300°F	

NOTES:

- 1) Instrument range 100°F → 3,000°F
 - 2) Thermocouple burnout causes full-scale indication
 - 3) Measured temperature swings full-scale several times per heat
 - 4) Indicated temperature during pour decreases to minimum indication
- * Recorder off towards end of heat #3, on after start of heat #4

Water flow rate to the spray nozzle banks in the fume quench chamber was successfully measured. These data show that an average water flow of 8.6 gpm is demanded for each furnace and that cold air in-flow through the joints of the flexible elbow is contributing to quenching the fume stream. Between the two furnaces, approximately 10.9×10^6 Btu/hr is transferred into the quench water to bring it to equilibrium downstream conditions. The additional quenching effect of ambient air leakage is nominally estimated at 14.1×10^6 Btu/hr. Ambient air dilution is approximately 48%.

Total mixed gas flow rate is calculated from a series of total and static pressure measurements taken across the duct at a convenient access port 350 feet from the furnaces. At this point, approximately 13% of the duct cross-section is occupied by settled dust. An area weighted average of the velocity survey measurements yields 40 ft/sec. Measured gas temperature at this point was 376°F, which yields a nominal mixed gas (fume, air, and water) flow rate of 257,000 lb/hr. These figures are consistent with a 1,300°F fume stream of 128,000 lb/hr partially quenched by 17.2 gpm (8,590 lb/hr) of water, partially quenched by 120,000 lb/hr of ambient air to an upstream (measured) temperature of 550°F. Further lost energy by radiation and convection from the uninsulated duct decrease the mixture temperature to 376°F at the plane of velocity measurement. These figures yield an available energy of 40×10^6 Btu/hr above 70°F.

2.4.2 Soak Pit Stack Gases

Gases from the soak pits represent a low-grade heat source since the high temperature streams are recuperated. The average temperature of gases leaving the recuperators is about 600°F. Gases entering the recuperators can be as hot as 1,800°F. Table 2 shows average temperatures and flow rates of gases leaving the soak pit operation and the recuperator. The recuperation process recovers about 16 million Btu/hr on the average for all three batteries. This reduces fuel usage by about 12%.

Table 2
SOAK PIT DATA

Soak Pit	A	B	C
Combustion gas flow, lb/hr	15,000	15,200	21,000
Recuperator exhaust gas temp., °F	670	600	600
Recuperator inlet gas temp., °F	*	1,720	1,550
CFM of natural gas	322	325	448
Tons of steel heated per hour**	59 tons/hour		

*Data not collected, but similar to "B" battery.

**Data collected for all soaking pits.

At Bethlehem Steel in Seattle, the soak pits consist of three batteries of four pits each. These batteries are designated A, B and C. The A and B batteries are similar in that they each have one brick recuperator associated with four soaking pits. The C battery has four metallic recuperators, one for each soak pit.

The data collected in Table 2 is averaged for each battery. Temperature recordings were made around each recuperator over a 3-day period. A sample of temperature recordings is shown in Figures 4 and 5. Figure 4 is before the recuperator and Figure 5 is after recuperation. As can be seen, the temperatures are fairly constant. The overall gas flow rate is calculated from the known fuel air ratio and measured fuel usage during the measurement period at 53,000 lb/hr.

2.4.3 32-Inch Mill Output Shapes

The residual sensible energy in the output shapes (bloom, billet or slab) from the 32-inch mill represents a rather large heat loss. These shapes are typically about 25 square inches in cross-section and 11 to 14 feet long. Cooling occurs on a angled bed with mechanical drives to move the cooling shapes incrementally, making room for the next shape; hence, the term "walking ramp". Shapes approach the walking ramp at 1,750°F and cool (by radiation and free convection) to 1,200°F as measured by an optical pyrometer. This cooling allows the formation of a different crystalline structure at the lower temperatures, so the shapes can be moved by a magnetic carrier. Cooling times range from 30 to 60 minutes, depending on the shape and type of steel. The average output of the mill based on the last 3 years is about 600 tons per 8-hour shift. This amounts to 8 million Btu's an hour lost, mostly by radiation.

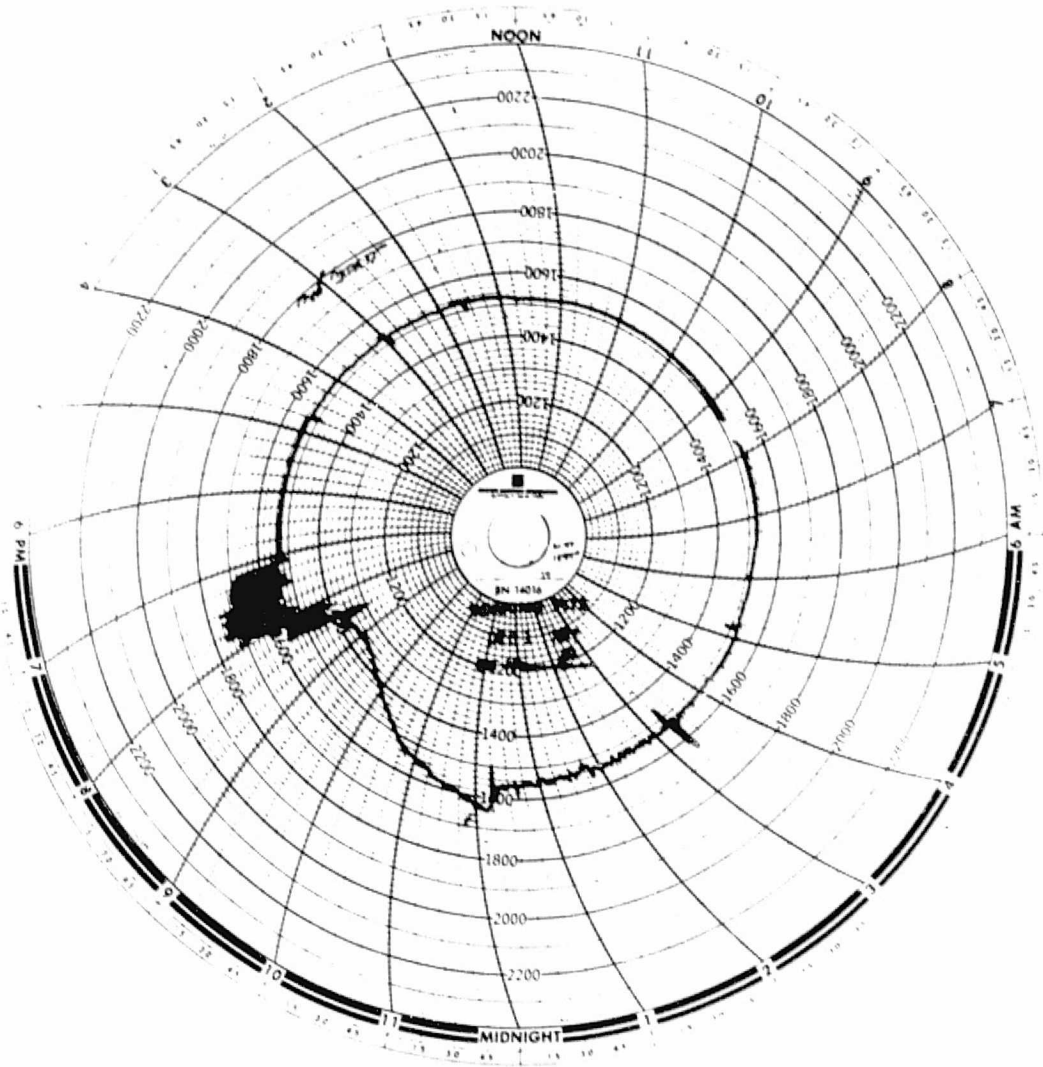
Measurements have been made to show temperatures of the supporting structure with and without radiation effects. Six thermocouples were placed along the bed 12 inches below the shapes themselves. Figure 6 shows a typical plot of the thermocouple readings. Thermocouple No. 4 was shielded and showed a rather low (about 100°F) consistent temperature. All other thermocouples were affected by radiation and read higher. The highest reading was on the order of 600°F on the hot end of the cooling bed. These measurements show that direct heat recovery from the bed structure itself would be limited to low temperature as the dominant heat transfer mechanisms are radiation and free convection.

Since the shapes cannot be "force cooled" without undesirable metallurgical changes, radiation heat transfer is the only means to recover the heat. While it may be technically possible to arrange shrouds around this area to intercept the radiation, any such device would interfere with handling machinery access and is not felt to be practical.

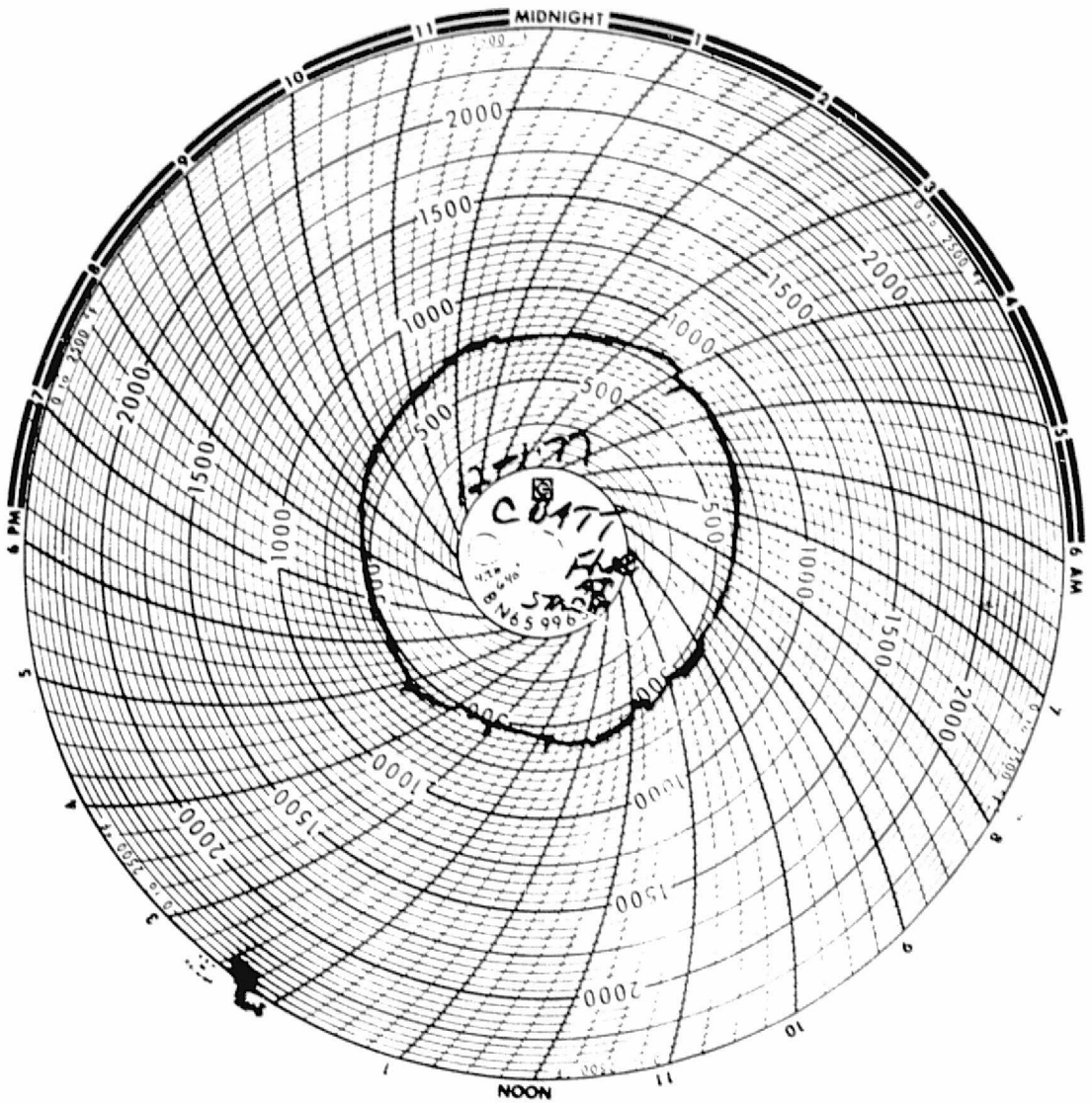
2.4.4 Mill Furnace Stack Gases

There are two reheat furnaces at the Seattle Bethlehem Steel plant in addition to the soak pits. These furnaces supply heated material to the 12- to 10-inch bar mill and the 22-inch

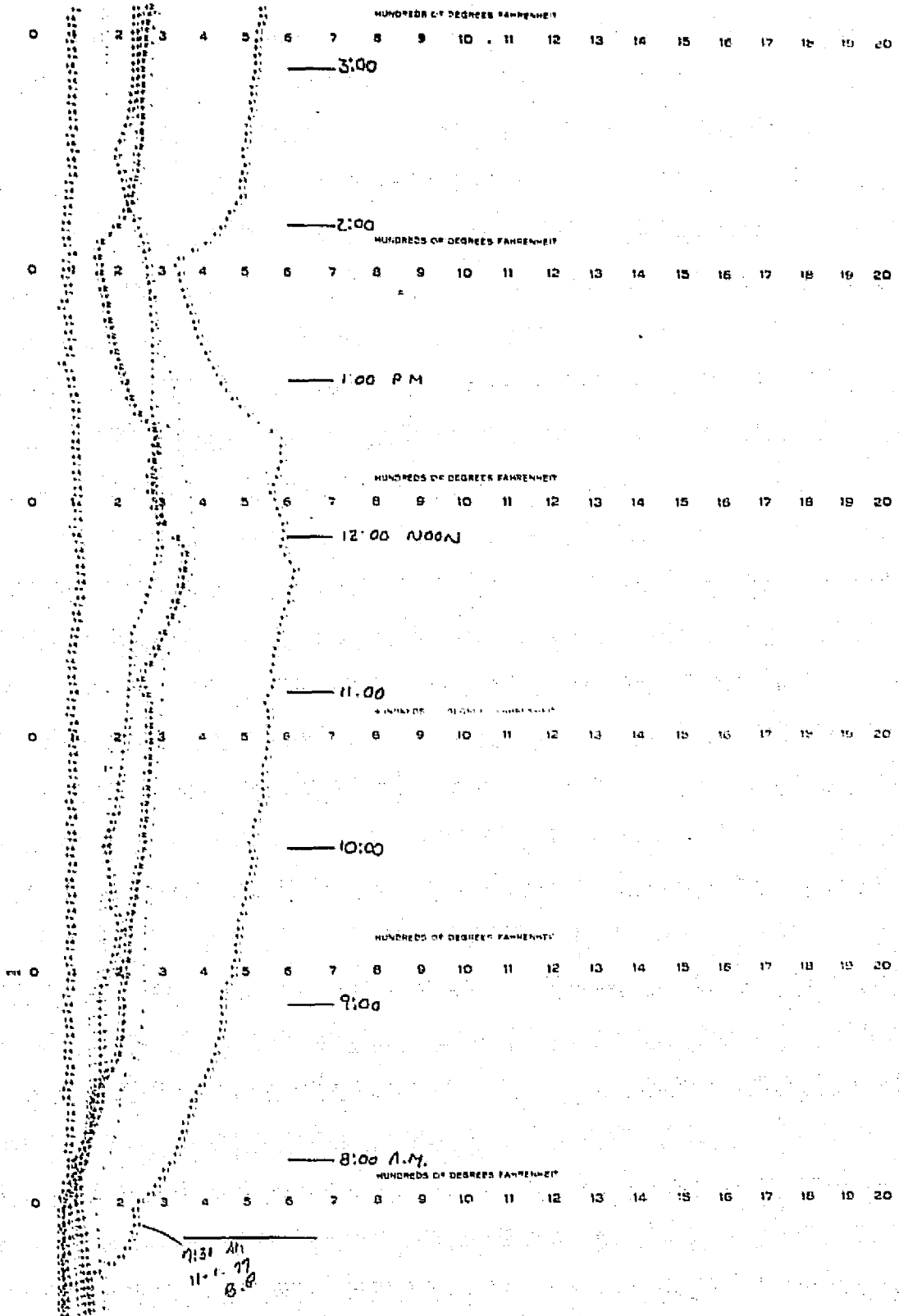
"C" BATTERY, SOAKING PIT NO. 10 GAS TEMPERATURE
BEFORE RECUPERATION



"C" BATTERY STACK GAS TEMPERATURE AFTER RECUPERATION



WALKING RAMP TEMPERATURE MEASUREMENTS



mill. Exhaust gases from these furnaces were defined. Table 3 shows the averaged data over a 24-hour period. These temperatures vary more with time than those of the soak pits, due to some cycling of mill operations. Flow rates of exhaust gases were determined from the fuel usage and known fuel-air ratio.

Table 3
REHEAT FURNACE DATA

<u>Furnace</u>	<u>12" to 10" Bar Mill</u>	<u>22" Mill</u>
Combustion gas flow, lb/hour	41,900	43,000
Exhaust temperature, °F	1,625°F	820°F
CFM of natural gas	886	909
Tons of steel heated per hour	32	13

The 12- to 10-inch mill furnace has a relatively high temperature with a suitable flow rate. Potential heat recovery from this source could be as high as 10 million Btu/hr. The 22-inch mill furnace is of lower availability and magnitude. Direct recuperator systems are likely to show a better cost payback than storage systems, as a synchronized demand exists for any energy which can be recovered.

2.4.5 Smaller Mill Output Shapes

The fifth waste energy stream identified is the sensible energy in the secondary mill output shapes. Temperatures of these products are on the order of 1,700°F and outputs are cyclic, depending on production schedules. Data from the last 3 years indicates 209 tons per 8-hour turn for the bar mill operating at 15 turns a week. The structural mill (based on 3 years) produces 137 tons per 8-hour turn operating at 10 to 15 turns a week.

As the output shapes from these mills are final products, the cooling rates are even more critical to metallurgical properties than are the cooling rates of intermediate shapes from the blooming mill. The shapes themselves tend to be very long and slender, thus the energy is dissipated in a very diffuse manner. Thus, while a sizable amount of energy is dissipated by this means, recovery is not felt to be economically practical.

3.0 SYSTEM SELECTION

The system identified by this study evolves from consideration of four items:

1. Choice of energy source
2. Choice of energy end use
3. Choice of energy storage means
4. Choice of system flow arrangement

The means of making the required decisions regarding the above variables are described in the following paragraphs.

3.1 ENERGY SOURCE SELECTION

Five energy flow paths are identified at the example site which are high enough in both temperature and energy content to be of interest. Each of these energy streams is currently dissipated to the ambient, hence could serve as a source for an energy storage and recovery system. Three of these sources are heated gas streams and two are sensible energy contained in the product. Table 4 lists these sources and shows the result of numerical scoring against each of four major selection criteria. Each energy stream was scored on a scale of 1 to 10 against each criterion, with a score of 10 indicating the stream is very advantageous relative to that criterion. The numerical scores were then summed to a figure of merit for each energy stream. In the following paragraphs, these criteria are discussed, together with the logic behind the assignment of each individual scores.

Table 4
ENERGY SOURCE SELECTION EVALUATION

Source	Requirement For Storage	Expense For Development	Impact to Existing Operation	Confidence of Success	Total
Primary fume stream	9	8	7	8	32
Soak pit stack gases	0	10	7	9	26
32" mill output shapes	5	3	3	4	15
Bar mill furnace stack gases	0	9	7	9	28
Smaller mill output shapes	8	1	1	3	13

The first criterion in the evaluation is the requirement for storage, or, in other words, the degree of variation in temperature or heat flow which precludes the use of common

steady-state recuperator technology. Both of the exhaust stack gas streams are substantially constant in both temperature and flow rate; hence, are capable of recuperative type energy savings. In fact, a recuperator already is in service on the soak pits and the bar mill furnaces are fitted with means to install recuperators. It is thus unlikely that the additional complexity and thermal loss associated with storage of the energy in these streams would be justified.

The second criterion is developmental expense associated with transfer of energy to a transport fluid. Essentially, the three sources in gaseous form can draw upon a wide body of existing experience, whereas little prior art exists for the capture of that energy which is in the mill output shapes. Thus, although it may be feasible to transfer the heat from the mill output shapes, the equipment required would be expected to require significant development expense.

Impact to existing operations associated with means to recover the energy in the various streams is essentially very much less for the three gas stream sources than for either solid form source. In particular, the secondary mill output shapes are very long and slender and would require a very large bulky system, inevitably interfering with materials handling equipment in the vicinity. The same problem at somewhat lesser magnitude exists for primary mill output shapes.

The final criterion is the level of confidence expected for success in using the various sources. In other words, what is the probability that fundamentally unsolvable problems exist, irrespective of the amount of developmental money which could be utilized to provide a workable system? There are no such problems foreseen for stack gas sources. The furnace fume stream could potentially have such problems associated with its dust load and is thus given a slightly lower score. Conflicting requirements for cooling rates from metallurgical considerations and from heat transfer system requirements may have a higher probability of producing fundamental problems for the cases of the solid shapes.

As a result of the above analysis, the arc furnace fume stream is selected as the best energy source for subsequent analysis. The two stack gas sources can be better utilized by steady-state recuperation. The two solid material sources will require significant further research before a demonstration project would be warranted.

3.2 CHOICE OF ENERGY END USE

Four applications for stored energy were identified. These were:

1. Specialty steel ingot preheating
2. Combustion air preheating
3. Substituting of stored energy for holding fire
4. Peak electrical load leveling via generation.

The four end uses are discussed in turn in the following paragraphs.

Specialty steel ingot preheating -- While technically feasible, this appears to offer a very low energy utilization. Reheating of cold specialty steel ingots occurs infrequently; periods of months pass without its occurrence. Thus, this application would require storage of a near seasonal nature, resulting in a very large system. In addition, the investment of capital in a facility which is seldom used is very unlikely to show an attractive payback period.

Combustive air preheating and hold-fire substitution -- Under normal furnace conditions, the steady-state energy stream in the reheat furnace and soak pit stack gases can provide the required energy for air preheating. Thus, it is only during night-time holding fire conditions, when these stack gases are cooler, that providing stored energy for air preheating might show a cost competitive position with the less complex direct recuperation means. In the limit, it might be possible to provide the total energy required for holding; hence, the combustion air preheating transitions smoothly to hold-fire substitution. A fundamental flaw exists for these applications in that at times the plant runs three shifts per day, and hence, there is no requirement for holding fire. Traditionally, these full capacity periods are weeks to months in duration. Hence, unless very large storage systems were considered, the energy storage system would have no use during the times when the daily energy available is the greatest. This end use concept is, thus, unlikely to show the most beneficial cost payback analysis.

Peak leveling -- Peak leveling through electric generation from stored energy remains the most attractive end use for stored energy. There is a demand for electrical energy at any generation level and duration compatible with the size of the energy source. Essential turbogenerator equipment is available "off-the-shelf".

3.3 ENERGY STORAGE MEANS

In Table 5, proven storage materials are listed together with peak temperature ranges and estimated costs. No fundamentally different storage techniques have been found which could be considered proven technology; hence, the storage material must be selected from Table 5.

Water storage is eliminated because of the significant loss of availability which would be incurred due to the relatively low maximum temperature of these storage means, the high expense of storage, and the significant hazard associated with tank rupture and the flashing to steam of large quantities of superheated water. Similarly, petroleum based heat transfer oil storage systems must accept a significant loss in availability as the maximum temperature consistent with long chemical life are lower than the mean source temperature. A second severe difficulty with these materials arises from the anticipated results of a system leak. Vapor pressures of these materials are significant near their maximum temperatures; thus, a line rupture would yield large quantities of vaporized material. As the steel-making environment is characterized by open surfaces at 3,000°F or higher, such vapors are nearly certain to ignite. Suitable protection against such an event is likely to push the storage cost well in excess of the \$3.224/M Btu listed in Table 5. Anhydrous sodium hydroxide, also,

Table 5
STATE-OF-THE-ART STORAGE MATERIALS

STORAGE MEDIUM	STORAGE CONTAINMENT	TEMPERATURE RANGE (°F)	TYPE OF HEAT	COST (\$/M Btu's)	STATUS	REF.
WATER	PRESSURIZED ABOVE GROUND TANK, UNDERGROUND TANK	TO 410°F	SENSIBLE	2,500	DESIGN DATA AVAILABLE, EXPERIMENTAL SYSTEMS TESTED	5
	PRESTRESSED CAST-IRON VESSEL	TO 575°F	SENSIBLE	13,000		
PETROLEUM-BASED OILS (I.E. CALORIC THERMINOL)	PRESSURIZED ABOVE GROUND, UNDERGROUND TANKS	TO 700°F	SENSIBLE	3,224	DESIGN DATA AVAILABLE	48, 49
REFRACTORY BRICK (I.E. MgO)	INSULATED CONTAINMENT VESSELS	TO 1,500°F	SENSIBLE	477	OPERATIONAL	42, 43
HOT ROCKS (PEBBLE BED)	PACKED BED	TO 1,200°F	SENSIBLE	21-297	DESIGN DATA AVAILABLE	18, 46
METAL INGOTS (I.E. IRON, ALUMINUM)	NONE	TO 1,200°F	SENSIBLE	4,000	DESIGN DATA AVAILABLE	45, 44
NaOH	DRUMS	TO 900°F	LATENT	1,025	DESIGN DATA AVAILABLE, EXPERIMENTAL DEVICE TESTED	5, 47

would require an undesirable decrease in the availability of stored energy through its maximum temperature limitation of 900°F. This may not be severe enough degradation to cause outright elimination of NaOH systems, but certainly is an undesirable disadvantage. A more severe disadvantage is the reluctance of steel personnel to consider large amounts of highly caustic material on their site. For 8 hours of storage from the system, approximately 200 tons of molten NaOH would be required. The required safety precautions to preclude the absorption of water or accidental spillage of anhydrous molten NaOH would inflate the cost of the system.

The several solid storage media have no problems foreseen with spills, fires, or steam scaldings. Pressurized storage is not required. All have upper temperature limits equal to or in excess of the mean source temperature; hence, the medium properties do not require a loss of availability per se from that of the source. A number of solid materials with various thermal properties are available. The decision of which specific material need not be made at this time, as the analytical studies can be arranged to simulate any solid material desired, depending upon the specification of thermal properties.

3.4 SYSTEM FLOW ARRANGEMENT

The fourth choice to be made is the system flow arrangement. There are three criteria for the flow arrangement:

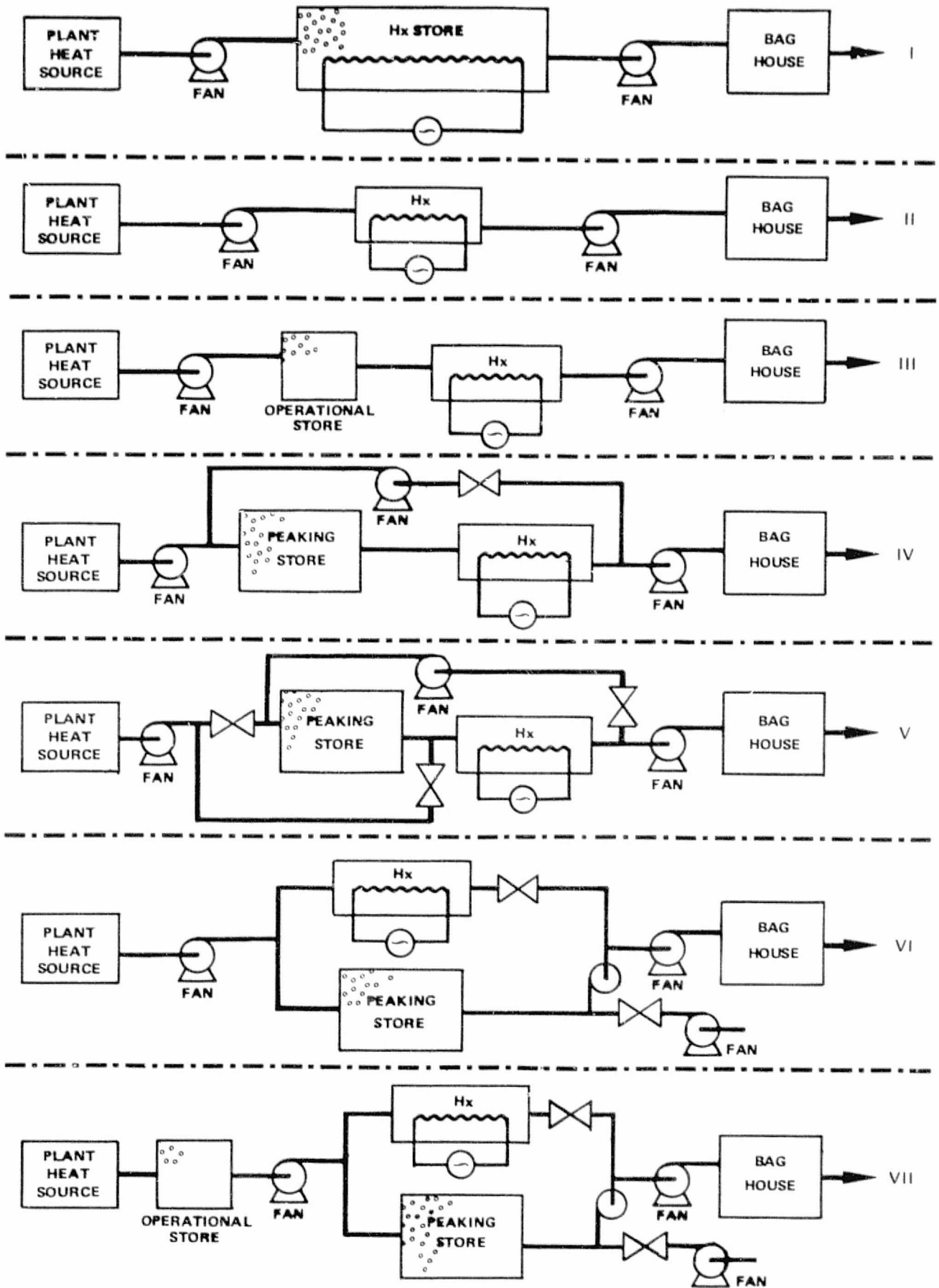
1. The flow arrangement should be as simple as possible, as this will result in the lowest costs.
2. The flow arrangement must allow for most efficient use of energy.
3. The flow arrangement must avoid potential problem areas.

The steam loop for the turbogenerator is not an independent variable in this series, the assumption being that the turbine will be designed around the output from the heat exchanger. Seven system flow arrangements were considered in the evolution of the proposed system. Figure 7 details these in order of simplest toward more complex.

Arrangement No. 1 is the simplest in concept. Gas from the heat source flows continuously through a storage bed and then to the baghouse. The bed is discharged by a heat exchanger buried in the bed operating on counter-flow. Such an arrangement would be versatile in that a partially charged thermal bed could be discharged if desired.

Several disadvantages of this system have surfaced during the work to date. The first of these is that a very large buried heat exchanger will be required. To discharge the bed progressively, yielding constant output temperature steam, the exchanger must essentially have sufficient area for the energy transfer in each of several zones down the bed axis. As the heat exchanger is likely to be a very high cost item, a system which makes more efficient utilization of the heat transfer surface would be desirable. A second disadvantage to the buried heat exchanger is the susceptibility to tube failure when the solid storage medium is

EVOLUTION OF SYSTEM FLOW ARRANGEMENT



charge (this especially is obvious when one considers using the scrap steel as the storage medium). The system would have to be carefully built up on site, layer by layer. A third disadvantage is seen in the expense of maintenance. Should a leak develop in the exchanger, the whole system might have to be torn down and rebuilt with associated high costs.

Conceptually, the second arrangement arises from the first by removing storage material from the heat exchanger. The heat exchanger can now be considerably smaller, as its area is in a hot zone all the time. This arrangement could be applied to a continuous generation system; however, the highly fluctuating temperature of the source will result in widely fluctuating inlet conditions to the steam turbine. To avoid condensation in the turbine, it must be designed for the minimum expected inlet temperature and flow rate. Excess in temperature over the design value results in off-design turbine operation and lower efficiency. Excess steam production must be bled off to prevent over-stressing the turbine. Thus, the turbine must be designed for minimum source conditions. In conclusion, system No. 2 has avoided the problems associated with the buried heat exchanger, but suffers from loss of turbine efficiency.

In system No. 3, a storage bed has been added to system No. 2. This bed acts to even out the fluctuations of the plant heat source, so that the turbine can be designed for more nearly average energy stream conditions, resulting in considerably improved overall system efficiency. There is no means to discharge this bed, however, as this is a continuously operating system. Thus, the operational store, once up to temperature, acts as a heat source for cooler than average source gas, a heat sink for warmer than average source gas, and stays nominally at the mean source temperature.

These first three steps have been limited to continuous duty, i.e., if the plant runs 16 hours per day, the system generates electricity 16 hours per day. Systems 4 through 7 all incorporate the ability to hold energy for a period and generate at a higher power level over a shorter duration.

The number of simple closed form relationships may be derived which link the nominal gas flow rates of these four systems with the relative duration of peaking bed charging and discharging. In any system designed to produce electricity for a shorter time than the duration of the source, the system flows can be calculated noting six factors:

1. The total energy generated is nominally the same, no matter what the discharge period.
2. Thus, short generating times will yield high power levels and large equipment.
3. The bed charging flow rate is the plant flow rate — a constant.
4. The largest generating time is the continuous charging system (in our analysis, 16 hours/day), and results in the smallest equipment.
5. The gas temperature drop in the heat exchanger will be nominally the same as the gas temperature rise in a peaking storage bed during discharge operation for optimum storage bed utilization.

6. The gas temperature drop in the storage bed during charge mode operation is the same as the gas temperature rise in discharge mode operation.

Under these conditions, if a system is designed to charge the peaking storage bed for θ_C hours and discharge the bed in θ_D hours, then the ratio of discharge flow rate to charge flow rate is θ_C/θ_D . Since the charge flow rate is a constant for all systems, the ratio of hours charging to hours discharging immediately sizes all the ductwork and equipment to a first approximation.

System No. 4 incorporates a storage bed large enough to hold energy over whatever period is desired, and the ability to discharge the storage bed to produce peaking power. A return gas loop and fan is arranged so that when the peaking store is charged, a higher flow rate can be arranged to discharge it. Charging flow and discharging flow are in the same direction through the storage bed, so that plant source temperature variations will be damped out by the storage bed.

System No. 4 will not show a high storage bed utilization (energy stored per unit mass) in many charging time/discharging time conditions. An example clarifies this point. Suppose a plant runs 16 hours per day, and one wishes to store energy for 8 hours and discharge the bed for 8 hours, generating electric power at roughly double the rate of a continuous duty system (like No. 3). Flow through the return loop will be nominally equal to the plant flow rate, yielding a discharge flow through the storage bed double the charge flow. The temperature to which the bed can be discharged, in the limit, is no lower than the inlet gas temperature during discharge conditions. In system arrangement No. 4, cooled gas from the heat exchanger exhaust is mixed with hot fume directly from the furnaces, before entering the bed, yielding a discharge inlet temperature halfway between the mean plant source temperature and the heat exchanger exhaust temperature. The storage bed utilization for this system will be about half what it could be, i.e., this system will require twice the storage mass.

Arrangement No. 5 cures the low storage utilization of system No. 4 by arranging a second bypass loop for the primary fume to bypass the storage bed during the discharge mode. Thus, the inlet gas to the storage bed is at the heat exchanger exhaust temperature. The difference between the charged temperature and the discharged temperature will be the same as the temperature difference across the heat exchanger, yielding double the storage bed utilization of the example used with arrangement No. 4. A second advantage to this system arises from the lowered flow rate in the bed during discharge, yielding lower parasitic power requirements.

The disadvantage of system No. 5 is that the storage bed must be designed with exactly the right dimensions. Too much bed material will cause inefficiencies as bad or worse than not enough bed material. The phenomenon arises because the charging and discharging flows in the bed are in the same direction. As the bed is charged, the locus of high temperatures

moves in the same direction as the charging flow. The transition from low to high temperature at any point in the bed takes place over a finite time. Hence, the transition region from low to high temperature at any time as a finite thickness. As the transition region passes through the downstream plane of the bed, the bed exhaust temperature rises. Until it has risen to the bed charge temperature (i.e., all the energy contained in the thermal transition wave has passed), there will not be enough energy to run the turbine, hence, this energy is wasted. The same phenomenon happens in reverse when the transition from low to high temperature passes through the exit plane. Temperatures will decrease to the point where the turbine can no longer be run safely before all the energy is extracted from the bed. The above problem exists even for a bed of optimum length. The problem is very much magnified when considering beds longer or shorter than optimum (as on days where the source runs significantly hotter or cooler than average, or conditions where a plant has a system designed for 16 hours/day operation and is running 24 hours/day). Essentially, the flow arrangement No. 5 must be fully charged and fully discharged each cycle, with excess energy from the source causing an early turbine startup, lower than average energy from the source causing delayed turbine startup.

System flow arrangement No. 6 allows for more efficient use of the storage bed. During storage bed charging, the fume gases are directed through the peaking store, then through a "free wheeling" fan to the baghouse. During discharge operation, the alternate line valve is opened, the "free wheeling" fan is driven, and flow is reversed through the peaking store. At the "T", the flow mixes with that coming directly from the heat source and the combined gas streams led to the heat exchanger. At the second "T", gas is divided, with a portion going to the baghouse, and a portion forming the discharge gas stream. As discharge flow in the storage bed is in the opposite direction from the charge flow, the bed can be designed with excess storage capacity so that the thermal transition wave in charging need never pass through the bed exit plane. In the discharge mode, the thermal transition wave need never pass through the inlet plane. This arrangement eliminates the largest source of losses for solid thermal bed storage devices.

The disadvantage of flow arrangement No. 6 is similar to that of arrangement No. 2. The source is characterized by a widely fluctuating temperature. When averaged over a given 3-hour heat, the temperature may be as high as 1,750°F or as low as 850°F. An example system is chosen which charges the peaking store for 8 hours and discharges the store, creating electrical power for 8 hours.

Flow through the peaking bed loop will be nominally the same magnitude as the plant flow rate. Hence, the temperature at the heat exchanger inlet may be calculated from the known fume temperature variation, and the assumption that the temperature of gas existing the store will be very close to the mean fume temperature (1,300°F). A heat exchanger inlet variation from 1,025 to 1,275°F is predicted. The heat exchanger and turbine must be sized based upon 1,025°F inlet conditions to the exchanger, with excess energy dissipated in higher heat exchanger exhaust temperatures and steam blowby.

The seventh flow arrangement restores the ability to design the turbine and heat exchanger for maximum utilization of the source stream, through incorporation of the operational storage bed discussed under arrangement No. 3. The device operates in the same manner as in arrangement No. 3, except that the degree to which temperature fluctuations must be damped need not be as great for the operational store in configuration seven. The very strongly damped flow from the peaking store will dilute residual temperature variations passing through the operational store. This effect is quite strong, so that for system with charging times longer than 12 hours, the design optimum operational storage bed size is zero (it is not necessary). At the other end of the charge/discharge spectrum, a system which operates continuously needs no peaking store, but the operational store must deliver a greater damping.

4.0 INTERFACE REQUIREMENTS

The energy conservation system will interface with both the physical site and with the steel-making procedure. A strong similarity exists between steel-making procedures at different shops, so that comments concerning the procedural interface are largely representative to the industry as a whole. Discussion concerning the physical interface is largely site specific. The two allowable sites at Bethlehem may represent near and far bounds from the industry-wide viewpoint.

Impacts to the site and operation represent expenses which are very difficult to quantify. The engineering approach, then, is to minimize such impacts to an (intuitively) acceptable level. To a certain extent, this task is simplified through the elimination of hazardous storage materials and the avoidance of logistically complex energy uses (ingot preheating).

4.1 SYSTEM LOCATION

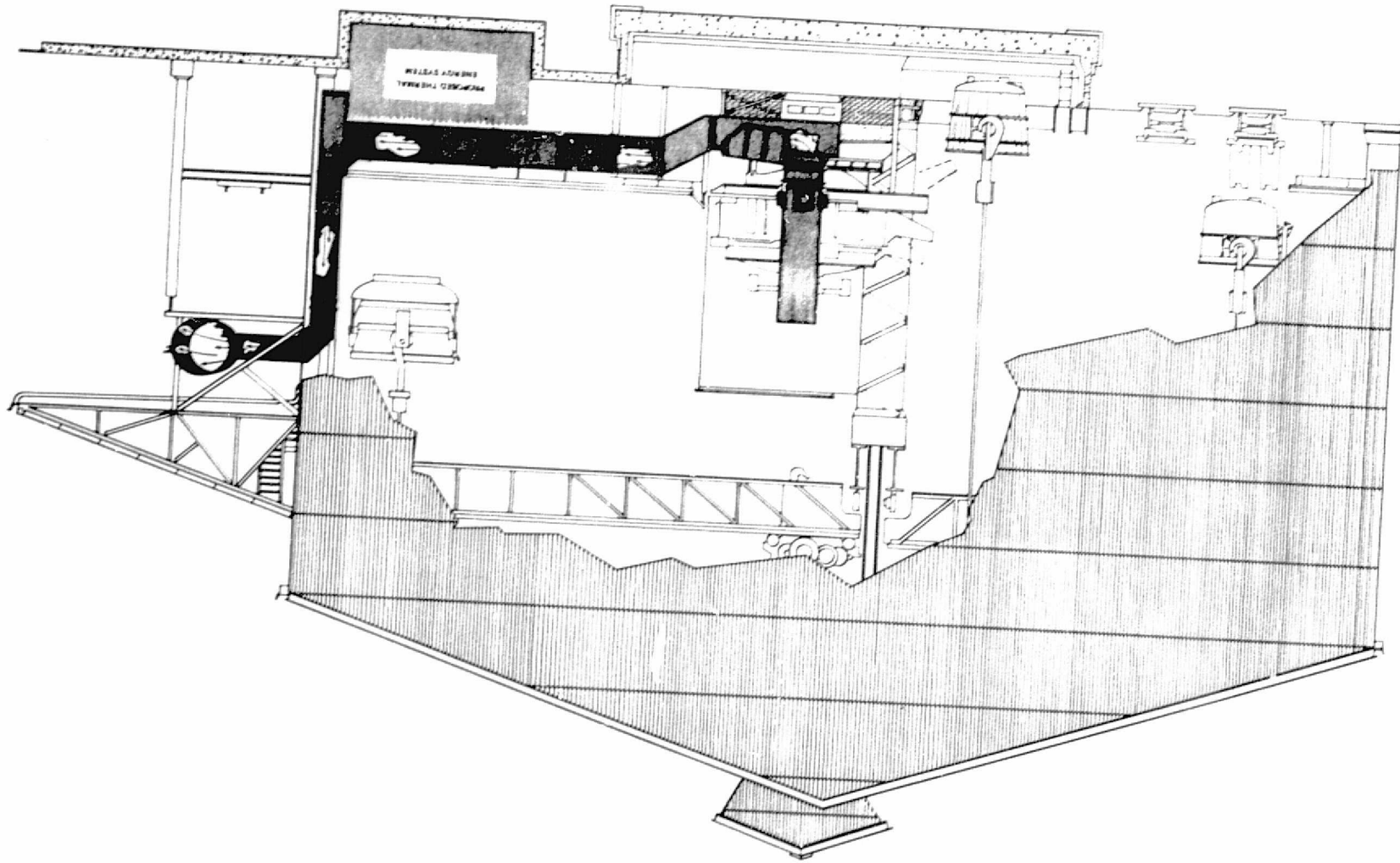
Discussions with Bethlehem personnel reveal that the closest significant volume in which the store could be located has a volume 60 by 20 by 15 feet (without excavation) and is 80 feet from the furnaces. This area is beneath the melt shop floor, as shown in Figure 8. The fume duct currently passes through the center of this volume. Figure 8 shows excavation, allowing more depth to the system. Should an even larger volume be indicated, an area of nearly unlimited dimensions could be accommodated another 150 feet downstream (west) along the duct outside the melt shop building. This area is shown in the general layout drawing of Figure 9.

Space for the turbogenerator is available near either store location, without significant impact on steel-making operations. Space for the condenser is available near the farther store location. As the nearer store location presupposes a smaller turbine, it may be possible to accommodate the condenser in a close coupled manner to the turbine. The benefit of low condenser pressures must be traded off against longer distances to the condenser in this case.

In establishing the two locations for the energy conservation system, several other possibilities were discussed. One was the possible use of the areas presently occupied by the additive storage bins. This would be accomplished by moving these bins to the east. If this were implemented, railroad track would be rearranged at the eastern end of the plant (not shown in Figure 9). Considerable impact to plant operations would occur during this phase of construction (at more expense), as well as required changes from current melt shop practice. After preliminary discussions, this area was eliminated from consideration.

A fourth possible location inside of the melt shop building is located one bay over from the smaller area discussed previously. The area is currently in use for anode cooling.

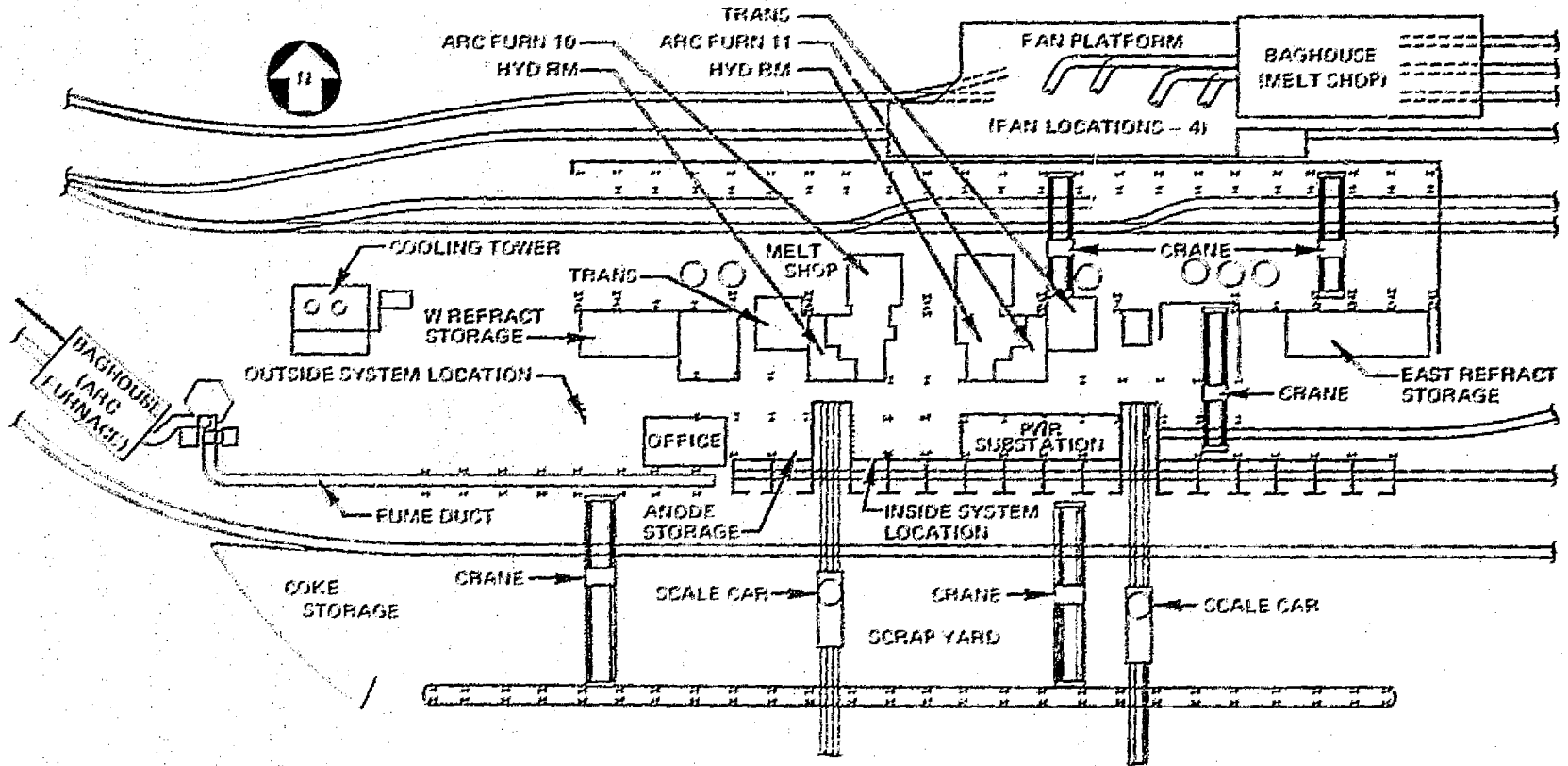
ORIGINAL PAGE IS
OF POOR QUALITY



MELT SHOP SECTION

MELT SHOP BUILDING AND SURROUNDING AREA PLAN

29016-53



31

ORIGINAL PAGE IS
OF POOR QUALITY

Figure 9

Development of an alternate anode cooling site is estimated to require both excessive expense and extensive modification to current melt shop operation, and was, therefore, eliminated from further consideration.

4.2 PROCEDURAL INTERFACE

Eliminating troublesome store sites and awkward heat recovery concepts eliminates major potential impacts to the ongoing operation. A few minor changes are unavoidable, however, as discussed below.

The additional cooling tower load required by the condenser, for instance, may lower the plant water flow rate or raise the water temperature a few degrees. Lowering the water flow rate would impact the operation, but delivering the same amount of water at a slightly higher temperature will not impact the steel-making operation. Most of the water used at Bethlehem Steel in Seattle is for lubrication of hot ingots through the rolling mills. The higher temperature would not matter here. The cooling operation supplied by water generally are for very large temperature differences, and again a few degrees warmer; cooling water would not effect the operations.

Another potential change to the existing operation may involve the handling of fume dust. Equipment in the waste energy recovery system could be designed so that each piece is "flushed" of dust at the end of a working day. If this were the case, special operations would have to be set up to handle the additional collection points of fume dust at the various locations. Another possible dust handling situation may involve a separating device before going to the energy conservation system. This, again, would involve an additional collection point for the dust.

No further permanent impact to operations is foreseen. Some temporary impact to operations is inevitable, while the system is being built and connected to the existing ductwork. During system construction, the impact will be minimal. System hookup and checkout will involve opening the existing ductwork, and must be accomplished when the plant is otherwise not working. Furnace refractory linings are replaced periodically. This process takes 4 days. The final hookup could be scheduled to coincide with the furnace reline, or might even be accomplished during a normal 50-hour weekend.

5.0 SIZING AND PERFORMANCE ANALYSIS

The goal of the analysis performed in the fifth task was to establish the optimum tradeoff between the peak-shaving system performance and the size and cost of the various system components. The results will yield a system with the most favorable payback. While much of the input data has been specific to the Bethlehem/Seattle plant, it is believed that the overall conclusions are applicable to the industry as a whole.

5.1 SYSTEM DESCRIPTION AND OPERATION

5.1.1 Waste Heat Recovery System Description

A schematic of the waste heat recovery system is shown in Figure 10. The hot gases in the primary fume evacuation system from a pair of electric air steel remelting furnaces serves as the source of energy for the system. The nominal flow rate of this source is 128,000 lbs per hour at an average temperature of 1,300°F, yielding an energy flow rate of 40×10^6 Btu's per hour above the 70°F ambient temperature.

Two energy storage beds are required. The operational storage bed serves to time-average the widely fluctuating temperature of the source. The peaking storage bed serves to hold energy until the demand arises.

A counterflow heat exchanger in the gas stream preheats water, raises steam, and superheats the steam to the desired temperature and pressure. Steam is expanded through a turbine which in turn drives a generator, yielding electric power. The water/steam cycle is completed with a standard condenser and turbopump.

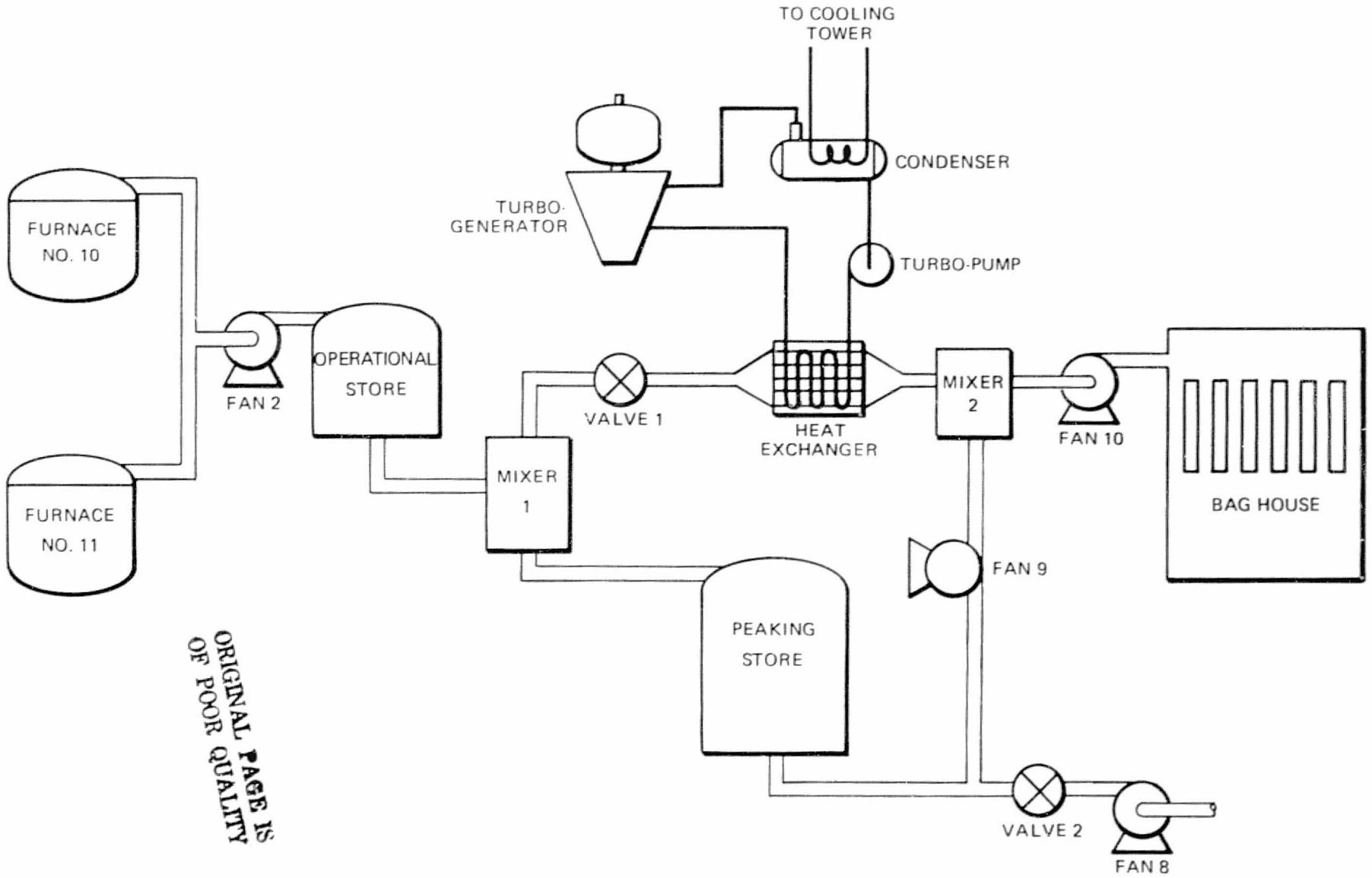
Four fans are arranged to overcome pressure drops occurring in the primary fume flow ducts and equipment. Primary fume exits the system through the existing baghouse filters to the ambient.

5.1.2 Operation

The system operates in two distinct modes, depending upon whether energy is being stored in or withdrawn from the peaking storage bed.

Charge Mode — Conditions during which energy is added to the peaking storage bed are termed charge mode operations. Referring to Figure 10, fume from the arc furnaces is combined to a single stream and led to the inlet of the operational store. The operational store will rise in temperature to the mean of the fluctuating fume temperature. Thereafter, hotter inlet gasses will tend to be cooled in passage through the device, while cooler inlet gasses will be warmed. The operational store is not ordinarily discharged, hence, stays at nominal temperature between system cycles.

STEEL ARC FURNACE ENERGY RECOVERY SYSTEM



ORIGINAL PAGE IS
OF POOR QUALITY

Gases exiting the operational store, while not necessarily at exactly the mean temperature, will exhibit a considerably damped time/temperature fluctuation.

During charge mode, valve 1 is closed; hence, all fume is directed to the peaking store. As the fume passes through the peaking store, its energy is lost to the cooler bed material. During any given charging cycle, a thermal front passes from the inlet side of the operational store toward the outlet end. Upstream of this front, the bed material has been heated to the system mean temperature. Downstream of this front, the bed temperature remains at the cooler value from the previous discharge cycle. Gases exiting the peaking storage bed will, therefore, have been cooled to the discharge temperature.

Valve 2 is closed during charge mode. Fume flows under the action of fans 9 and 10 to the baghouse, through its filters, and is released to the ambient.

Discharge Mode - Conditions during which energy is removed from the peaking store are termed discharge mode operation. Flow through the furnaces through the operational store is the same as during the charge mode. During discharge mode, valve 1 is opened and fan 9 reversed so that flow through the peaking store is reversed. Cool fume is withdrawn from the stream at mixer 2 and forced by fan 9 through the peaking store. Cool gas is heated as it passes through the thermal front and exits the peaking store at the mean gas temperature.

The gas streams from the operational store and from the peaking store combine in mixer 1 and flow to the heat exchanger. In the heat exchanger, the gas flows over three sets of coils in a multi-pass, counterflow arrangement. First, cooling of the gas accomplishes the superheating of the steam; next the boiling of water; and, finally preheating the water to the boiling point. Upon leaving the heat exchanger, gas flows to mixer 2. Here it divides into two streams, one returning to the peaking store inlet while the second stream continues to the baghouse.

Changeover Transient Operation - The period of time required to switch from steady-state charge mode operation to steady-state discharge operation is termed the changeover transient. At the beginning of this period, valve 1 is opened, and the system nominal flow rate (128,000 lbs/hr) circulates to the heat exchanger and is drawn by fan 9 towards the peaking store. There is no flow to the baghouse until sufficient gas has been accumulated in the system to yield the design discharge rate of the peaking storage bed. Valve 2 and fan 8 are incorporated into the system schematic so that ambient air may be drawn in rapidly, thus shortening the changeover transient if desired.

5.2 WASTE HEAT SYSTEM SIZING AND PERFORMANCE COMPUTER CODES

Two computer codes were written to describe the system operation - a system sizing model which predicts system performance during steady-state operations in charge and discharge modes, and a thermal model which predicts the transient behavior of either storage bed. The

general analytical approach, using these two models, is presented in the following paragraphs. Details of the model development are included in Appendices B and C, respectively.

5.2.1 Independent Variables

Charge/Discharge Ratio -- The major independent variable for this analysis is the system charge to discharge ratio θ_C/θ_D , the ratio of time spent in the charge mode to time spent in the discharge mode. All analyses were performed parametrically with this variable, yielding a series of design curves rather than an isolated design point. The logic behind this approach is that the value of energy generated to reduce peak power demand is strongly dependent upon the duration over which the power is generated. This effect is apparent in the trend to time-of-day pricing of energy charges by electric utilities. It is possible to avoid an arbitrary decision regarding the form of future time-of-day energy price by treating the θ_C/θ_D ratios as an independent variable.

Storage Bed Materials -- Three storage bed materials were carried along for the analysis: slag, scrap steel, and silica brick. Each has its advantages and disadvantages. Slag is cheap, but relatively untried, lower in thermal conductivity and specific heat, and has questions concerning the thermal and dimensional stability. Scrap iron is next in cost, high in thermal conductivity, though still relatively untried. Depending upon certain site specifics (ease of loading and unloading the bed), a scrap bed could be considered a raw material stockpile in temporary service, hence, a zero cost item (other than costs associated with loading and unloading). There are questions concerning the chemical stability of scrap in the fume environment. Brick checkerworks are the most expensive storage material considered, but are well known by the industry and in common use.

5.2.2 Dependent Variables

Two criteria exist against which system variations will be evaluated. The first of these is the desire to conserve as much energy as possible. The second of these is to do so as cost-competitively as possible. The final output system dependent variables are then, the total system cost and the total energy savings. The ratio of these two is termed the capital cost factor (CCF) defined as follows:

$$CCF = \frac{\text{Total System Capital Cost}}{\text{Daily Energy Savings}} \frac{\$1000}{(\text{MW-hr})/\text{day}}$$

The CCF is an interim variable used in the optimizing analysis. Cost of energy produced is a convenient and straightforward indication of the most economical system, independent of the subtleties of inflationary pressures, escalating fuel costs, and variations in the value of electric energy by time of day and geographic location.

5.2.3 Analytical Approach

The overall energy conservation system will operate in steady state, both charging and discharging the peaking storage bed. The short transient operation between modes is not

expected to exert a strong influence on the overall system design. The efficiencies of the two energy storage beds, however, can only be found through transient analysis. Although the whole system could be described in the transient mode, the result would be a very complex computer program with attendant high running costs. An alternate approach, taken in this project, is to divide the steady-state (system) analysis and the transient (thermal storage bed) analysis into separate computer programs. The details of these two programs are presented in Appendices B and C.

Figure 11 illustrates the method by which the two models are used to predict the system engineering and economic performance. The major tradeoffs in component size are defined using the system design model. The transient thermal losses from the two storage beds are initially estimated by an assumed energy loss equivalent to a decrease in system mean temperature from 1,300 to 1,100°F. The result is a set of designs for various charge/discharge ratios and storage bed materials, where the best economic tradeoff between major system elements has been located.

The transient thermal storage bed model is then used to predict more accurately the peaking storage bed losses in the charge mode. The energy savings from an increased length of the peaking storage bed is then traded off against the resulting increased parasitic power to define the peaking storage bed length.

The transient thermal model is then used to predict the output gas temperature characteristic with time from each storage bed (peaking storage bed in the discharge mode). The temperature/time characteristic of the mixed gas at the inlet to the heat exchanger is then found and compared to the original 1,100°F assumption. If the temperature is found to fall below 1,100°F before the end of the discharge time, then the effective time of production of turbine power is decreased to be consistent with the 1,100°F heat exchanger inlet condition (this is conservative). Thereafter, the parasitic power for the fans which overcome pressure drops in the storage bed is calculated, as well as any revisions indicated in fan cost and storage bed cost. The predicted system cost and net power output may then be calculated.

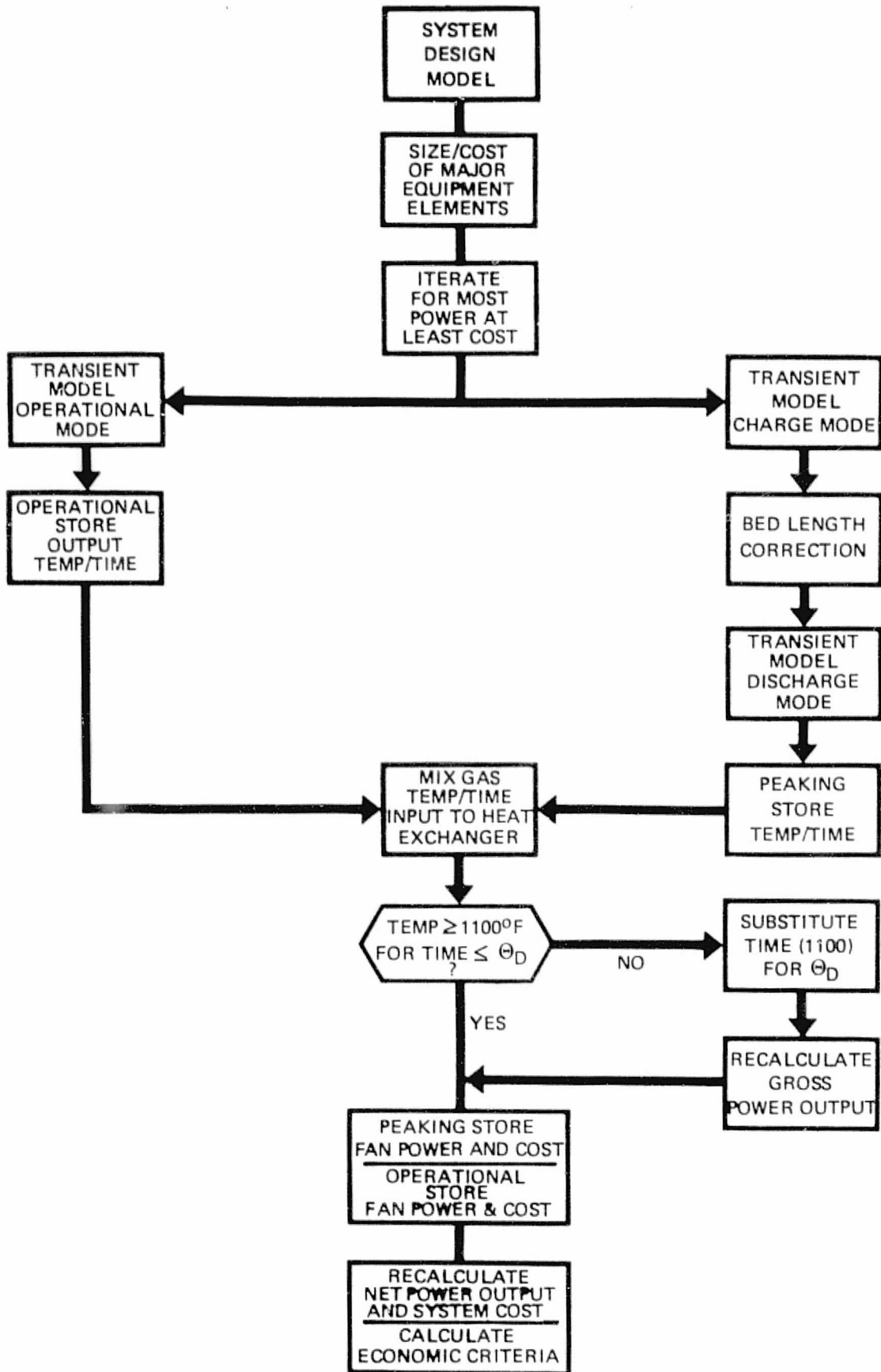
The analysis concludes with the calculation of economic criteria: payback, net present value, return on investment, and rate of return.

5.3 RESULTS OF SIZING AND PERFORMANCE ANALYSIS

5.3.1 Turbine Inlet Design Conditions

Turbine inlet conditions are set through the desire to generate as much power as possible, in keeping with reasonable turbine cost and design. Higher inlet temperature and pressures will yield greater turbine efficiencies. However, considerable increase in turbine costs result when the design must incorporate exotic, high-temperature materials. This effect occurs at 800 psig and 950°F for the turbine size range (1 to 10 megawatts) under consideration. Therefore, the study contained herein selected a turbine inlet pressure and temperature of 800 psig and 950°F, respectively.

LOGIC DIAGRAM: SYSTEM OPTIMIZATION PROCESS



5.3.2 Storage Discharge Temperature

The maximum output power is found when the storage discharge temperature (T_R) is as low as possible. Very low storage discharge temperatures require very large heat exchangers and, hence, high system costs. These competing effects result in a broad minimum in capital cost factors when plotted against storage discharge temperature. Figure 12 is an example of this effect, showing the optimum storage temperature for the four charge/discharge ratios considered. Storage medium in the example shown is scrap iron. The optimum discharge temperature was found not to be a function of the storage material and a fairly weak function of charge/discharge ratio. All four minima fall in the region of 350 to 450°F, with the larger systems (larger θ_C/θ_D ratio) justifying the lower discharge temperatures.

5.3.3 Model Continuation

Once the optimum discharge temperature is found, the design model proceeds to size the heat exchanger, fans, turbopump, ductwork, the turbine condenser, and the peaking store. Capital costs are calculated for each item and summed. The gross power generated is calculated, and the parasitic power associated with the fans in charge and discharge modes is calculated along with the power required for the turbopump. The net power produced is calculated as the difference between the gross power and total parasitic power. Having calculated the net power produced, and sized each of the major system components, the capital cost factor can be calculated. The variation in capital cost factor with discharge time is presented in Figure 13 for the three bed materials. The higher thermal storage density of the scrap iron results in smaller storage beds (and lower containment costs), but does not quite make up for the higher material costs when compared to the system incorporating slag. The additional cost to be paid for brick may be worthwhile when its development status is considered.

5.4 CORRECTION OF SYSTEM DESIGN FOR TRANSIENT STORAGE BED EFFECTS

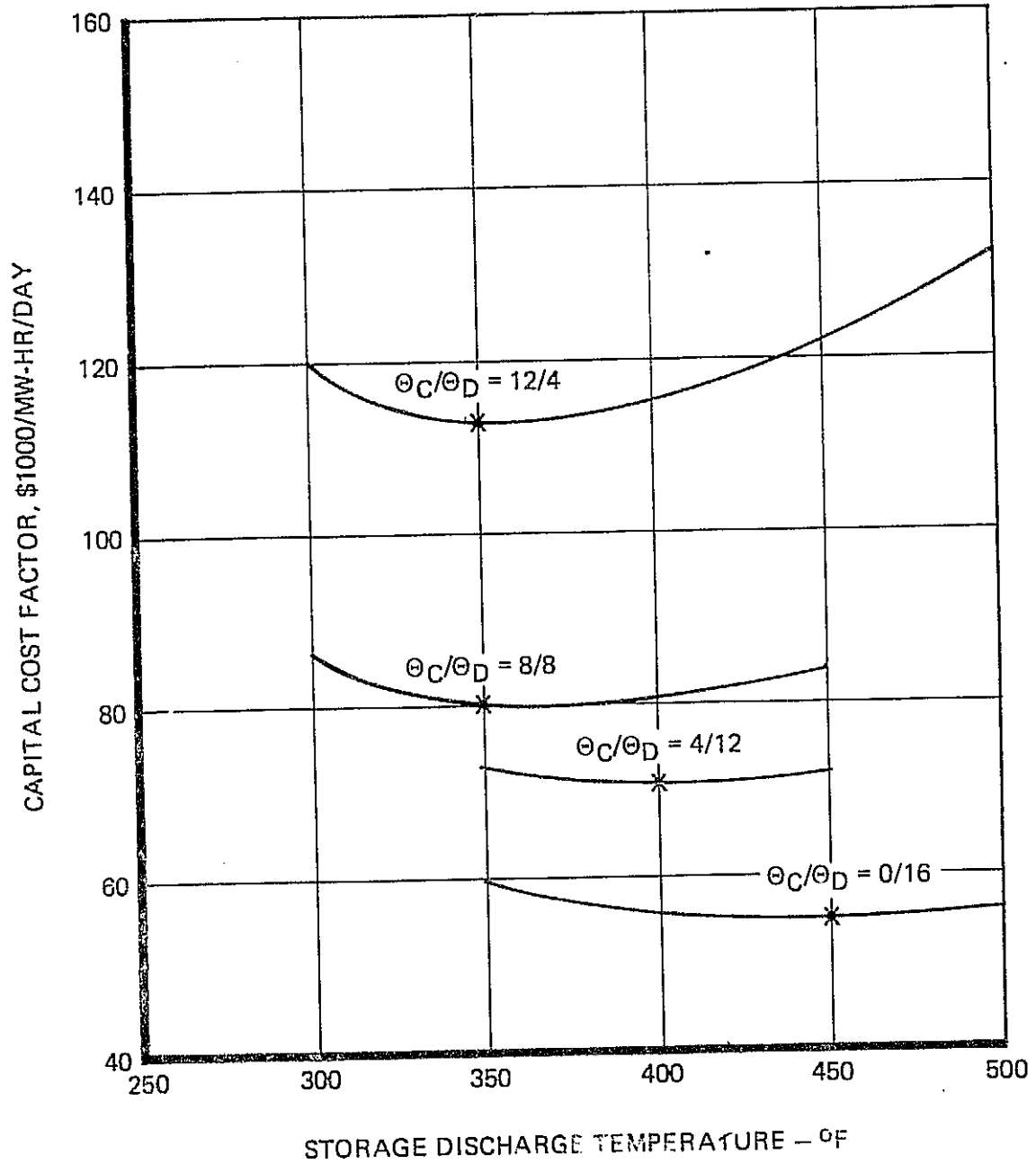
The steady-state design model assumed a lump loss to account for real storage bed transient thermal effects and losses. It remains to check the accuracy of this assumption and correct the thermal storage bed design, if indicated. Real bed effects enter in four ways:

1. Output temperature of operational store is not constant
2. Radial thermal losses are experienced from both storage beds
3. The temperature of air exiting the peaking store will rise towards the end of the charge cycle due to axial energy transfer in the bed
4. The temperature of air entering the heat exchanger will decrease with time toward the end of the discharge cycle due to axial energy transfer in the bed.

The transient model was utilized to determine the magnitude of these effects. The following paragraphs discuss these results.

OPTIMUM STORAGE DISCHARGE TEMPERATURE

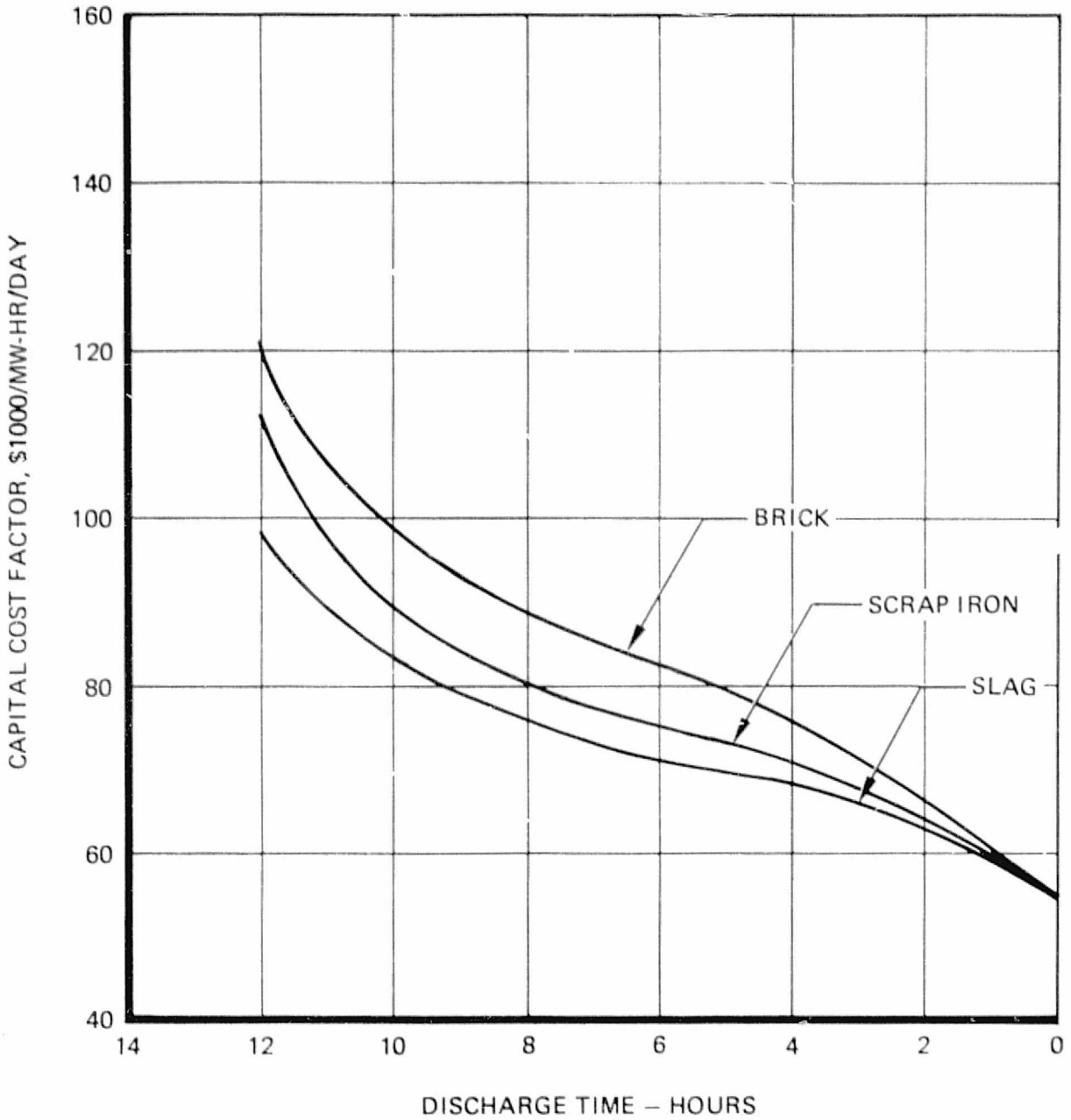
STORAGE MATERIAL – SCRAP IRON
TURBINE INLET TEMPERATURE – 950°F



ORIGINAL PAGE IS
OF POOR QUALITY

CHARGE TIME VS. CAPITAL COST FACTOR

TURBINE PRESSURE = 815 psia
TURBINE TEMPERATURE = 950°F
OPTIMUM T_R RANGE = 350°F TO 450°F



5.4.1 The Operational Store

The purpose of installing the operational store bed in the thermal energy storage system is to reduce the temperature fluctuation of the hot fume stream from the steel plant. The main concern in the design of the operational store bed is limiting of the amplitude of the outlet air temperature fluctuation of the operational store. Although the transient model, discussed in Appendix C, can be applied to find the outlet air temperature and thus the amplitude of the fluctuation, a closed form theoretical analysis can more readily provide some insight into the problem.

Assuming that the fluctuation of the inlet air temperature can be approximated with a sine wave function, the outlet temperature fluctuation will be sinusoidal at the inlet frequency. The outlet fluctuation will lag behind the inlet fluctuation by an angle, ϕ , and will have a smaller amplitude. Using the Laplace Transform technique, we can find the amplitude ratio of A_o/A_i . If $T_i(S)$ is the Laplace Transform of the inlet fluctuation, $\Delta T_i = T_i - T_m$, and $T_o(S)$ is the Laplace Transform of the outlet fluctuation, $\Delta T_o = T_o - T_m$, then:

$$\frac{T_o(S)}{T_i(S)} = G(S)$$

where $G(S)$ is the transfer function defined as the ratio of the Laplace Transform of the responding variable to the Laplace Transform of the disturbing variable. (See Appendix A for term definitions.) $G(S)$ is obtained by appropriate transformation of equations C-1 and C-2 of Appendix C.

To obtain the amplitude ratio, we merely need to substitute $j\omega$ in $G(S)$ and take the magnitude of the resulting complex number (Reference 31). Such an analysis leads to the following result after nondimensionalization:

$$\frac{A_o}{A_i} = \exp \left[-\left(\frac{1}{r}\right) \left(a\right) \left(\frac{1}{1+\beta^2}\right) - \left(\frac{1}{r}\right)^2 \left(\frac{DP}{LB}\right) \left(\frac{1}{Pe}\right) (\gamma)^2 \frac{1 - \left(\frac{1}{\beta}\right)^2}{\left[1 + \left(\frac{1}{\beta}\right)^2\right]^2} \right]$$

where:

$$a = \frac{LB/V_B}{\rho_B CP_B/h_v} = \frac{\text{Residence time}}{\text{Thermal time constant of packing}}$$

$$\beta = \frac{1/\omega}{\rho_B CP_B/h_v} = \frac{\text{Period of disturbance}}{\text{Thermal time constant of packing}}$$

$$\gamma = \frac{L_B/V_B}{1/w} = \frac{\text{Residence time}}{\text{Period of disturbance}}$$

$$r = \frac{\rho_a C_{pa}}{\rho_B C_{pB}} = \frac{\text{Thermal capacity of air}}{\text{Thermal capacity of bed}}$$

w = angular velocity of the disturbance, radian/time.

$$j = \sqrt{-1}$$

The first term on the right-hand side is the damping effect due to the absorbing thermal capacity of the packing, and the second is the damping effect due to the axial thermal conduction. Examination of this equation reveals the following results regarding the design of the operational store bed:

1. The amplitude ratio decreases with increasing fluctuation frequency. Amplitude ratio approaches zero as w approaches infinity.
2. Amplitude ratio becomes smaller as the fluid residence time in the bed, L_B/V_B , increases. A long bed helps damp out the fluctuation.
3. Small thermal capacity ratio of air versus solid particle gives better damping effect.
4. As $h\nu$ becomes zero ($\beta \rightarrow 0$) or infinity ($\beta \rightarrow \infty$), the damping effect contributed by the packing becomes negligible. The optimal value of $h\nu$ depends on w . Since $h\nu$ is dependent on the size of the particle, it is important to have an accurate estimation of $h\nu$ as a function of d_p . The choice of d_p is critical to the design of the operational store bed.

To illustrate the application of the amplitude ratio equation to the design of the operational store bed, the dimensional and operating variables of the bed are:

$$\left. \begin{aligned} d_p &= 6", D = 15 \text{ ft}, L = 10 \text{ ft} \\ w &= 150,000 \text{ lb/hr} \end{aligned} \right\} \text{Sample case}$$

For analysis comparison purposes, the packing is assumed to be 6-inch spheres with a thermal conductivity of 10 Btu/hr-ft-°F. Based on the real data, the amplitude ratio from the computer program STORE 1 is 16.86%. By using the approximation of the sine wave function, the amplitude ratio is 10.1% if the period of the fluctuation is assumed to be 3 hours, and the amplitude ratio is 14.1% if the period is assumed to be 4 hours. In view of the irregular fluctuation of the real data, the closed form equation gives a reasonably close estimation of the amplitude ratio.

The bed cost is derived as \$40,000, using scrap iron as the storage material. The additional fan power to overcome the pressure drop in the operational storage bed is 0.156 megawatts. As this fan runs continuously, 2.5 megawatt hours is added to the daily parasitic power total.

An amplitude ratio of 16.86% yields an output temperature fluctuation of $\pm 76^{\circ}\text{F}$ about the $1,300^{\circ}\text{F}$ mean, guaranteeing a minimum output temperature of $1,224^{\circ}\text{F}$. This is a suitable design for a 4-hour charge, 12-hour discharge system at the example site.

5.4.2 Peaking Store

Losses in the peaking store occur from radial heat transfer effects (surface losses), and from axial heat transfer effects. The latter are evidenced by rising exit temperatures at the end of the charge mode and falling exit temperatures at the end of the discharge mode. The axial transfer effects can be reduced by extending the bed length at the expense of additional parasitic power, and slightly increased capital cost for bed material, bed containment, and increased fan capability. An optimum is found between these competing criteria.

Figure 14 presents an example of the prediction for the combined charge and discharge thermal loss as a function of bed length increase from the length selected by the simplified component sizing model. Scrap iron is the example bed material. Charge/discharge ratio shows a weak effect. Adding the estimates for surface heat losses yields the total thermal loss (Figure 15), a somewhat stronger function of charge/discharge ratio. The additional parasitic power required for various bed length increases is presented in Figure 16. Again, scrap iron is the example material. The parasitic power is a strong function of bed length increase as well as charge/discharge ratio.

In Figure 17, the optimization result is presented as capital cost factor versus bed length increase. The location of the minimum is a very weak function of charge/discharge ratio. A 14 to 20 percent bed length increase is justified, yielding a 5 percent decrease in CCF for the 12:4 system or 8 percent decrease in CCF for the 8:8 system, and a 12 percent decrease in CCF for the 4:12 system.

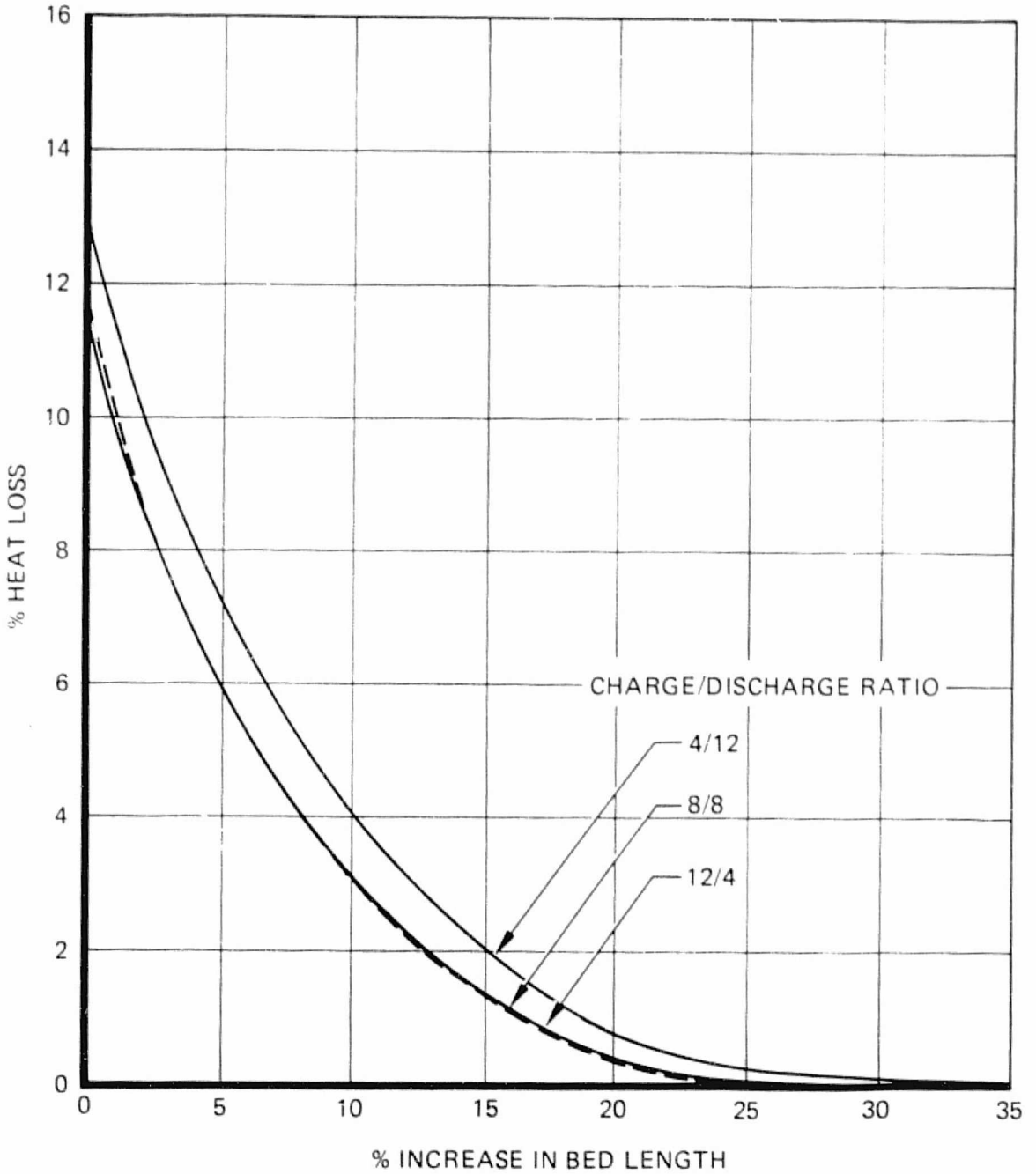
5.5 OVERALL SYSTEM PREDICTIONS

After accounting for transient thermal affects, the overall system performance is calculated assuming the indicated optimum increases in bed length. Figure 18 shows power output from the system as a function of discharge time. Different storage bed materials have almost no effect upon system power output except at the very short discharge times. Overall system capital cost is presented in Figure 19. The lower cost of containment for the higher density scrap iron store nearly compensates for its higher bulk price, while brick storage is significantly more expensive for all but the smallest (near-continuous generation) systems.

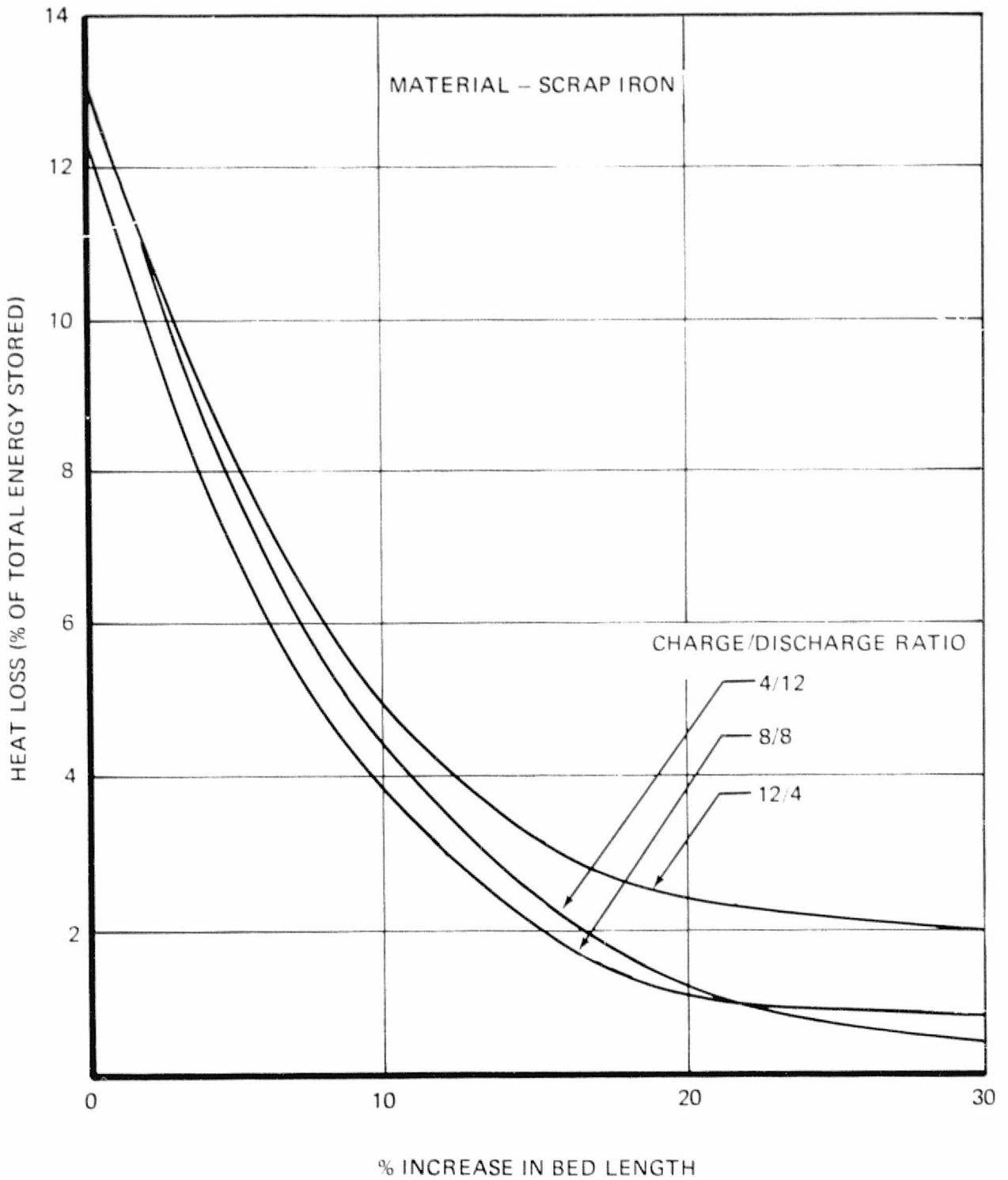
Figure 20 presents a breakdown of the capital costs for the scrap iron storage system. The major cost item is the turbogenerator system (including turbopump and condenser). It is

PEAKING STORE CHARGING AND DISCHARGING
PERCENT HEAT LOSS VERSUS
PERCENT INCREASE IN BED LENGTH

STORAGE MATERIAL – SCRAP IRON
PARTICLE DIAMETER – 0.125 FEET

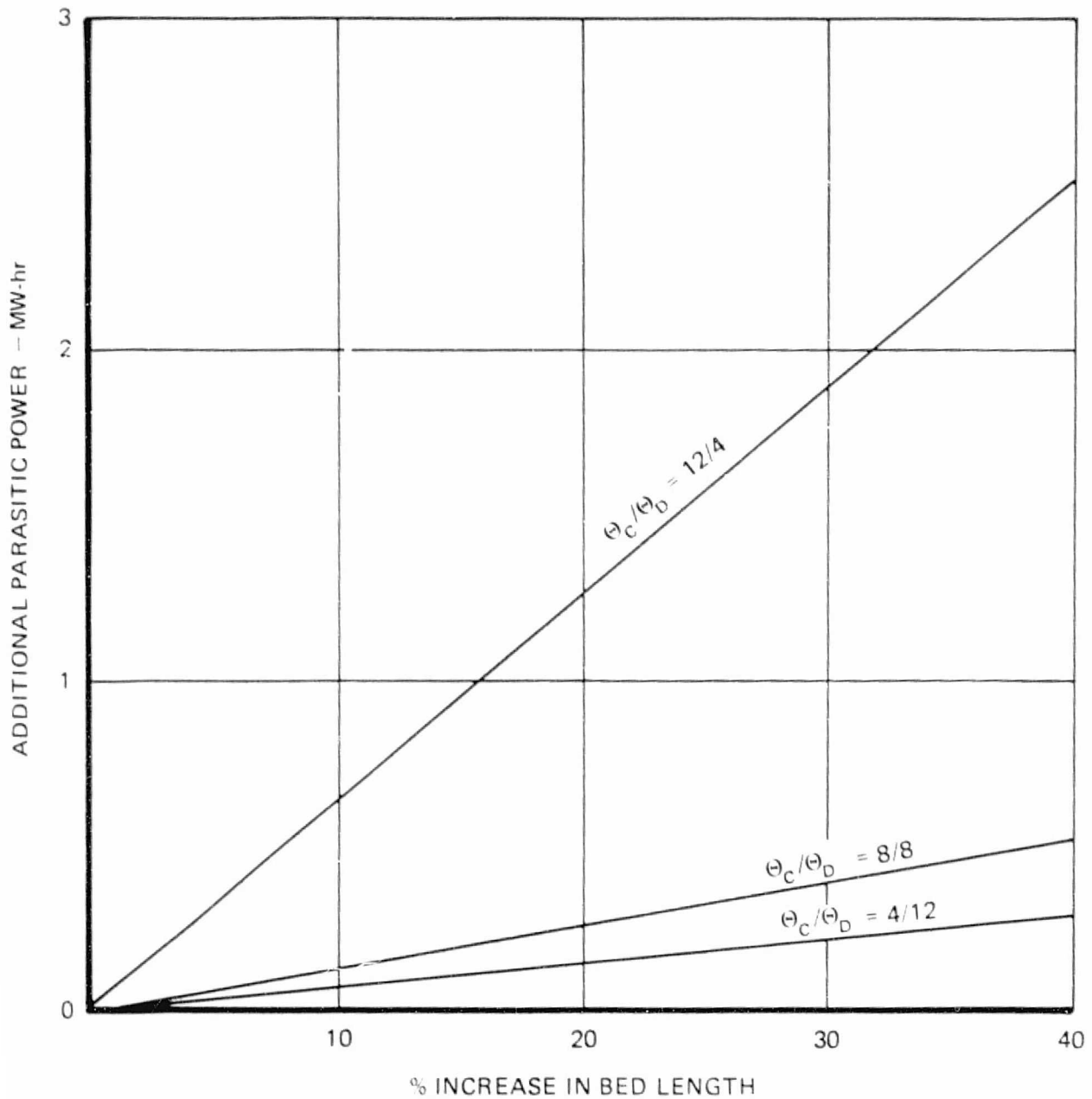


PEAKING STORE
EFFECT OF INCREASED STORAGE BED
LENGTH UPON STORAGE BED HEAT LOSS

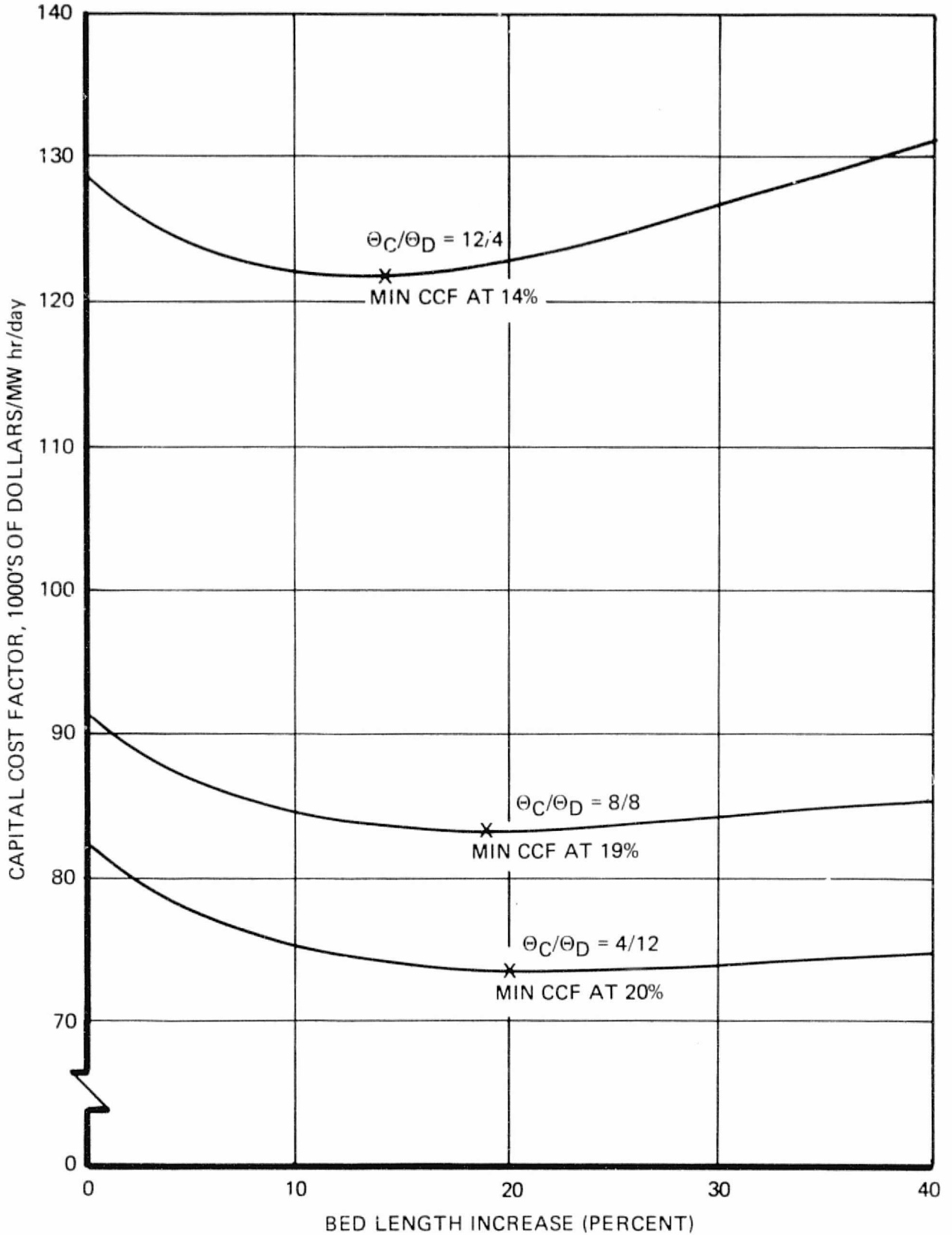


PEAKING STORE
EFFECT OF INCREASED STORAGE BED LENGTH ON
SYSTEM PARASITIC POWER

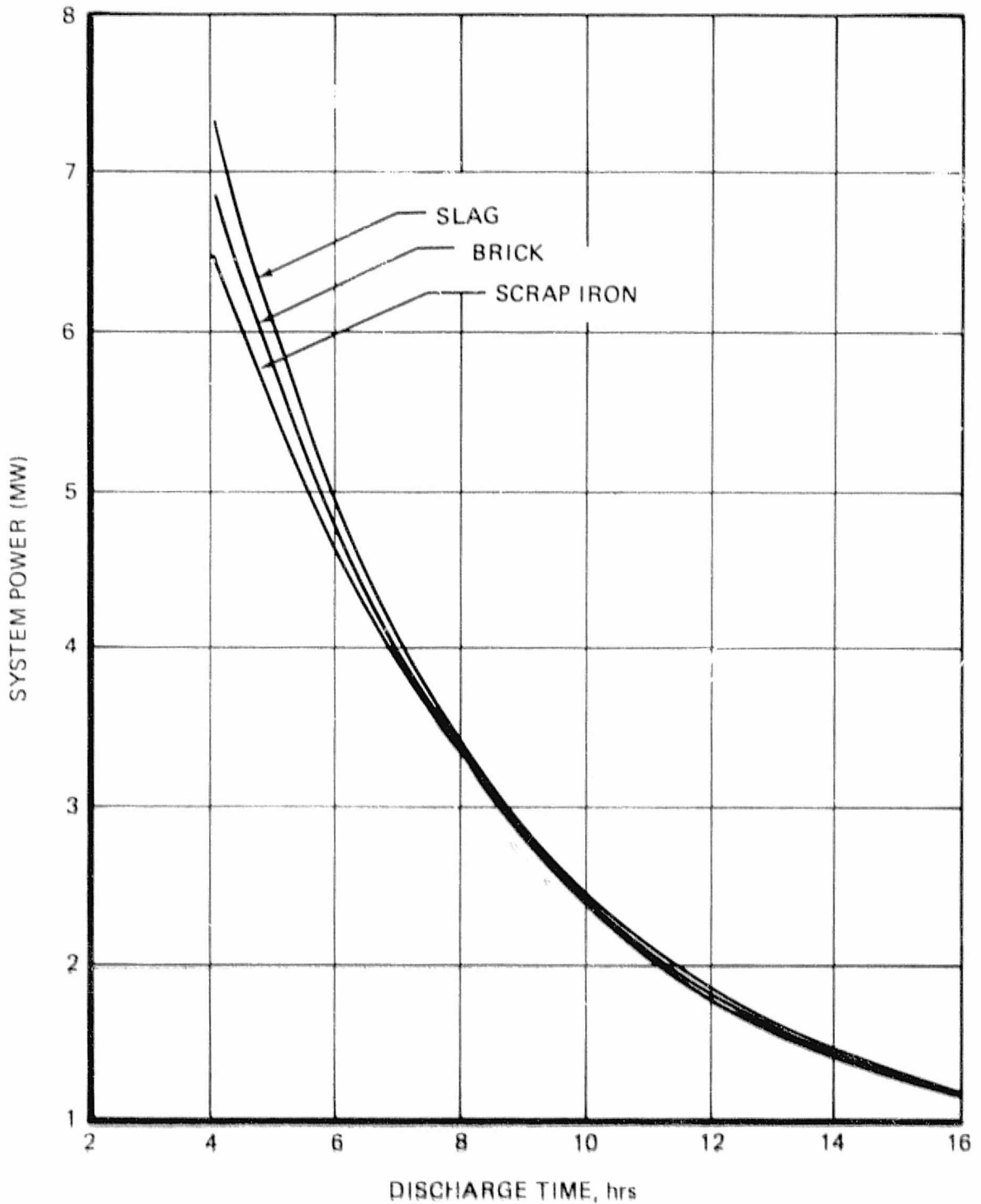
BED MATERIAL - SCRAP IRON



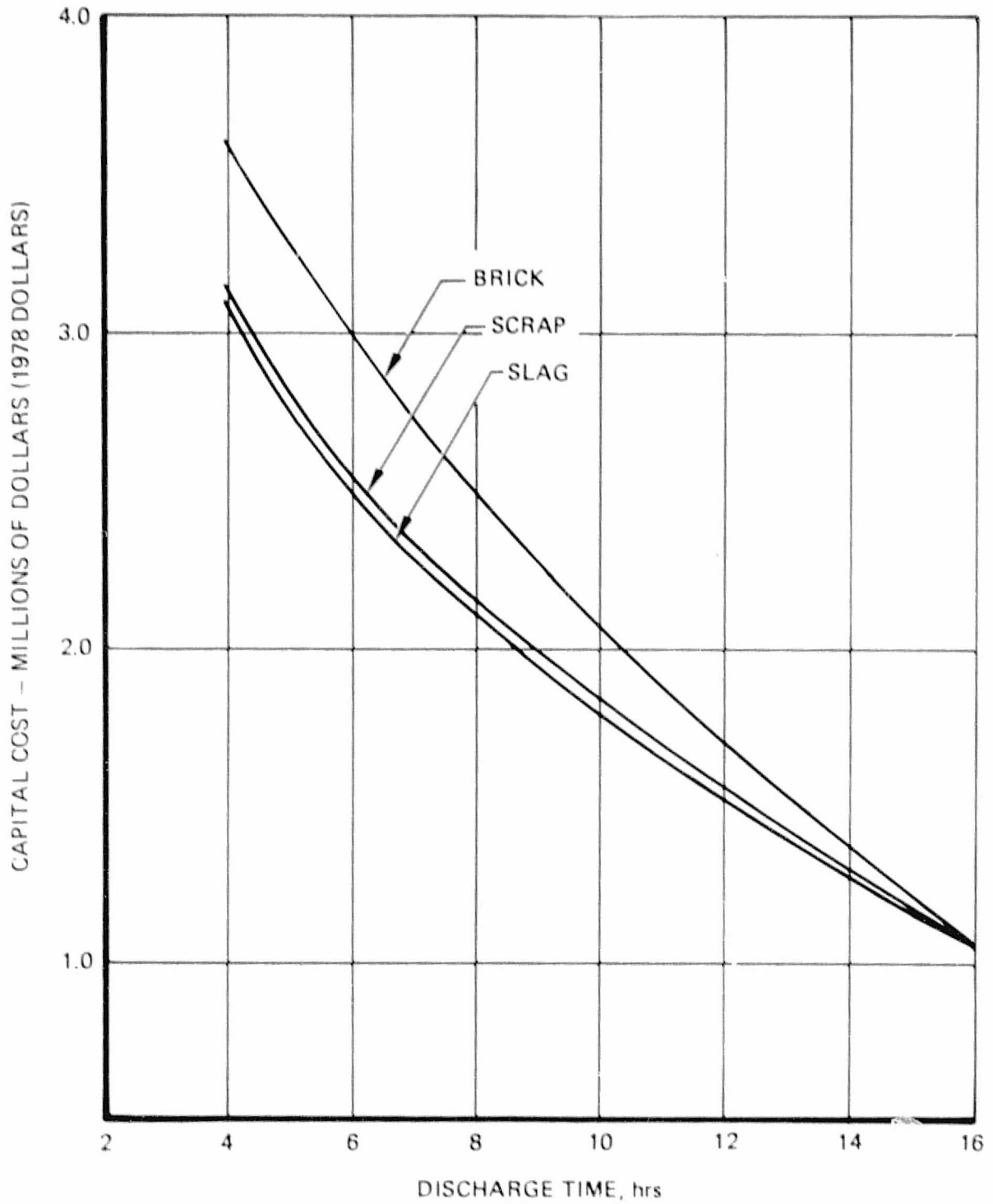
PEAKING STORE
CAPITAL COST FACTOR OPTIMIZATION VERSUS % BED LENGTH INCREASE
MATERIAL – SCRAP IRON



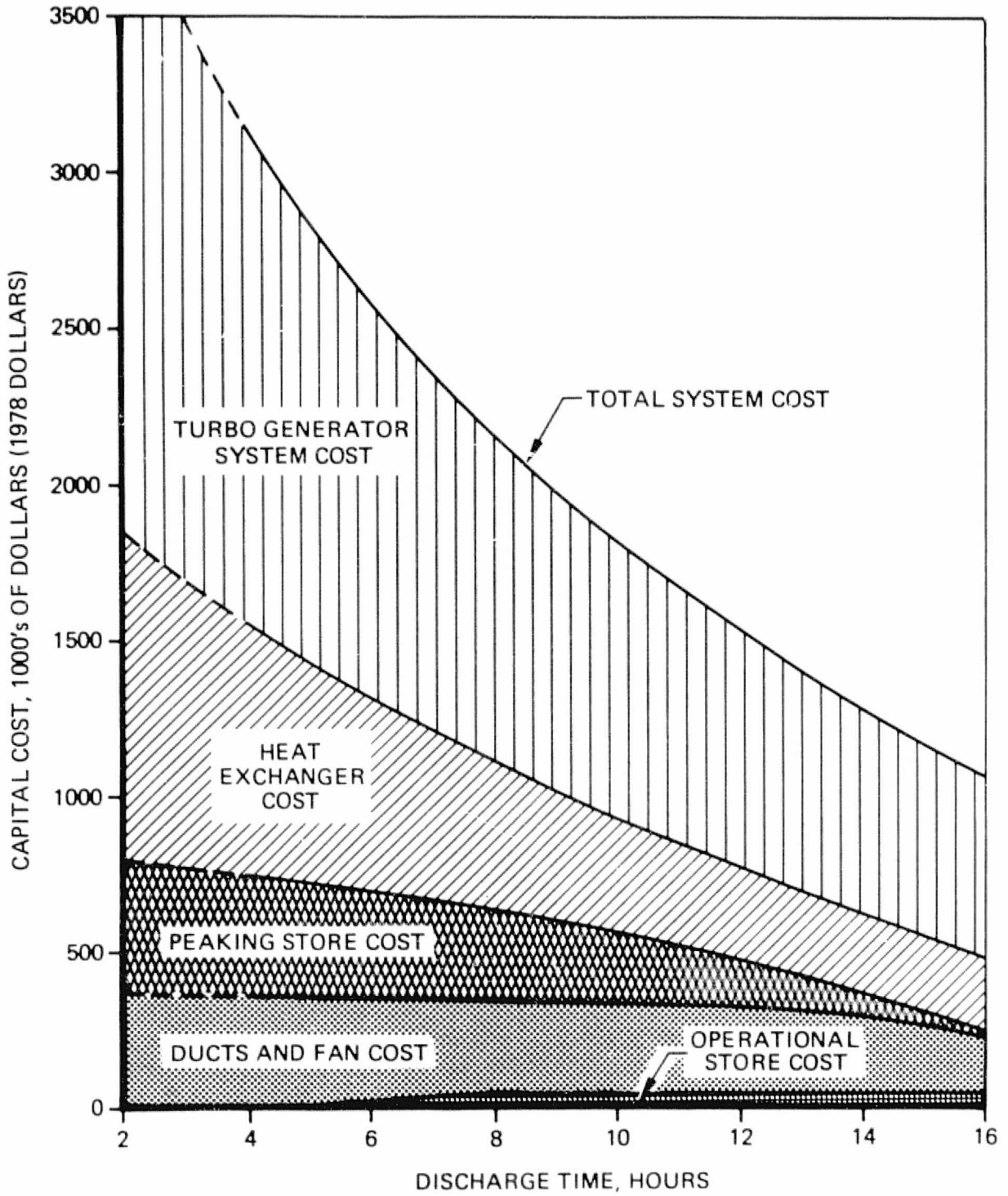
EFFECT OF DISCHARGE TIME AND STORAGE MATERIAL ON SYSTEM NET POWER OUTPUT



OPTIMIZED AND CORRECTED OVERALL SYSTEM CAPITAL COST VERSUS DISCHARGE TIME



COMPONENT CAPITAL COST COMPARISON FOR SCRAP IRON SYSTEM



ORIGINAL PAGE IS
OF POOR QUALITY

approximately half of the total cost. The heat exchanger is the next largest cost. The peaking store cost depends on the discharge time. The operational store cost is a small and constant item, as was discussed in paragraph 5.2.1. At some point of decreasing discharge time, the operational store will not be needed. For the 4-hour discharge time, in all cases, there was no operational store as the flow rate coming from the peaking store would dampen out the temperature fluctuations of the plant gas, since storage flow is three times greater. On the graph, the operational storage cost is shown to decrease between 4 and 8 hours.

5.6 ESTIMATED NATIONAL ENERGY SAVINGS

An estimate of the savings in fuel oil from nation-wide application of the techniques of this conservation system is found as the product of the estimated energy savings per ton of steel produced at the example site, and the estimated national production in 1985. It is assumed that the system displaces electric energy which would have otherwise been produced by gas turbine-driven peak power generating plants, using fuel with a heating value of 18,500 Btu per pound, having a specific gravity of 0.84, and operating at an overall thermal efficiency of 37 percent.

The net energy produced has been found to be a weak function of charge/discharge ratio, and nearly insensitive to the choice of storage material. Figure 18 shows these effects. Higher energy savings occur from the shorter discharge times as the larger turbogenerators required for these systems operate at higher thermal efficiency. Choosing an 8-hour discharge time as an example, an average power generation of 3.4 megawatts is predicted for the example site. (While this is not the most cost-effective choice for that site chosen for the cost effectiveness calculation of Section 6.0, it is perhaps more indicative of the average choice industry wide.) The 3.4 megawatts, generated for 8 hours, yields 27.2 megawatt hours displaced energy each day. The daily steel production at the site is 1,200 tons. The specific energy savings is, therefore, 0.0227 megawatt hours per ton.

Estimates of the total national production by process type to 1985 is shown in Figure 1. Electric steel production is estimated at from 44 to 51 million tons by 1985. The existence of water-cooled refractory technology (Reference 6) allows the potential to double steel production from existing electric arc facilities with very much less investment than building new ones. This effect makes the higher end of the range more probable than the lower. Assuming 50 million tons production in 1985 yields an estimated energy savings of 1.133 million megawatt hours.

Fuel with a specific gravity of 0.84 weighs 7.0 pounds per gallon, or 294 pounds per barrel, and has a heating value of 5.44×10^6 Btu per barrel. At 3.41 Btu per watt-hour, and an overall efficiency of 0.37, this fuel will produce 0.590 megawatt hours per barrel. Thus, 1.133 million megawatt hours displaces 1.9 million barrels of refined oil.

6.0 SYSTEM DESIGN AND COST

This section describes design conditions which must be met by the components of the energy conservation system. Several layout drawings are shown assuming installation at the Bethlehem plant in Seattle. An economic study is also presented herein using the costs as described in the preceding section (Section 5.0). An example of time-of-day pricing is shown which will affect the choice of a particular charge/discharge ratio.

6.1 PRELIMINARY DESIGN

The system described in this section is the 4:12 charge/discharge ratio configuration utilizing scrap iron as the peaking store and operational store material. Plant installation is assumed to be at Bethlehem Steel in Seattle. Figure 21 is an isometric of the present fume evacuation system. Figure 22 shows the 4:12 system installed with the condenser and turbopump (not shown) located outside of the building. The drawings show the system as it would be installed at the example site. The main body of equipment is located under the melt shop floor just south of the arc furnace foundations. To install most of the system at this location requires some excavation to allow more height to the area for the storage containers and ductwork.

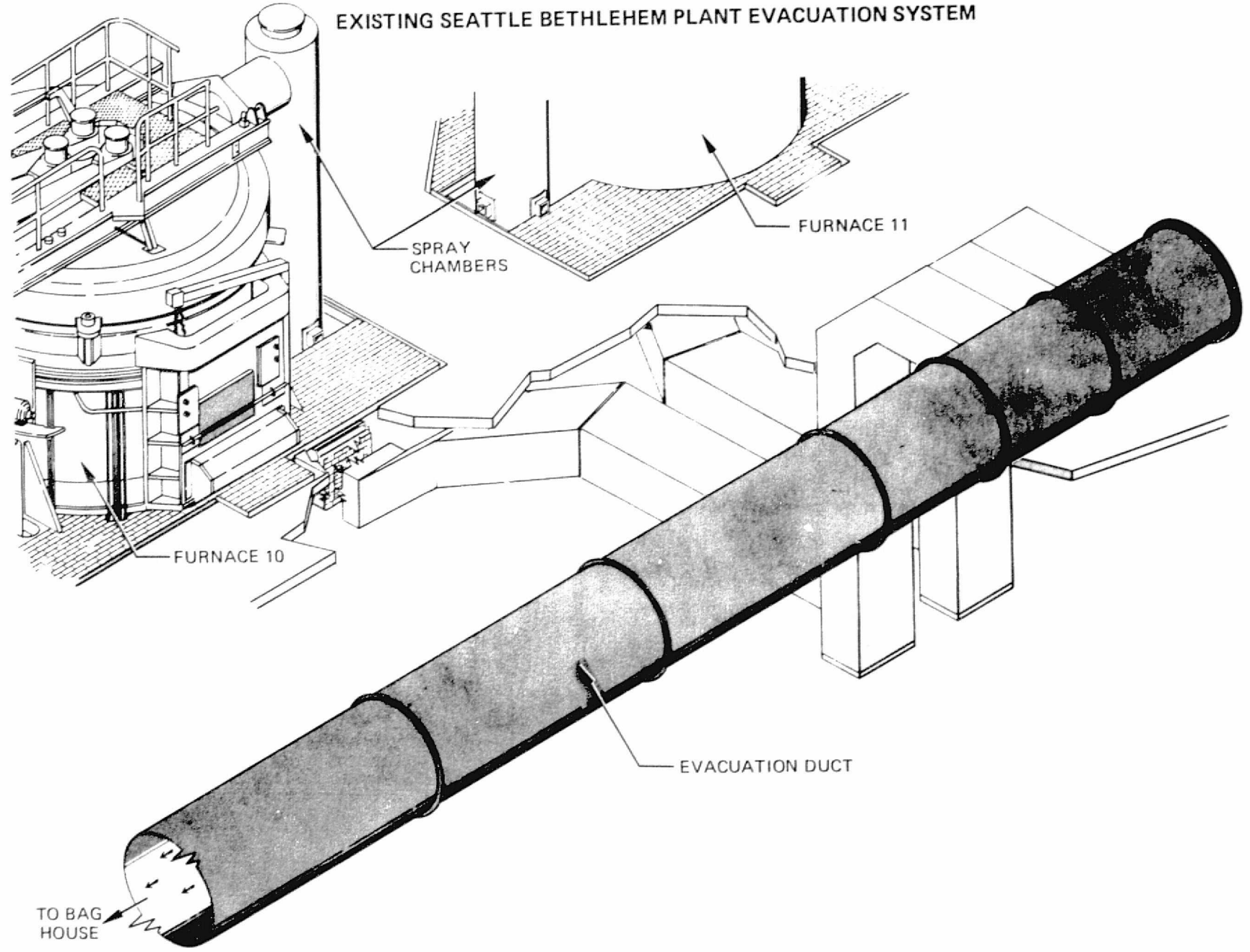
As can be seen in Figures 21 and 22, geometric changes will be made on the existing ductwork. The two ducts coming from the arc furnaces will "tee" together before entering the operational store (in background of drawing). All new ductwork will be constructed, interconnecting the pieces of equipment and entering the main duct outside of the building. The existing ductwork leading to the baghouse will not change, as high temperatures will not exist once the fume stream passes through the conservation system.

The existing ductwork leading up to the "tee" will either be modified to handle the high temperature stream or replaced. Modification may be a difficult task with these ducts as linings to insulate and protect the duct material may prove to be uneconomical to install. Replacement of the ductwork and the sliding fume elbow appears more favorable, as proper materials of construction can be selected to handle the high temperature.

The operational store functions at an amplitude ratio of 16.86% allowing a minimum input temperature of about 1,200°F (as described in Section 5.0). The peaking store, which is shown in the foreground, is slightly larger than the operational store, having dimensions of 19 feet in diameter by 22 feet high. The heat exchanger, which is the small "box" between the operational store and the turbogenerator, is 6 feet in width and about 5 feet long. The turbogenerator is shown in the left foreground. The condenser and turbopump are located approximately 100 feet to the west of this system.

29013-64A

EXISTING SEATTLE BETHLEHEM PLANT EVACUATION SYSTEM



S4

Figure 21

PROPOSED ENERGY RECOVERY SYSTEM INSTALLED IN BETHLEHEM SEATTLE PLANT

29013-63A

55

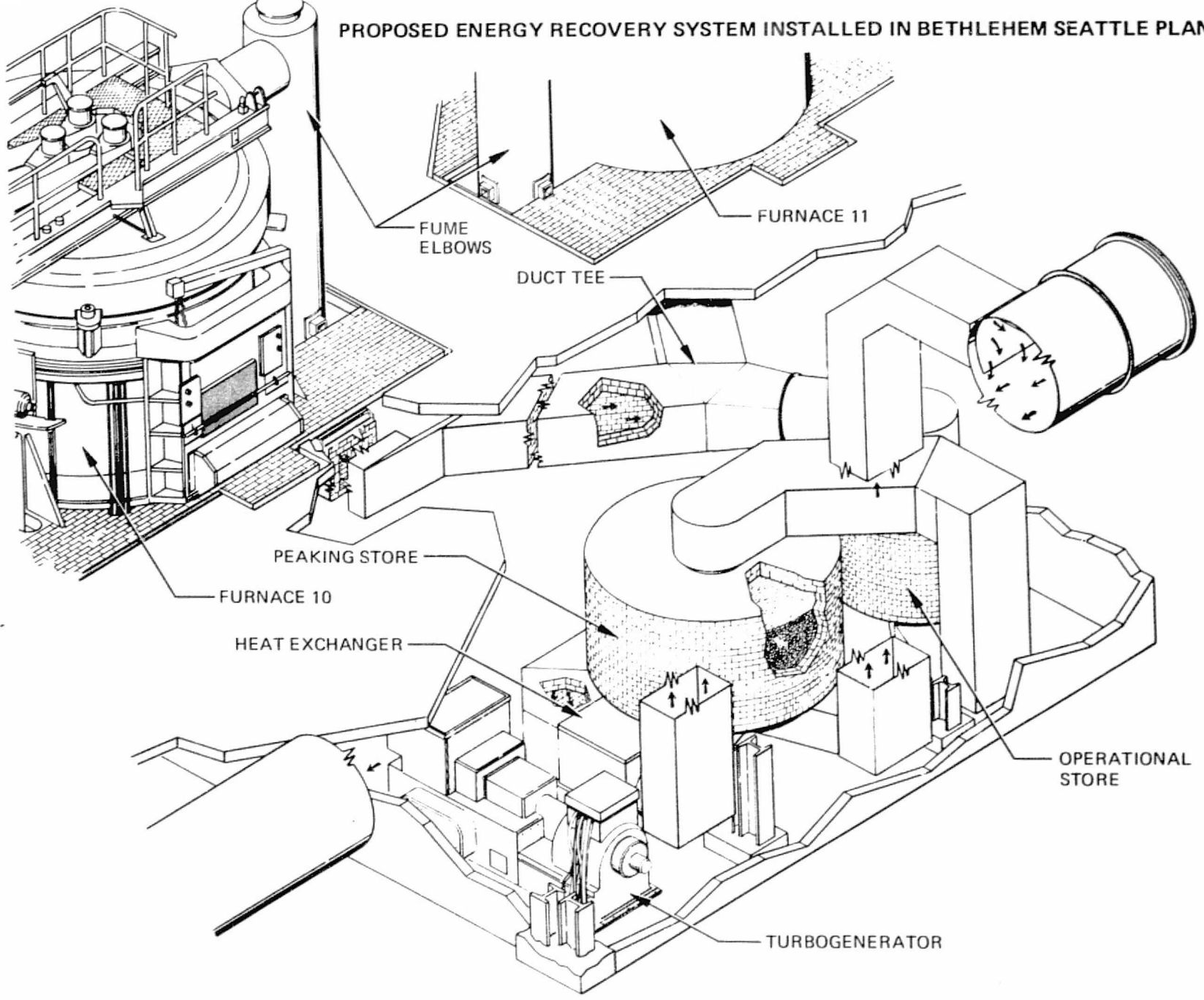


Figure 22

ORIGINAL PAGE IS
OF POOR QUALITY

The 4:12 system, as it would be installed at the Bethlehem plant in Seattle, would be built up without interfering with the existing operations. The main components of the system would be constructed and interconnected before tying into the existing fume disposal system. The new ductwork to be located between the arc furnaces and the operational store would be prefabricated. By this series of construction steps, the actual implementation of the system would require a minimum of shutdown time.

The 4:12 system cost will be 1.55 million dollars (1978 dollars) as predicted by the analysis method described in Section 5.0 and illustrated in Figures 19 and 20. The power output with parasitic correction will be 1.76 megawatts of electric power for a 12-hour period (see Figure 18). A savings of energy of 21.1 megawatt-hours per day is realized. The power produced can readily be used for operation of the existing overhead pollution equipment.

6.2 SYSTEM ECONOMICS

The economics of energy conservation systems depend strongly upon the cost of displaced energy. Energy cost depends upon a variety of factors but most strongly upon the geographic location of the plant. Other factors include the ongoing nationwide energy cost escalation and variations among utility rate-schedules (such as time-of-day pricing schemes). The economic analysis presented in this section is based on a projected cost of electrical energy to industrial users in 1985 of 77 mills/kw-hr. The escalation of energy cost is based on the data shown in Figure 23, where a rate of 15%/year has been realized for the period 1970 through 1978. The potential effects of time-of-day pricing are also evaluated. Figure 24 shows a time-of-day rate schedule which might be in effect for the Seattle Bethlehem Steel plant in 1985. Economic effects of rate variations in this type are discussed in subsequent sections.

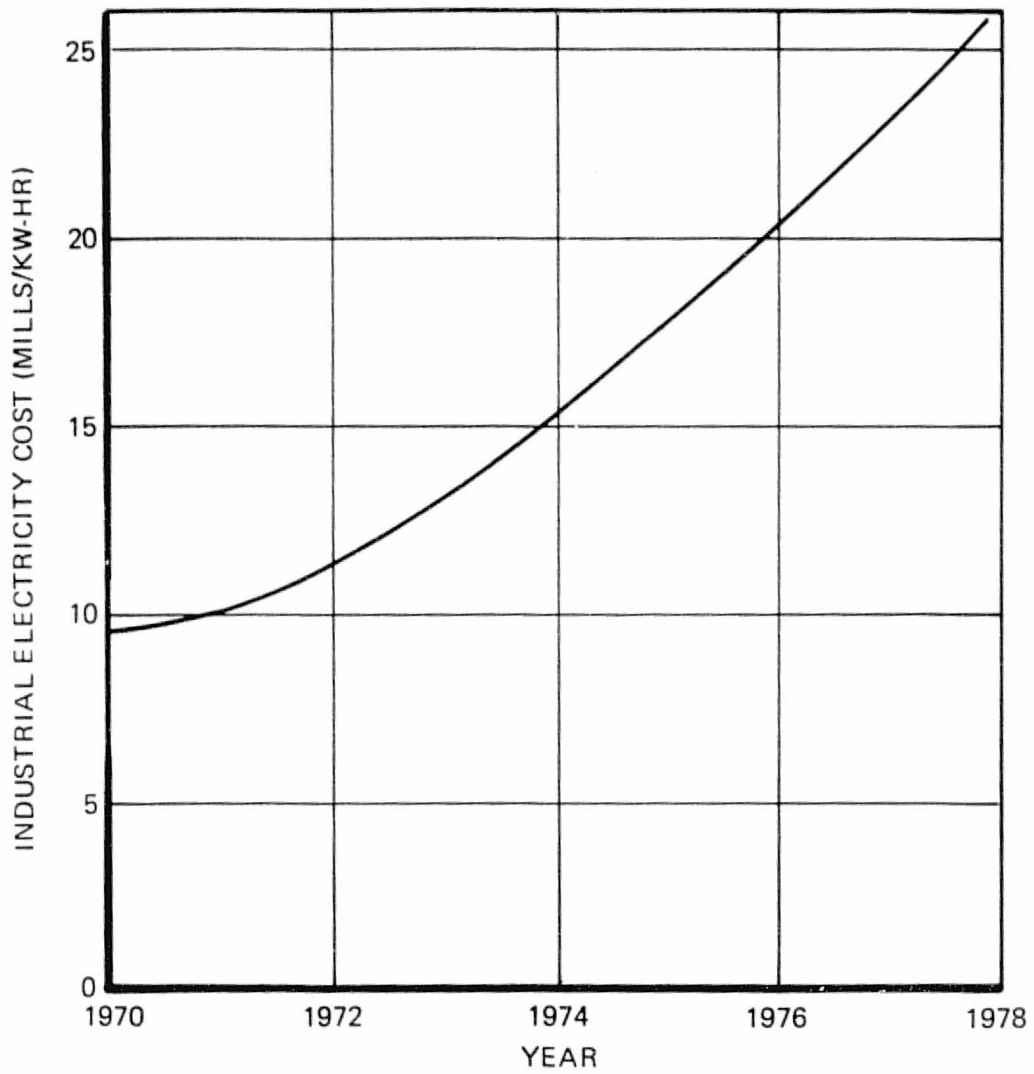
Also assumed is use of scrap iron for the peaking storage material which is intermediate in cost between the alternatives of slag or brick storage beds. Costs and power outputs derived include the effect corrections for optimum peaking storage bed lengths.

The operating cost of the system consists most entirely of the cost of electrical energy for powering the added fume-circulation fans. This cost is accounted for in the calculation of net energy saved. Other operating and maintenance costs are estimated to be small and negligible for purposes of comparing systems of differing θ_C/θ_D ratios. System startup and miscellaneous costs have been lumped into an estimated additional initial expenditure of 20% of the system capital cost (Reference 39).

The economic analysis results presented in the following sections have been derived based on pretax revenues because of the very wide variation in marginal income tax rates paid by industrial organizations.

Table 6 summarizes economics data used in the analysis of the example $\theta_C/\theta_D = 4/12$ case. The daily energy output (saving) and system capital costs are read from Figures 18 and 19 respectively.

COST OF ELECTRIC POWER TO INDUSTRIAL USERS



SCURCE: "ELECTRICAL WORLD" NOV. 15, 1977, pp 43

EXAMPLE OF TIME OF DAY PRICE SCHEDULE

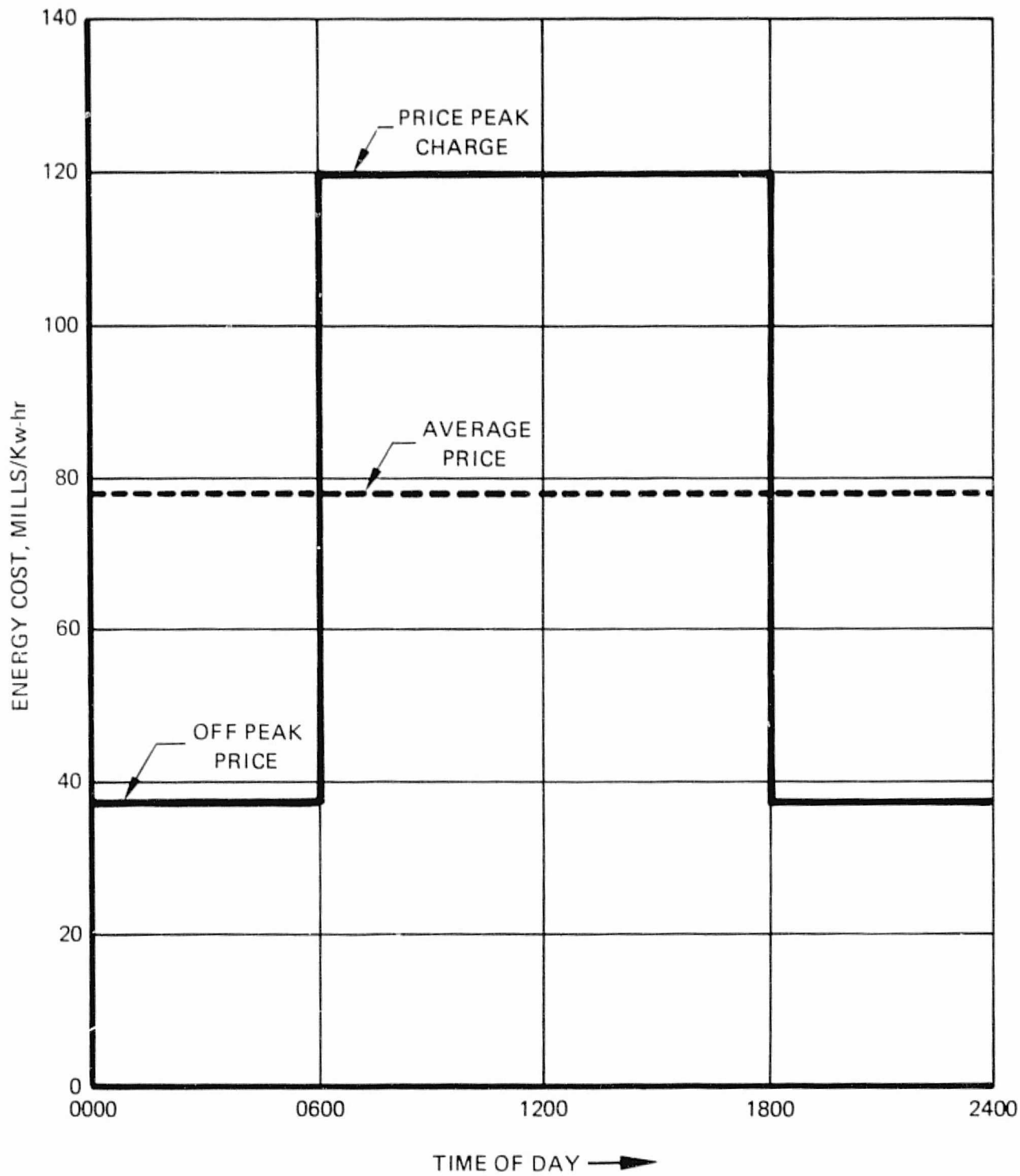


Table 6
ECONOMIC ANALYSIS EXAMPLE CASE

Charge/discharge ratio	$\theta_C/\theta_D = 4/12$
Starting year	1985
Energy escalation rate	15%/year
1970 energy cost (1970 \$)	9.5 mills/kW
Current capital cost (1978 \$)	\$1,550,000
1985 energy cost (1985 \$)	$(9.5)(1.15)^{15} = 77 \text{ mill/kW hr} = 77 \text{ $/MW hr}$
1985 capital cost (1985 \$)	$(\$1,550,000)(1.05)^7 = \$2,181,000$
1985 daily energy saving	$(1.82 \text{ MW})(12 \text{ hr/day}) = 21.8 \text{ MW/day}$
1985 annual energy saving	$(21.8 \text{ MW/day})(5/7 \text{ work days/day})$ $(365 \text{ days/yr}) = 5,680 \text{ MW hr/year}$
1985 annual revenue (1985 \$)	$(5,680 \text{ MW hr/year})(77 \text{ $/MW hr}) = \$438,000/\text{year}$
1985 startup cost (1985 \$)	20% of \$2,181,000 = \$436,000

The following sections show the application of several economic analysis techniques to the example case and discuss the results of application of these techniques to systems of various θ_C/θ_D ratios.

A net present value analysis was performed on each of four θ_C/θ_D cases for various economic plant lives. The results are summarized in Table 7 which shows that for very short economic lives, the lower θ_C/θ_D plants tend to pay back capital more quickly (because of their smaller capital investment); but for more realistic economic lives such as 10, 15, and 20 years, the greater energy output of the higher θ_C/θ_D ratio systems overcomes the initial capital cost disadvantage. At a 20-year life, the $\theta_C/\theta_D = 8/8$ system has the highest net present value. The 12/4 system is an exception to the above because it produces slightly less energy than the 8/8 system but has a higher capital cost.

Time-of-day pricing schedules will have an effect on the system tradeoff which will tend to be very site-specific. For a time-of-day schedule such as shown in Figure 24, the 4/12, 8/8, and 12/4 systems can all be operated to supply energy during periods of peak price, while some of the discharge of the 0/16 system will necessarily be during off-peak hours. Time-of-day schedules having shorter peak price times will tend to increase the relative value of the shorter discharge time (higher θ_C/θ_D ratio) systems because of their greater flexibility with respect to schedule variations.

Table 7
PRETAX NET PRESENT VALUE (\$1000) COMPARISON
FOR VARIOUS θ_C/θ_D AND ECONOMIC LIFE

<u>Plant Life (Years)</u>	<u>Charge/Discharge (θ_C/θ_D) Ratios</u>			
	<u>Continuous Discharge (0/16)</u>	<u>4/12</u>	<u>8/8</u>	<u>12/4</u>
	*(1,490)	(2,181)	(3,040)	(4,430)
	*(300)	(436)	(610)	(890)
5	414	-	-	-
10	3,166	3,022	3,276	1,374
15	6,604	6,932	8,080	5,017
20	10,897	11,817	14,079	11,816

*Plant investment and startup costs.

6.2.1 Net Present Value Analysis (NPV)

The NPV of a capital investment is obtained when the sum of the present values of all expenditures is subtracted from the sum of the present values of all incomes. The present value is obtained by discounting at a rate representative of the opportunity cost of capital. An assumption as to the life of the plant is needed to determine the overall NPV of the plant. The expenditures of the plant are the capital cost (1985) and additional costs such as contingent costs that occur. Table 8 illustrates the application of the NPV method to the example case which shows a net present value of \$6,932,000 assuming a 15-year economic plant life.

6.2.2 Internal Rate of Return (IROR) Analysis

The internal rate of return is defined as that discount rate which equates the present value of cash outflows with the present value of cash inflows over the expected economic life of the plant. Table 9 illustrates the application of the IROR analysis to the example case and shows a rate of return of 31.7% for a 15-year plant life.

An internal rate of return comparison is given in Table 10 for the four θ_C/θ_D cases for varying average energy prices. The calculation method and energy escalation rates are identical to those of Table 9. The energy savings and capital costs are as read from Figures 18 and 19 for the respective values of θ_C/θ_D .

For any given average energy price, the IROR is a strong function of the initial investment and is highest for the 0/16 system. As discussed in the preceding section, time-of-day

Table 8
PRE-TAX NET PRESENT VALUE ANALYSIS FOR BASELINE CASE

Year		Future Value of Revenue (\$1000)	1985 Value of Revenue (\$1000) (Discounted at 10%/Year)	Net Present Value (\$1000)
No.	Calendar			
0	1985*	(2,617)	(2,617)	(2,617)
1	1985*	504	458	(2,159)
2	1986	579	479	(1,680)
3	1987	666	500	(1,180)
4	1988	766	523	(657)
5	1989	881	547	(110)
6	1990	1,013	572	462**
7	1991	1,165	598	1,060
8	1992	1,340	625	1,685
9	1993	1,541	653	2,338
10	1994	1,772	683	3,021
11	1995	2,038	714	3,735
12	1996	2,343	747	4,482
13	1997	2,695	781	5,263
14	1998	3,099	816	6,079
15	1999	3,564	853	6,932

*Plant investment and startup costs incurred at start of 1985, revenues occur at year end.

**Value of original capital investment recovered in 5.2 years.

Table 9
PRETAX INTERNAL RATE OF RETURN ANALYSIS FOR BASELINE CASE

Year		Revenue \$1000 (15% Escalation)	Revenue \$1000 Discounted at IROR = 31.7%**	Net Present Value \$1000
No.	Calendar			
0	1985*	(2,617)	(2,617)	(2,617)
1	1985*	504	382	2,235
2	1986	579	334	1,901
3	1987	666	291	1,610
4	1988	766	254	1,355
5	1989	881	222	1,133
6	1990	1,013	194	940
7	1991	1,165	169	771
8	1992	1,340	148	623
9	1993	1,541	129	494
10	1994	1,772	113	381
11	1995	2,038	98	283
12	1996	2,343	86	197
13	1997	2,695	75	122
14	1998	3,099	65	57
15	1999	3,564	57	0

*Plant investment and startup costs incurred at start of 1985, revenues occur at year ends.

**The calculation procedure is iterative. A trial IROR is assumed, and the yearly revenues are discounted at the IROR to obtain their present values. If the net present value after all revenues expected during the plant economic life are accounted for is negative, a smaller trial IROR is chosen and the calculation is repeated. Similarly, if the final calculated NPV is >0, a larger trial IROR must be selected. The IROR which gives a final NPV ≈ 0, is the correct IROR. The sample case IROR of 31.7% is the result of this iterative process, and gives the required NPV of 0, as shown.

Table 10
**PRETAX IROR COMPARISON FOR VARIOUS θ_C/θ_D AND ENERGY COST
(FOR 15-YEAR PLANT ECONOMIC LIFE)**

1985 Energy Cost Mills/kW-hr	Charge/Discharge Ratios, θ_C/θ_D			
	0/16 (%)	4/12 (%)	8/8 (%)	12/4 (%)
50	26	23	21	14
70	36	30	27	19
77	38	32	29	21
100	46	38	35	26
120	53	44	40	30

pricing may strongly affect this trade-off. Any system which must discharge during an off-peak-price period will naturally lose some economic value, and the 0/16 system is most likely to suffer from these effects. Time-of-day pricing schedule effects will combine with local operating constraints to create a very site-specific tradeoff to determine the optimum system θ_C/θ_D .

6.2.3 Return on Investment (ROI) Analysis

An accounting method return on investment value is usually stated as an average rate of return defined by:

$$\text{Average rate of return} = \frac{\text{Average annual profit}}{\text{Average investment}}$$

A simplified form, known as the operating return, is defined as:

$$\text{Operating return} = \frac{\text{Gross operating profit}}{\text{Initial investment}}$$

These methods provide a simple approach to investment evaluation by ignoring the timing of cash flows and the time value of money.

The return on investment is calculated as "operating return" for the various θ_C/θ_D systems. For the example case, the ROI (operating return) is calculated from the data of Table 6 as:

$$\text{ROI (operating return)} = \frac{\$438,000}{\$2,181,000 + \$436,000} = 16.7\%$$

ROI measured as operating return is shown in Table 11 for the four θ_C/θ_D ratios, using the same method as for the baseline case with energy savings and capital costs being read from Figures 18 and 19. The comments of the preceding section regarding time-of-day price scheduling effects apply to the ROI results.

6.2.4 Payback Period Analysis

Another simplified method of capital investment analysis is payback period analysis which calculates the number of years from the time of plant startup to the point where the initial investment is recovered.

Table 12 illustrates this method for the example case, again using the basic data of Table 6. For the payback analysis as for the preceding ROI calculation, the 1985 energy cost is used without escalation, and pretax revenues are used without discounting. Table 12 shows that the payback period for the example case is 5.97 years.

Table 11
ROI ANALYSIS (AS OPERATION RETURN)
 (Percent)

Year	Charge/Discharge Ratio			
	0/16	4/12	8/8	12/4
1985	21.5	16.7	14.7	9.8

Table 12
ECONOMIC ANALYSIS BASELINE

	Year	Item	Costs (\$1000)	Revenue (\$1000)	Net of Costs and Revenues (\$1000)
0	1985	Installed plant	(2,181)		(2,181)
0	1985	Startup cost	(436)		(2,617)
1	1986			438	(2,179)
2	1987			438	(1,741)
3	1988			438	(1,303)
4	1989			438	(865)
5	1990			438	(427)
6	1991			438	11*
7	1992			438	449

*Payback period 5.97 years.

Table 13 summarizes the payback periods calculated for the different systems for varying average energy prices. As in the previous section, the payback analysis shows the 0/16 system to be favored if constant energy cost is assumed. Under time-of-day pricing schedules, systems with greater flexibility due to shorter discharge times will become relatively more favorable. As for the other indicators of economic value discussed previously, the payback period versus θ_C/θ_D ratio trade-off will be very site-specific.

Table 13
PAYBACK PERIOD ANALYSIS

PAYBACK PERIOD (YEARS) VS. ENERGY COST FOR VARIOUS θ_C/θ_D

1985 Energy Cost Mill/kW-hr	Charge/Discharge Ratio			
	0/16	4/12	8/8	12/4
50	7.2	9.2	10.4	15.7
70	5.1	6.6	7.5	11.3
77	4.6	6.0	6.8	10.2
100	3.6	4.6	5.2	7.9
120	3.0	3.8	4.4	6.6

7.0 SYSTEM ASSESSMENT AND PLAN FOR RECOVERABLE REJECT ENERGY

Under the contract work described herein, the conceptual design has been established for a reject energy recovery system for the Bethlehem Steel Plant in Seattle, Washington. Literature searches were conducted of reject heat availability within the steel industry in the United States, coupled with discussions with selected representative companies in the iron and steel industry. Results of the analysis of other iron and steel companies indicate that the recoverable reject heat from other United States plants is similar to that being analyzed at the Bethlehem Steel Plant, and that the economics of utilization of the reject heat should be as good or better than that of the Seattle Bethlehem plant.

Economic analysis of the reject heat recovery system within the Bethlehem Steel plant in Seattle, Washington, has shown a payback time of 5 to 6 years (Tables 8 and 12). Under normal economic conditions in the steel industry, a proposed investment which shows a payback of 5 years or less will receive serious consideration; thus, it would be expected that the proposed reject energy recovery system would be competitive for consideration for implementation. Current conditions, where capital rationing is severe, may tend to delay this implementation.

Historically, users of large quantities of electric power have purchased that power under a long-term contract from their suppliers at prices approaching baseload cost. The continued growth of demand for electricity, coupled with demonstrated lesser growth in capacity, will likely result in the price of contract power approaching that of retail power. Thus, by 1985, the economic risk situation will most likely be suitable for the start of wide-spread industrially financed implementation as long as the technical risk is low (i.e., the technology/feasibility has been demonstrated on a full-scale basis).

Based on resultant energy savings predicted for the Bethlehem Steel plant, the projected energy savings has been estimated on a national basis. Results of this analysis, discussed in detail in paragraph 5.6, indicate the national energy savings per year is equivalent to 1.9 million barrels of oil.

As a result of favorable economic payback and a significant energy savings, further development of the reject heat recovery system appears warranted. No fundamental problems/constraints have been identified which would prevent its implementation. There are two major areas for which feasibility must be demonstrated prior to widespread implementation of the utilization of reject heat from the iron and steel industry. These two areas are:

PRECEDING PAGE BLANK NOT FILLED

1. Resolution of potential technical problem areas associated with the utilization of reject heat from the iron and steel industry
2. Demonstration of the technical and economic aspects of utilization of reject heat by installation and demonstration of a full-scale system which can be utilized as a model for the rest of the industry.

The potential technical problems which RRC believes must be resolved prior to proceeding with demonstration efforts on the program are:

1. Development of techniques for removing dust from the fume gas stream and/or demonstrating the ability of the thermal storage bed to operate with the dust in the fume gas.
2. Development of design criteria for sizing of thermal beds utilizing conventional high-temperature storage materials (i.e., rocks, steel slag, scrap steel, brick, etc.).
3. Development of design criteria for predicting the transient behavior of thermal beds operating in the charge and discharge modes.
4. Effect of residual dust in fume stream on heat exchanger performance.
5. Electrical transient problems associated with bringing turbogenerator up to speed and tying in output into existing electrical grid.

The proposed program leading to full-scale implementation is divided into five phases, as shown in Figure 2.5. These five phases are:

- | | | |
|-----------|---|---|
| PHASE II | — | TECHNOLOGY DEVELOPMENT |
| PHASE III | — | PILOT PLANT DETAIL DESIGN |
| PHASE IV | — | FABRICATION, ASSEMBLY AND TEST OF PILOT PLANT |
| PHASE V | — | DETAIL DESIGN OF FULL-SCALE DEMONSTRATION SYSTEM |
| PHASE VI | — | FABRICATION, ASSEMBLY AND TEST OF FULL-SCALE DEMONSTRATION SYSTEM |

The following sections describe each of the above program phases in detail.

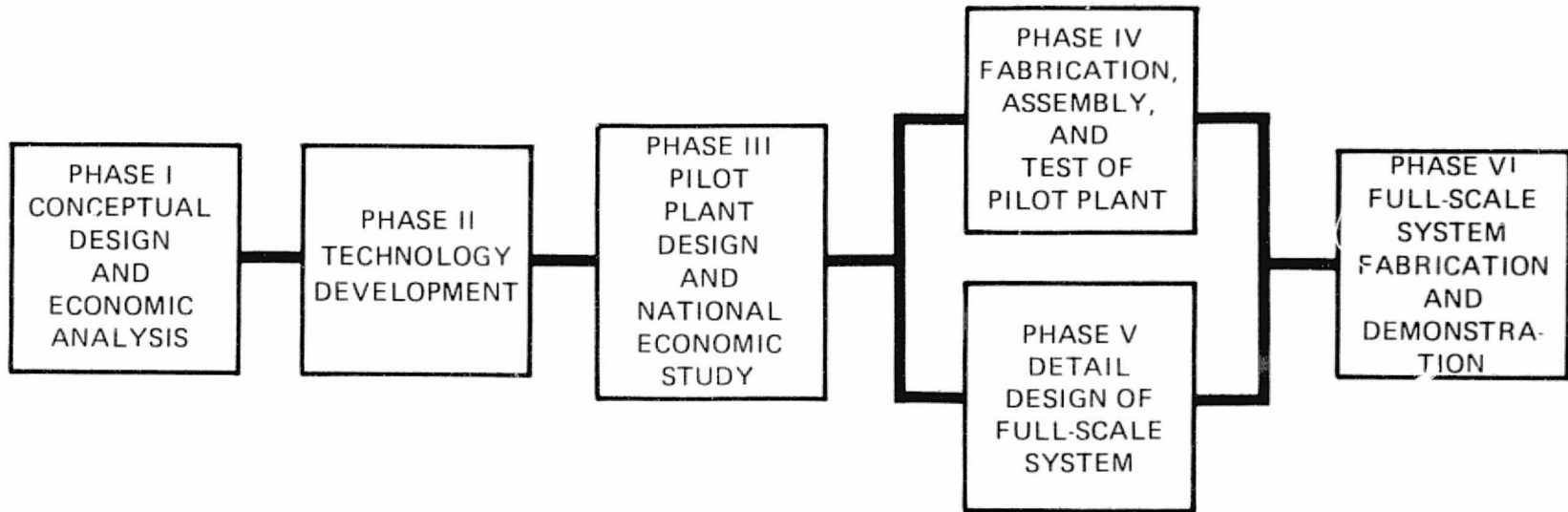
7.1 PHASE II — TECHNOLOGY DEVELOPMENT

The proposed technology development program in Phase II is broken into four tasks as follows:

- | | | |
|----------|---|---|
| Task I | — | Development of Thermal Storage Bed Design Criteria |
| Task II | — | Development of Techniques for Removing Dust from Fume Stream |
| Task III | — | Evaluation of the Effect of Dust in Fume Stream on Heat Exchanger and Storage Bed Performance |
| Task IV | — | Establishment of Optimum Design Criteria for Tying Generated Power into Steel Plant |

Each of these tasks are described in the ensuing sections.

IMPLEMENTATION PLAN FOR UTILIZATION OF REJECT HEAT
FROM IRON AND STEEL PROCESSING



69

V03064

Figure 25

7.1.1 Thermal Storage Bed Design Criteria

High temperature storage is a major element of the iron and steel reject energy utilization system. With such a storage device, the energy of heat streams may be stored during off-peak hours and then used to generate electric power during on-peak periods, thus avoiding the resistance of utilities to purchase of off-peak surplus power. Sensible heat storage in granular packed beds is clearly the most feasible technique in the near term for high temperature storage and has the least potential problem with environmental constraints.

The heat transfer and fluid flow phenomena in packed beds have been described by many authors since early studies circa 1928, directed generally at predicting the operation of blast furnaces and chemical reaction columns. Of prime importance are the assumptions which have been made in these analyses, which severely limit the confidence with which these past analyses can be applied to the design of the thermal storage bed. Assumptions which limit the applicability of the analyses include:

1. The thermal expansion of the fluid flowing through the packed bed is neglected, i.e., the fluid is assumed incompressible. This is a reasonable assumption for a liquid reaction column, and likewise, a low temperature energy storage device. For a device which handles gases over the 500°F to 1,750°F range, however, density variations by a factor of 2 will be experienced.
2. Thermal conductivity in the axial direction (flow direction) within the bed is neglected. This, again, is a reasonable assumption when the system under consideration composes a liquid flowing through a packed solid, as the energy transported by convection in the liquid will likely overshadow the conduction through the solid-to-solid contact points. If the flowing fluid is gaseous, the assumption is still perhaps not too bad, if the granules are small, as many such point contact resistances will be met in a unit length. For a gaseous medium flowing in a bed of larger solid masses, however, axial solid conduction may act to decrease the overall efficiency of the storage bed.
3. Temperature differences between the surface of the solid particles and the center (or bulk temperature) are neglected, i.e., particle conductivity is assumed infinite. This assumption, too, is reasonable for the small particles normally under investigation. If, however, other physical constraints require larger granule sizes, the finite conductivity of real material may further decrease the efficiency of the storage device. For instance, Reference 1 found it necessary to propose different correlation equations for his measured data, depending upon whether the bed was being heated or cooled by the gas stream. Commentators upon this paper presented good arguments that this was precisely what to expect from the finite size/finite conductivity of the bed materials. (Individuals up to 7.6 cm diameter, with a mean diameter of 4 cm for at least one test, other tests used still smaller fragments.)

4. Heat loss from the bed is usually neglected. This assumption can result in prediction of higher bed efficiencies than those which will result in actual application.
5. The granular bed is usually assumed to be composed of spherical or cylindrical particles or particles of a geometry which has been thoroughly studied. For the iron and steel industry, use of scrap iron or slag is being strongly considered, and the properties and shapes of these materials may vary markedly from past analysis assumptions.

The above simplifying assumptions are made in most analytical studies. Experimental investigations to date have been designed, generally, to check the analytical models. Thus, regular shapes (spheres, etc.) are used by all but Reference 1. In general, rather small spheres (~1/4-inch nonmetal to 1-1/2-inch metal) have been used which tends to mask the effect of material conductivity. Most experiments have been of laboratory scale (~18-inch diameter, 3-ft long), and only a few have operated at temperatures in excess of 1,000°F.

A gap thus exists in both analytical and experimental treatments to date, namely realistic scale studies of large, granular masses in the high-temperature region (approaching 1,500°F), using a gaseous medium as the flowing fluid.

During this task, a detailed analytical model will be developed for the thermal storage beds using conventional materials (hot rocks, steel slag, scrap steel, brick, etc.). This model will be constructed to eliminate simplifying assumptions made in prior models which limit their usefulness for high-temperature applications, and will treat both transient and steady-state operating conditions. Experimental studies will be conducted to verify the models, and a design manual will be published which gives equations and criteria for sizing of the thermal storage beds.

7.1.2 Task II – Development of Design Techniques for Removing Dust From Fume Stream

Since the advent of mandatory pollution controls, high temperature, particulate laden gas streams are commonly cooled to temperatures consistent with filter materials and cleansed of their dust in large filtering facilities commonly termed baghouses. The energy content of these streams pose problems to the plant operators as: 1) either massive volumes of ambient air must be entrained to dilute the gas down to reasonable temperatures, or 2) water must be sprayed into the stream to "quench" the gas temperature. In either case, a much greater volumetric capacity of the filters and fans is required. As shown in this report, the energy content of these gases can be recovered for electrical generation. The presence of dust and particulates, however, will force such designs to incorporate rather large granules in the thermal storage beds to avoid clogging problems and/or the dust must be removed from the gas stream prior to flowing through the bed. This problem has not been covered in any detail by theoretical and experimental work to date and must be resolved to permit reject energy recovery in the steel industry. During the Task II program, approaches will be evaluated for resolving the dust problem.

ORIGINAL PAGE IS
OF POOR QUALITY

7.1.3 Task III – Evaluation of Heat Exchanger Performance in Fume Stream

The dust in the fume stream poses the potential problem of particulate buildup in the heat exchanger and potential corrosion of the heat exchanger material due to gas/particulate products in the fume stream. Task III is aimed at evaluation of the severity of this problem and at establishing design solutions if a problem exists.

Task II of the program will quantify the dust which is in the fume stream or that which may remain after separation techniques are imposed. Task III will utilize this data to conduct additional studies.

7.1.4 Task IV – Establishment of Optimum Design Approach for Utilization of Generated Electricity

Depending upon the final selection of charge/discharge ratio for operation of the reject heat utilization system, the turbogenerator will produce several megawatts of electrical energy. Task IV will study the optimum approach for utilization of this energy and will consider direct use within the plant, or grid-feeding cogeneration-type applications.

7.2 PHASE III – PILOT PLANT DESIGN

In Phase III, detail design will be conducted of a pilot plant to prove feasibility of the system approach prior to proceeding to full-scale work. The goals of this phase are two-fold:

1. Complete a detailed design of a pilot plant system that will demonstrate the technical and economic aspects of the heat recovery and power generator subsystems.
2. Use pilot plant detailed design to update Phase I conceptual design and evaluate national economic impact.

To achieve these goals and provide adequate program control, the Phase III program is accomplished in five tasks.

7.2.1 Task I – Pilot Plant Requirements

During Task I, a complete study to establish the pilot plant design requirements will be conducted. The cyclic demand levels will be fixed and the interface requirements with the steel plant will be established.

An interface specification will be prepared to summarize the findings of the above study. Provisions for maintenance will be specified, based upon the steel plant operational constraints. Also during this task, the location of the store will be finalized, along with the turbogenerator and associated ducting. The storage system capacity will be specified during this task.

Task II – Component Design – After establishing the interface and performance requirements of the pilot plant system in Task I, the detailed design of the pilot plant system will be initiated. The three major components that comprise this system, the plant heat exchanger, store, and the turbogenerator, will be analyzed and designed in detail.

Plant Heat Exchanger Subsystem Design – Detailed design drawings of the pilot plant heat exchanger will be prepared. All necessary materials, manufacturing processes, and code requirements will be specified. A structural analysis will be conducted to ensure that the effects of induced vibration and thermal stresses will not alter system life expectancy.

Ducting – The ducting includes all piping, fittings, valves, fans, etc., necessary to connect the fume stream, plant heat exchanger, store, and turbogenerator. Utilizing the design requirements established in Task I, the system layout will be completed. Thermal/performance analysis will be conducted to determine duct and fan sizes for the network. Detailed working drawings of the ducting, fans, and valving will be prepared and a preliminary construction specification will be completed. This information will be used to prepare Phase IV system costs.

Storage System – Tradeoff studies will be conducted to finalize store size and material necessary to provide acceptable temperature fluctuations to the heat exchanger and to finalize the store size necessary. Detail analysis will be conducted of store heat losses and efficiency to assure proper sizing is conducted. During this task, the storage tank and components of the pilot plant will be designed in detail, and existing components will be utilized where appropriate.

Turbogenerator – Detail analysis will be conducted to define the turbogenerator requirements and a detail procurement specification will be written. A major goal will be to use an existing industrial turbogenerator.

Controls and Instrumentation – Several sets of controls are required in this system to maintain system optimization, reliability, and prevent operational problems. During this task of the total steel waste heat demonstration program, those controls necessary to assure proper pilot plant operation will be defined. Pilot plant instrumentation will be established based upon performance requirements. Since the prime purpose of a pilot plant is to determine if predicted performance is achieved, the design effort will specify type and location of instrumentation to assure adequate data recovery for system analysis.

7.2.3 Task III – Review of Full-Scale System Design and Economics

During this task, the Phase I conceptual design will be reviewed and changes incorporated based upon the detailed plant design. Changes to operational constraints will be made where appropriate. Cost modification to the system will be incorporated based upon current

state-of-the-art technology. It is the intent of this task to reanalyze the economic studies conducted during Phase I and determine if full-scale system economics remain favorable with projected displaced energy costs.

7.2.4 Task IV – National Economic Impact Analysis

Upon completion of the Task III cost update, a cost study will be conducted on utilizing this waste heat recovery/application system for the United States steel plants. Cost studies will be similar to the Phase I cost study effort. Systems will be sized by plant capacity and electrical energy rates and effect of peaking rate requirements. The information retrieved during the Phase I surveys will be used to conduct a system cost study for selected plants. Information to be determined during this phase includes the following for the various locations:

1. System capital cost per plant
2. Energy displaced per plant
3. Projected payback periods
4. Energy generation

7.2.5 Task V – Program Plan for Fabrication, Assembly, and Test of Pilot Plant

During this task, the program plan to construct and test the Phase IV pilot plant will be established. Detailed cost and schedule information will be prepared and the team members to implement this phase will be selected. A work statement will be prepared and submitted.

7.3 PHASE IV – FABRICATION, ASSEMBLY, AND TEST OF PILOT PLANT

During this phase, fabrication and testing of the pilot plant designed in Phase III will be implemented. It is anticipated that this phase will be divided into four tasks representing the major subsystems of the pilot plant.

7.3.1 Task I – Fabrication, Assembly, and Test of Plant Heat Exchanger

The heat exchanger designed in Phase III will be fabricated per design specifications. Performance testing will be conducted prior to installation. After achieving satisfactory operation and performance of the heat exchanger, the unit will be installed in the selected location.

7.3.2 Task II – Fabrication, Assembly, and Test of Storage Plant

In parallel to the Task I effort, the selected storage system will be fabricated and tested. The unit will be built at the designated location, and testing will be conducted with controlled input gas temperatures.

7.3.3 Task III – Fabrication, Assembly, and Installation of Ducting, Fans and Valving

In parallel to Task I and Task II, the required ducting, fans and valving will be fabricated and installed.

**ORIGINAL PAGE IS
OF POOR QUALITY**

7.3.4 Task IV -- Pilot Plant Operation

Final assembly of the pilot plant will be completed. Controls will be installed per pilot plant design requirements and system performance will be monitored. Test data will be reduced to verify predicted performance parameters for nominal and off-nominal conditions.

7.4 PHASE V -- FULL-SCALE SYSTEM DESIGN

Pilot plant operational data will be utilized to optimize the design of a full-scale demonstration system. The final product from this phase will be the detailed drawings and specifications of the full waste heat utilization system.

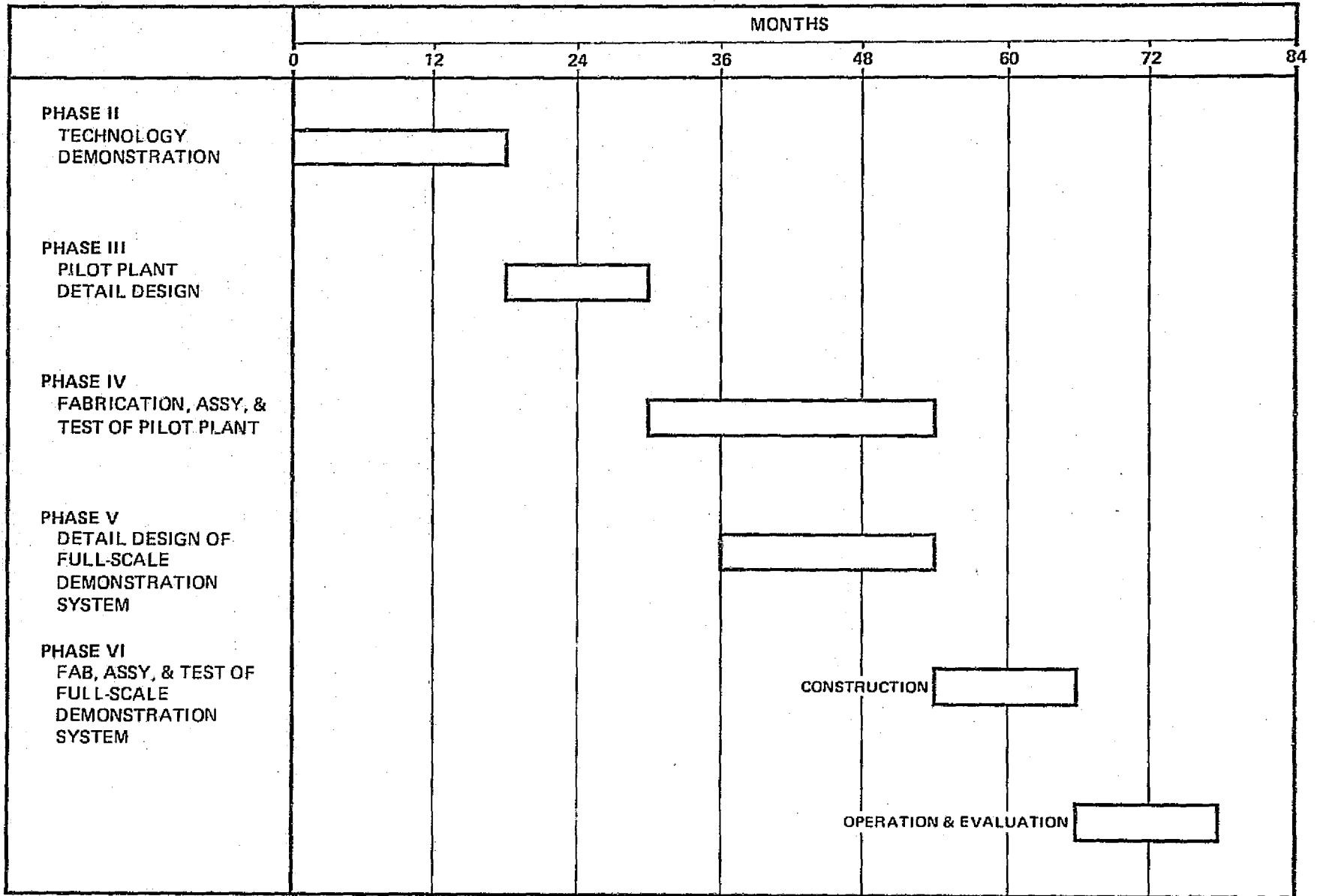
7.5 PHASE VI -- FABRICATION, ASSEMBLY, AND TEST OF DEMONSTRATION SYSTEM

This phase will entail construction of the demonstration system and performance monitoring. Data will be available to assess total system cost, component size/performance sensitivity on total system cost, and economic payback. Component design information will be of sufficient detail to implement system construction at other economically attractive locations.

7.6 OVERALL PROGRAM SCHEDULE

A summary schedule showing the estimated duration of each program phase is shown in Figure 26.

PROGRAM SCHEDULE



29016-54

76

Figure 26

8.0 SUMMARY AND CONCLUSIONS

A study has been performed to identify applications for near-term thermal energy storage technology applied to waste energy recovery in the iron and steel industry. A number of waste energy streams from this industry were considered. Those energy streams which could be more efficiently utilized without energy storage were eliminated from the final selection process even though the application of storage techniques might have shown reasonable efficiency. Based on the analysis of these energy streams, the primary fume gas collected from the electric arc steel remelting furnaces was selected as the optimum energy source for detailed study.

The study evolved a waste energy collection system design in which high temperature (approximately 1,300°F) energy is collected and stored in a bed of solid material as sensible energy. Upon demand, this energy is utilized to generate steam which drives a turbogenerator to produce electricity for peak power shaving. A preliminary design of this approach was studied in detail for the Bethlehem Steel plant in Seattle, Washington. Application of this approach to all electric arc furnaces in the United States yields a projected savings of 1.9×10^6 barrels of fuel oil per year, which could commence as early as the 1985 time period if an all-out implementation program were started immediately.

Detailed analyses were conducted on the economics of the aforementioned approach. The payback for the proposed application will be a strong function of the value of the energy displaced. This value currently varies by a factor of over ten (from 9 mills to 90 mills), depending upon customer size and geographic location. Time-of-day pricing is under strong consideration in many localities and already adopted by a few. This adds another variable to be considered in the economic analysis of the most cost-effective system. The implementation of time-of-day pricing will result in showing a strong economic benefit for the waste energy conservation system described herein. Due to the significant state of flux in the electric price structures in force nationally, the cost payback analysis (hence, all technical analyses as well) have been done parametrically against the duration of area peak price differential. This was done since this duration and price difference are the major considerations in the selection of an energy storage system for peak shaving as opposed to a continuously generating system for simple electric energy conservation. Traditionally, the steel industry considers a 5-year payback as a reasonable investment criterion. For the example site (Bethlehem Steel Company, Seattle plant), using retail electric price schedules postulated for the 1985 time frame, payback times of approximately 5 to 6 years are predicted.

Due to the favorable fossil fuel displacement predicted by this system and the results of economic studies which show favorable investment returns, further development of the system approach is recommended as described in Section 7.0. The first phase of this effort

would be technology-oriented work aimed at resolving design criteria necessary to accurately size the thermal storage beds and to utilize the system with the heavily dust-laden fume gas stream. Following successful definition of design solutions in these areas, a pilot plant demonstration of the system is recommended followed by a full-scale system demonstration. In this manner, work leading to the full-scale feasibility may be incrementally funded and technical assessments made at each phase to avoid a large initial investment prior to all technology being demonstrated.

Analysis indicates that the technology work and the demonstration programs can be accomplished to provide sufficient data to allow start of implementation on a national basis by 1985.

APPENDIX A GLOSSARY OF TERMS

A_{CHX}	free flow area of gas through heat exchanger, ft^2
A_{frc}	frontal area of condenser, ft^2
A_{frHX}	frontal area of the heat exchanger, ft^2
A_{OC}	shell side heat transfer area in condenser, ft^2
A_{OHX}	total shell side heat transfer area in heat exchanger, ft^2
A_{ox}	heat transfer area for section x of the heat exchanger, ft^2 $x = 1, 2, 3$
A_{TC}	inside cross-sectional area of one tube in condenser, ft^2
A_w	surface area of wall, general application, ft^2
a, b	constants used in the turbogenerator sizing equation which are functions of P_3 and T_3 derived from Reference 30 (mixed units)
a_1, b_1	constants used to determine Ψ from N_{RE} dependent on TS/D_o and derived from Reference 17, dimensionless
a_3	constant for axial direction heat transfer calculations in a packed bed, dimensionless
\bar{B}_i	vector representing the temperature profiles at time θ_i
C_a	thermal fluid capacity rate, gas side of a heat exchanger, $Btu/hr \text{ } ^\circ F$
C_h	fluid capacity rate of the hot fluid in a heat exchanger device, $Btu/hr \text{ } ^\circ F$
$C_{H_2O, x}$	thermal fluid capacity rate of steam in the heat exchanger for section x , $Btu/hr \text{ } ^\circ F$ $x = 1, 2, 3$
C_{max}	maximum fluid capacity rate of a heat exchanger device, $Btu/hr \text{ } ^\circ F$
C_{min}	minimum fluid capacity rate of a heat exchanger device, $Btu/hr \text{ } ^\circ F$
$C_{min c}$	minimum fluid capacity rate in condenser, $Btu/hr \text{ } ^\circ F$
$C_{min x}$	minimum fluid capacity rate of section x in the heat exchanger, $Btu/hr \text{ } ^\circ F$ $x = 1, 2, 3$
C_r	ratio of C_{min}/C_{max} , dimensionless
C_{pa}	specific heat at constant pressure
C_{pc}	specific heat of water (liquid), $Btu/lb \text{ } ^\circ F$
C_{pp}	specific heat of thermal storage bed material, $Btu/lb \text{ } ^\circ F$
C	specific heat of water side fluid in the heat exchanger for section x , $Btu/lb \text{ } ^\circ F$ $x = 1, 2, 3$

D_B	diameter of packed bed, ft
D_C	condenser diameter, ft
D_D	diameter of duct, ft
D_{ic}	inside diameter of condenser tubes, ft
$D_{i, HX}$	inside diameter of heat exchanger tubing, ft
D_{oc}	outside diameter of condenser tubes, ft
$D_{o, HX}$	outside diameter of heat exchanger tubing, ft
D_p	diameter of particle, ft
D_{LC}	log mean diameter difference for condenser tubes, ft
D_{LHX}	log mean of the inside and outside diameters of tubing used in the heat exchanger, ft
E	effectiveness of a heat exchanger device, used both for the condenser and heat exchanger, dimensionless
f	friction factor, general application, dimensionless
f_B	friction factor for packed bed, dimensionless
f_D	friction factor for ducts, general application, dimensionless
G	mass flow velocity, general application, lb/hr ft ²
G_{SH}	mass flow velocity of steam in section x of heat exchanger, (lb/ft ² hr)
G_x	mass velocity of gas in section x of heat exchanger, (lb/ft ² hr) x = 1, 2, 3
g_c	Newton's conversion factor, 417 x 10 ⁶ , (ft-lb/lbf - hr ²)
Height	Height of heat exchanger, ft
h_{ic}	internal heat transfer coefficient, Btu/hr ft ² °F
$h_{i, x}$	internal heat transfer coefficient in section x of the heat exchanger, (Btu/hr ft ² °F) x = 1, 2, 3
h_{oc}	external (shell side) heat transfer coefficient for condenser tubes (Btu/hr ft ² °F)
$h_{o, x}$	external (shell side) heat transfer coefficient for heat exchanger tubes of section x (Btu/hr ft ² °F). x = 1, 2, 3
hp	horsepower
H_{steam}	base enthalpy of steam at specific conditions, a generalized term used in determining ΔH_3 in the heat exchange calculation (H_{steam} is determined at constant pressure, P_2 , and at inlet condition, T_{03} , and exit condition, T_{32} , in section 3), (Btu/lb °F)
h_v	heat transfer coefficient based upon bed volume

ΔH_3	section 3 heat exchanger change of enthalpy for steam, Btu/lb
K_a	thermal conductivity of air (Btu/hr ft °F)
K_e	effective thermal conductivity of packed bed (Btu/hr ft °F)
K_e^o	static effective thermal conductivity of packed bed (Btu/hr ft °F)
K_m	thermal conductivity of tube material for the heat exchanger and the condenser (Btu/hr ft °F)
K_w	thermal conductivity of wall for storage devices (Btu/ft hr °F)
K_x	thermal conductivity of the water or steam stream in section x of the heat exchanger (Btu/ft hr °F) x = 1, 2, 3
K_1	thermal conductivity of individual layer in wall (Btu/ft hr °F)
K_2	thermal conductivity of individual layer in wall (Btu/ft hr °F)
L_B	length of storage bed, ft
L_C	condenser length, ft
L_D	equivalent length of duct section, general application, ft
L_x	length of section x in the heat exchanger, ft x = 1, 2, 3
MW_e	megawatts of electric power
m_a	flow rate of gas used for fan power calculations, lb/hr
m_c	cooling water flow rate in the condenser, lb/hr
m_{ct}	mass flow rate of cooling water through one tube, lb/hr
m_D	flow rate in an individual section of duct, lb/hr
m_{HX}	gas flow rate to heat exchanger, lb/hr
m_s	steam flow rate throughout system, lb/hr
m_{plant}	gas flow rate from plant source, lb/hr
m_{store}	gas flow rate from peaking store during discharging, lb/hr
N_c	number of tubes in condenser, dimensionless
N_{NU}	Nusselt number, dimensionless
N_{PE}	Peclet number, dimensionless
N_{PR}	Prandtl number, dimensionless
NP_x	number of steam-side passes in section x of heat exchanger, dimensionless x = 1, 2, 3

N_{RE}	Reynolds number, general application, dimensionless
$N_{RE, A}$	Reynolds number based on particle surface area, dimensionless
$N_{RE, P}$	Reynolds number based on particle diameter, dimensionless
$N_{RE, x}$	Reynolds number of water or steam in section x of the heat exchanger, dimensionless $x = 1, 2, 3$
N_{row}	number of tubes in one row of the heat exchanger, dimensionless
NTU	number of transfer units required in a heat exchanger device, dimensionless
NTU_c	number of transfer units in condenser, dimensionless
NTU_x	number of transfer units for section x of the heat exchanger, dimensionless $x = 1, 2, 3$
P_D	pressure of steam in condenser, 1.4 psia
P_{op}	operating pressure of system, psia
P_1	turbopump exit pressure, lb/ft ²
P_2	section 2 heat exchanger vaporization average pressure for steam, psia
P_3	section 3 heat exchanger exit average pressure (heat exchanger exit pressure and turbine inlet pressure) for steam, psia
ΔP	pressure drop, lb/ft ²
ΔP_B	pressure drop of packed bed, lb/ft ²
ΔP_D	pressure drop in a duct section, lb/ft ²
ΔP_F	pressure drop in a total section applying to one fan, lb/ft ²
ΔP_{sx}	pressure drop for steam side in section x of heat exchanger, lb/ft ² $x = 1, 2, 3$
ΔP_x	shell side pressure drop in section x of heat exchanger, lb/ft ² $x = 1, 2, 3$
q_w	heat loss through wall, general application, Btu/hr
$r_{h, o, HX}$	hydraulic radius shell side cross-sectional area per wetted perimeter in the heat exchanger, ft
r_{hs}	hydraulic radius for tube side of heat exchanger, ft
S_e	external particle surface area per unit volume of bed, st ⁻¹
T_B	temperature of gas in packed bed, °F
T_{air}	average gas temperature used for fan power calculations, °F

T_{BC}	bulk temperature of cooling water in the condenser, °F
T_D	temperature of steam in condenser, 115°F
$T_{in, c}$	inlet temperature of cold fluid to a heat exchanger device, °F
$T_{in, co}$	temperature of cooling water entering the condenser, °F
$T_{in, h}$	inlet temperature of hot fluid to a heat exchanger device, °F
$T_{out, co}$	temperature of cooling water exiting the condenser, °F
$T_{out, h}$	exit temperature of hot fluid from a heat exchanger device, °F
T_p	particle temperature within the packed bed, °F
T_s	condensing steam temperature, °F
TS_c	tube spacing in the condenser, ft
TS_{HX}	square pattern tube spacing distance for the heat exchanger, ft
T_w	wall temperature of tubes in condenser, °F
T_w	thickness of wall, ft
T_{03}	inlet temperature to section 3 of heat exchanger (inlet to heat exchanger), °F
T_2	section 2 heat exchanger vaporization temperature for steam, °F
T_3	section 3 heat exchanger exit temperature (heat exchanger exit temperature and turbine inlet temperature) for steam, °F
T_{10}	exit temperature from section 1 of heat exchanger (exit from heat exchanger), °F
T_{21}	temperature of gas between sections 1 and 2 of heat exchanger, °F
T_{32}	temperature of gas between sections 2 and 3 of heat exchanger, °F
$T\Delta$	temperature drop across wall, general application, °F
U_{oc}	overall heat transfer coefficient of condenser based on shell side, Btu/hr ft ² °F
U_{ox}	overall heat transfer coefficient based on the shell side of section x in the heat exchanger, Btu/hr ft ² °F x = 1, 2, 3
V_a	velocity of air, ft/hr
V_B	superficial bed velocity, ft/hr
V_C	fluid velocity of the cooling water in the condenser, ft/sec
V_D	velocity in the duct, ft/hr

V_{sc}	velocity of incoming steam to the condenser, ft/sec
V_x	velocity of water or steam in section x of the heat exchanger, ft/hr $x = 1, 2, 3$
VOL_c	volume of condenser, ft ³
v_1, v_2, v_m	specific volume of fluid, subscripts 1, 2, and m refer to inlet, exit, and mean conditions, ft ³ /lb
Width	width of heat exchanger, ft
X_{wc}	wall thickness of tubes in the condenser, ft
x_{WHx}	thickness of the tube wall in the heat exchanger
Z	axial distance in the packed bed, ft
$a_{o, HX}$	shell side heat transfer area per unit volume of the heat exchanger, ft ⁻¹
a_{oc}	shell side heat transfer area per volume of the condenser, ft ⁻¹
ϵ	void fraction in packed bed, dimensionless
Θ_c	charge time, hr
Θ_D	discharge time, hr
λ_c	heat of vaporization for steam in the condenser, Btu/lb
λ_1	section 2 heat exchanger heat of vaporization for steam, Btu/lb
μ_a	viscosity of gas, lb/ft-hr
μ_x	viscosity of the water or steam stream in section x of the heat exchanger, lb/ft-hr $x = 1, 2, 3$
ρ_a	density of gas at a particular point in the system, lb/ft ³
ρ_B	bulk density of storage bed material, lb/ft ³
ρ_x	density of the water or steam stream in section x of the heat exchanger, lb/ft ³ $x = 1, 2, 3$
ρ_w	density of liquid water, lb/ft ³
$\sigma_{1, HX}$	tube side free flow area per frontal area of heat exchanger, dimensionless
$\sigma_{o, HX}$	shell side free flow area per unit frontal area of heat exchanger, dimensionless
σ_{oc}	shell side free flow area per frontal area of heat exchanger, dimensionless
Ψ	group factor = $(N_{NU})(O_{PR})^{2/3}$
Ψ_x	group factor for gas in section x of heat exchanger, dimensionless $x = 1, 2, 3$

APPENDIX B SYSTEM DESIGN MODEL

Major elements of the energy conservation system shown in Figure B-1 are:

1. Heat exchanger
2. Peaking store
3. Operational store
4. Ductwork
5. Fans
6. Turbogenerator
7. Turbopump
8. Turbine condenser

With the exception of the two storage beds, these items are essentially steady-state devices. The system design model is written to describe steady-state relationships between the various elements of the system. Cost equations for each element as a function of important dimensions are developed from manufacturer's data and from Reference 38. In the latter case, costs are carried to installed costs by factors accounting for materials, labor, etc. Reference 38 also recommends an additional indirect cost factor to cover subcontractor administration, profit, etc. The indirect cost factor was not included, as in all likelihood the actual installation of the system would be performed by on-site maintenance crews.

Specific item costs are summed and net energy savings are calculated. Overall system economic parameters may then be calculated directly from the computer program outputs and assumptions concerning the value of energy saved in the future, the future cost of capital, and the inflation rate.

A generalized flow diagram of the design model is presented in Figure B-2. Table B-1 lists the major dependent and independent variables in the model.

The following paragraphs are devoted to the specific engineering and economic relationships incorporated in the model.

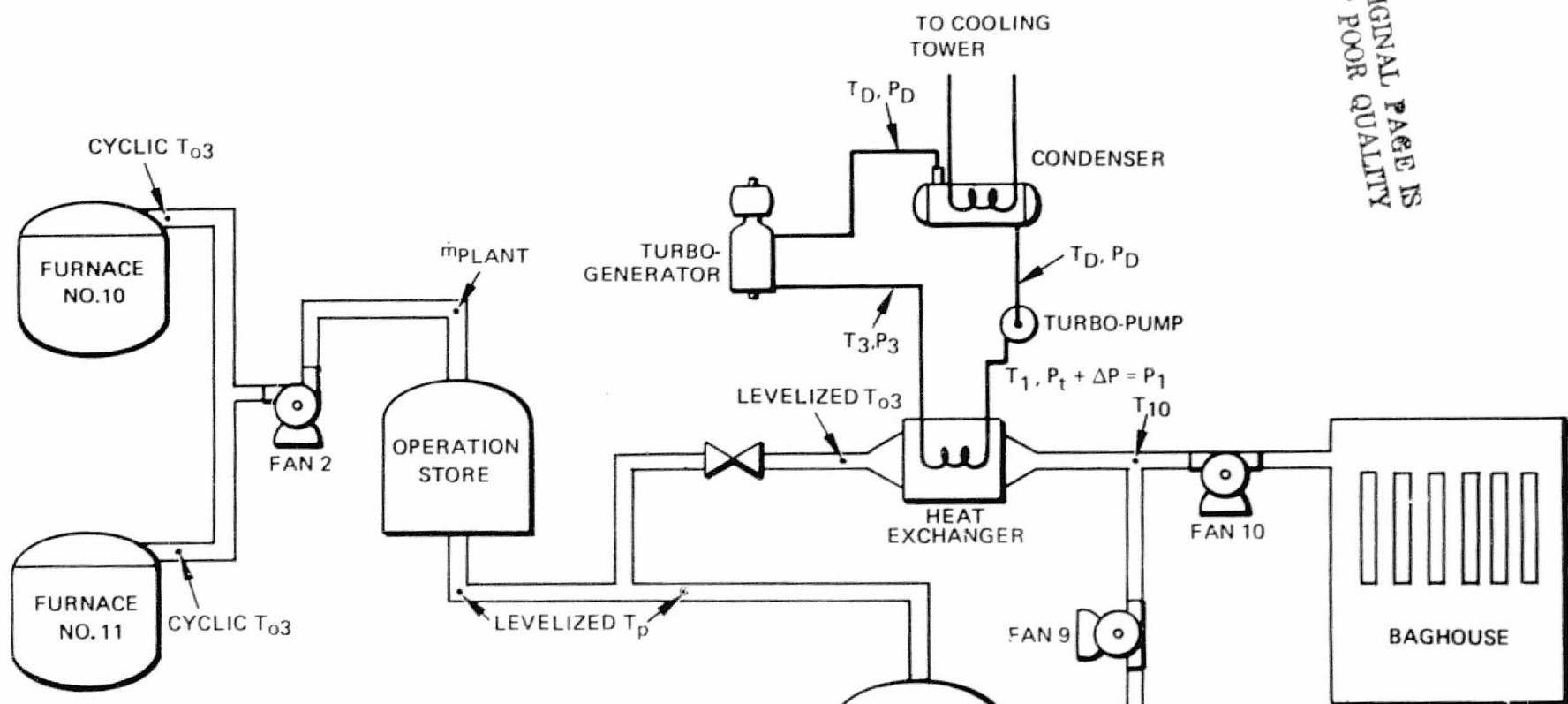
B.1 HEAT EXCHANGER

In the design model, the heat exchanger sizing is the most complex calculation performed. The method of calculation follows that of Reference 17. The major assumptions are as follows:

1. Three separate calculations performed – one each for liquid preheater, boiler section, and superheater, due to the fundamentally different heat transfer processes entailed.
2. Constant temperature and flow rate operation (inlet and outlet for each section).
3. Linear heat transfer coefficient with temperature through each section.
4. Heat losses to outside of exchanger are negligible.

STEEL ARC FURNACE ENERGY RECOVERY SYSTEM SCHEMATIC

ORIGINAL PAGE IS
OF POOR QUALITY



OPTIMIZING VARIABLES FOR SYSTEM		
VARIABLE	I.D.	VALUE
T₀₃	PLANT AVERAGE TEMP.	1100°F
T ₁₀	STORAGE DISCHARGE TEMP.	250 - 600°F
T ₃	TURBINE INPUT TEMP	500°F - 950°F
T _D	TURBINE DISCHARGE TEMP.	115°F
P ₃	TURBINE INPUT PRESSURE	815 psia
P _D	TURBINE EXHAUST PRESSURE	1.4 psia
ΔP	HEAT EXCHANGE ΔP	CALCULATED
m _{PLANT}	GAS FLOW RATE	137,000 lb/HR

29013-43A

86

Figure B-1

COMPUTER FLOW DIAGRAM

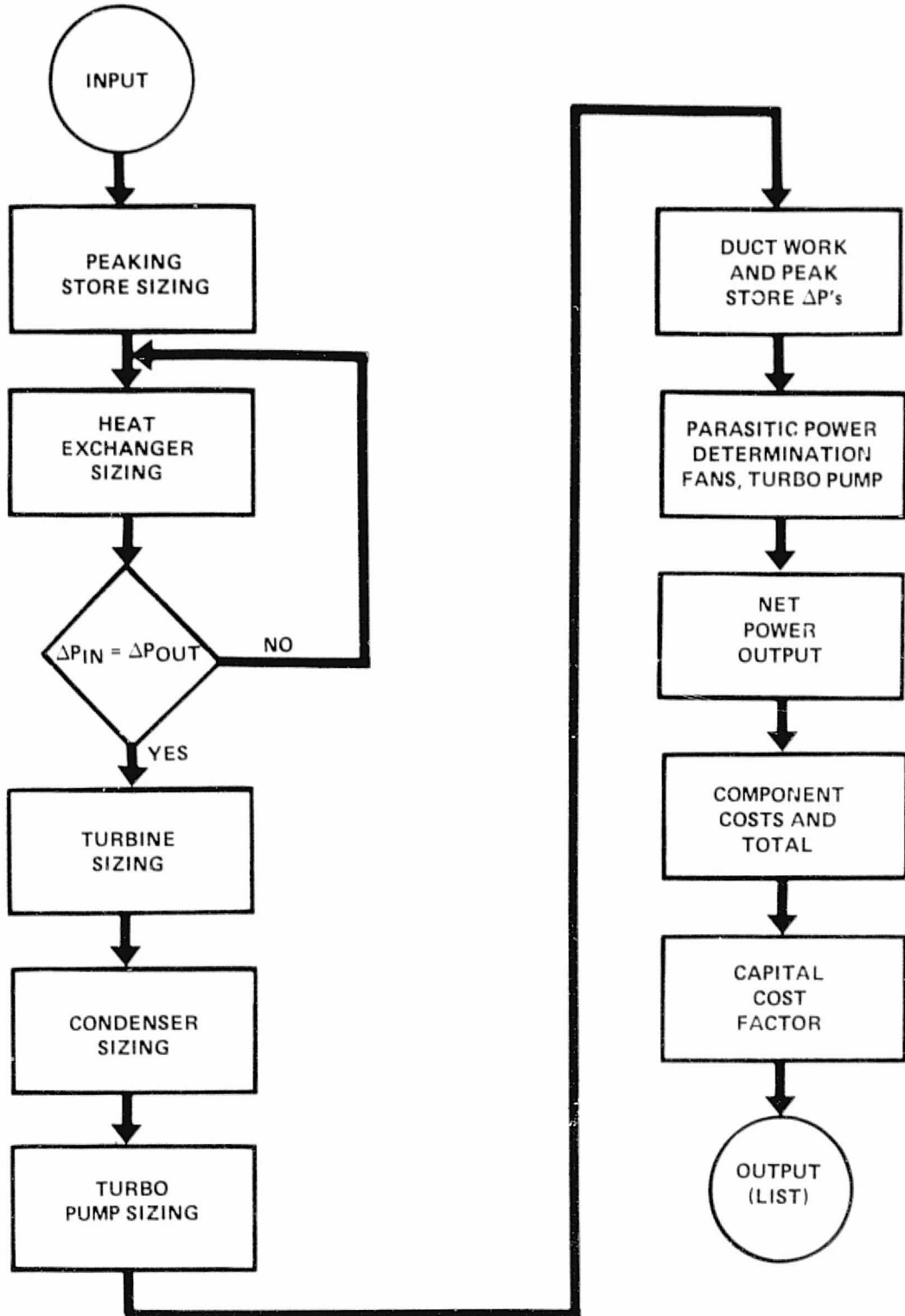


Table B-1

MAJOR INDEPENDENT VARIABLES IN MODEL

- GAS FLOW RATE
- GAS TEMPERATURE
- STORAGE DISCHARGE TEMPERATURE
- TURBINE INLET TEMPERATURE
- TURBINE INLET PRESSURE
- TURBINE DISCHARGE TEMPERATURE AND PRESSURE
- CHARGE/DISCHARGE RATIO
- STORAGE MATERIAL
- HEAT EXCHANGER GEOMETRY
- CONDENSER GEOMETRY
- LOCAL ELECTRIC RATE SCHEDULE

MAJOR DEPENDENT VARIABLES IN COMPUTER MODEL

- CAPITAL COST FACTOR
- HX AREA (SIZE)
- CAPITAL COST
- POWER OUTPUT
- STORAGE SIZE
- TURBINE SIZE

5. Countercurrent flow between water and gas.
6. For calculations, the gas is assumed to be air.

All three sections of the heat exchanger are sized in the same manner except that one section determines the cross-sectional dimensions. This section is the superheating section, and a velocity of gas must be input to start the sizing calculation for this section. The other two sections use the same cross-sectional dimensions as determined in the superheating section. Figure B-3 represents a typical temperature profile for the two fluids, and Figure B-4 illustrates the geometry for the entire heat exchanger.

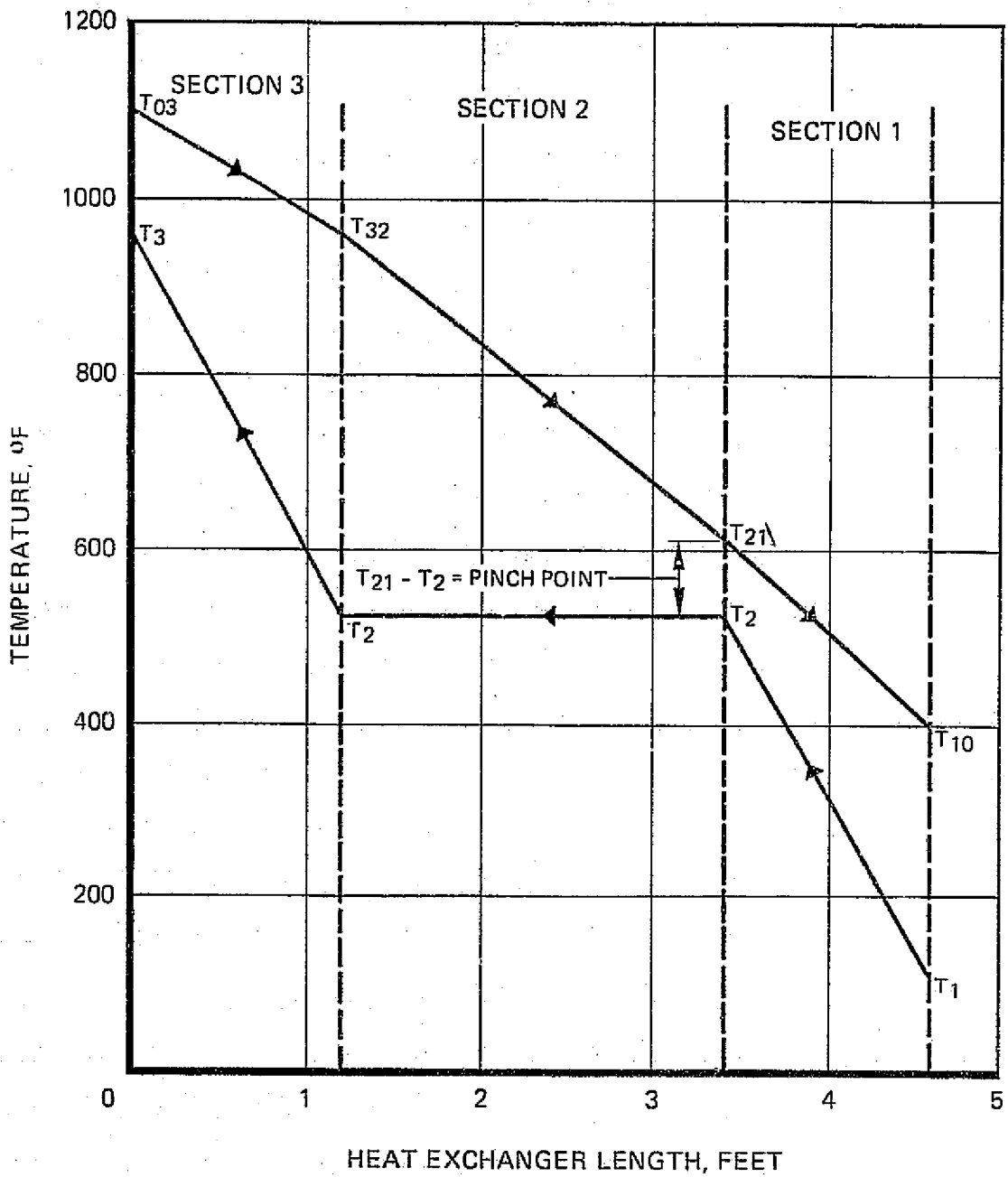
As Figure B-3 shows, the superheating section is numbered as section 3, and the liquid preheater and boiler sections are numbered 1 and 2. This diagram represents a waste heat recovery boiler. Figure B-3 shows a design condition often referred to as the pinch point. This occurs between sections 2 and 3 of the heat exchanger. It is important to note this condition, due to the calculating procedure for this piece of equipment. Since the steam (and water) flow rate is calculated from the mean temperature difference across Section 3, and then the lengths of Sections 2 and 1 calculated from the required total heat transfer, and the mean temperature differences, the analytical possibility exist for a negative temperature difference at the pinch point. If a negative pinch point is calculated, the program halts; and a message is printed that the exit temperature from the heat exchanger must be greater than a particular value to run the case. The pinch point then becomes an important optimizing parameter because it has the economic effect on how much heat can be removed from the gas stream and at what cost of the heat exchanger.

Figure B-4 represents the geometry of the heat exchanger. The assumption that the flows are countercurrent as opposed to cross-flow are justified due to the number of passes that the water side makes. From Reference 17, four passes closely approximate countercurrent flow. The heat exchanger in the simplified model has a pass for every row of tubes, thus exceeding four passes by a considerable multiple in all cases. The flow, then, is countercurrent.

The tube spacing selected reflects engineering design conditions. A square pattern with unfinned tubes has more design information as opposed to staggered, finned tube arrangements. Additional justification for the simple tube geometry is found upon consideration of the potential for eventual cleaning of the heat exchanger. In the heat exchanger model, tube spacing, tube outside diameter, and tube inside diameter can be changed to obtain a proper design of the heat exchanger without extrapolating heat transfer characteristics. Data fits almost any arrangement of the geometry in a simplified manner.

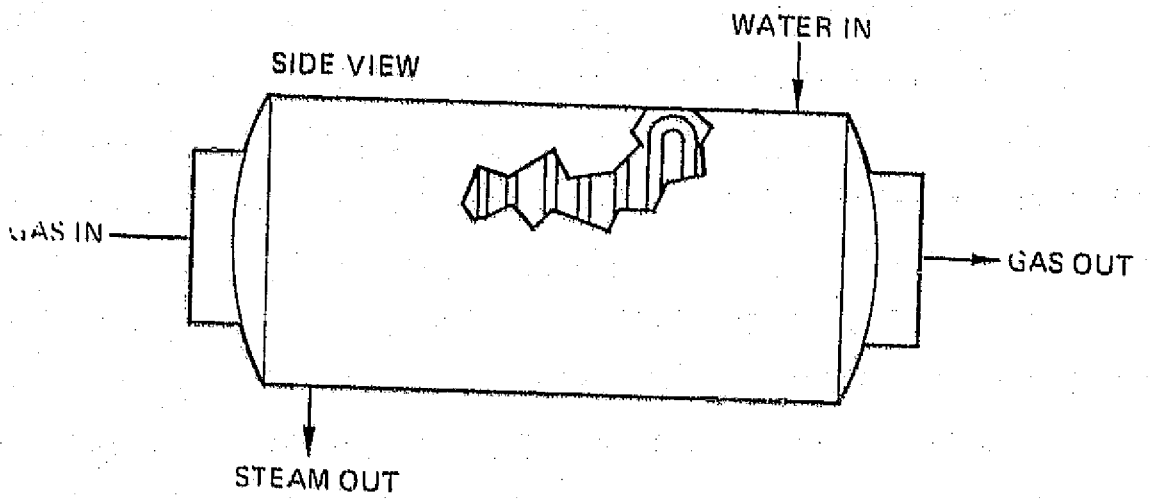
The geometry variables to determine are sigma ($\sigma_{O, HX}$), alpha ($\alpha_{O, HX}$), and the hydraulic radius ($r_{h, O, HX}$).

TEMPERATURE PROFILE IN HEAT EXCHANGER

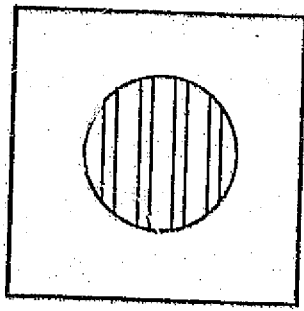


C-2

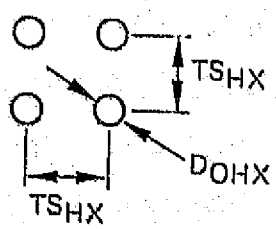
HEAT EXCHANGER GEOMETRY



END VIEW (SQUARE ENDED)



TUBE SPACING (SQUARE PATTERN)



ORIGINAL PAGE IS
OF POOR QUALITY

For each tube arrangement, there exists heat transfer and pressure drop data which depends on the ratio, T_{SHX}/D_0 , HX. The pressure drop relationship will be discussed in paragraph A.1.1. The heat transfer relationship will be discussed later in this section.

The calculation procedure discussed here applies to all three sections of the heat exchanger. The cross-sectional dimension calculation will also be shown. The nomenclature to be used in the heat exchanger calculations is shown in Figure B-5. The computer sequence will be followed (for one section) in the following sections.

An energy balance is performed on the heat exchanger to determine the section variables. An initial trial pressure drop of 5% is assumed to calculate P_2 for the water side:

$$P_2 = 1.05 P_3 \text{ (psia)}$$

P_2 is used to determine T_2 , λ_2 , and ΔH_3 values.

$$T_2 = 118.87 (P_2)^{0.22018}$$

$$\lambda_2 = 896.19 \text{ Exp } (-0.0003399 P_2)$$

$$Cp_3 = \frac{\Delta H_3}{(T_3 - T_2)}$$

where the enthalpy of steam is calculated from a steam table curvefit:

$$H_{\text{steam}} = [-431.59 \text{ Exp } (-0.001501 P_2)] T^{[0.19236 \text{ Exp } (0.000808 P_2)]}$$

For the steam flow rate:

$$\dot{m}_s = \frac{\dot{m}_{HX} C_{pa} (T_{03} - T_{10})}{[C_{p,1} (T_2 - T_1) + \lambda_2 + \Delta H_3]}$$

where:

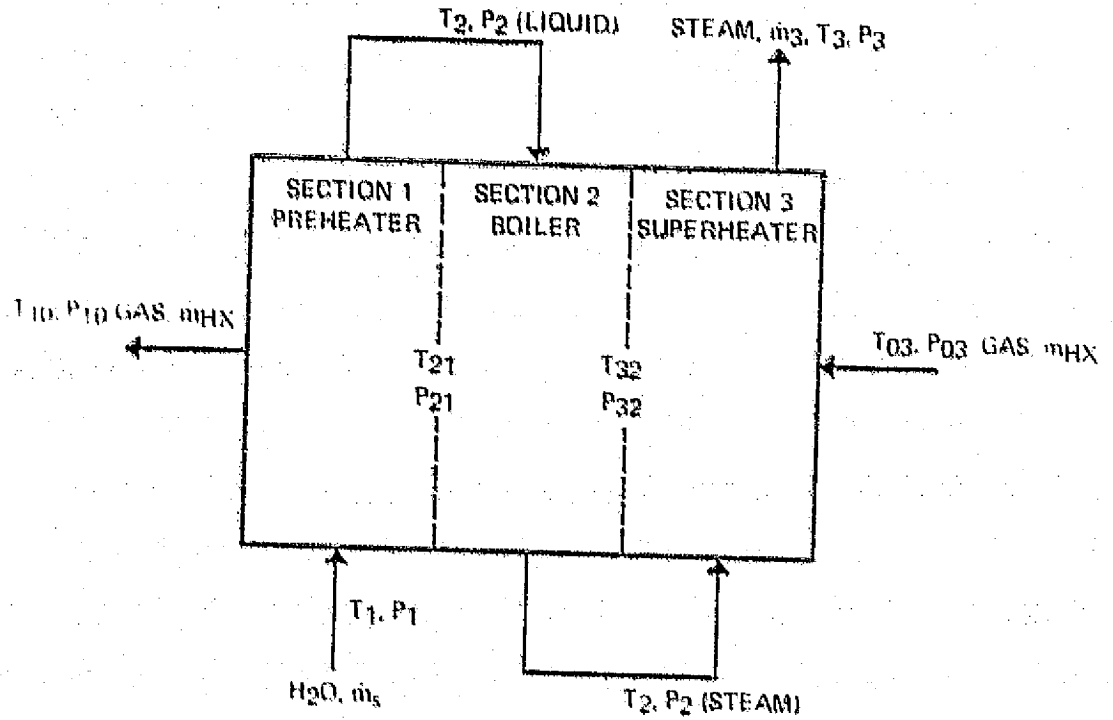
$$\dot{m}_{HX} = \dot{m}_{\text{plant}} + \dot{m}_{\text{stove}}$$

T_{32} and T_{21} for air are from an energy balance and the previously calculated variables.

$$T_{21} = \frac{\dot{m}_s C_{p,1} (T_2 - T_1)}{\dot{m}_{HX} C_{pa}}$$

$$T_{32} = \frac{\dot{m}_s \lambda_2}{\dot{m}_{HX} C_{pa}} + T_{21}$$

HEAT EXCHANGER SCHEMATIC



ORIGINAL PAGE IS
OF POOR QUALITY

The equations used in the overall energy balance relating the physical properties of water are accurate to $\pm 3\%$ through the operating range of the heat exchanger.

For each section, an NTU effectiveness method of heat transfer calculation is used. The following series of equations is used:

$$CH_2O, X = \dot{m}_s C_{p, X}$$

$$C_a = \dot{m}_{HX} C_{pa}$$

$$C_{min}/C_{max} = CR$$

$$\text{Effectiveness} = E = \frac{C_h (T_{in, h} - T_{out, h})}{C_{min} (T_{in, h} - T_{in, c})}$$

For counterflow heat exchangers:

$$NTU = \frac{\ln(1 - ECR) - \ln(1 - E)}{1 - CR}$$

For the physical properties of water, different relations exist for each section. The following general form applies to all three sections:

$$\text{Density} = \rho_X = f(P, T)$$

$$\text{Heat capacity} = C_{pX} = f(P, T)$$

$$\text{Viscosity} = \mu_X = f(P, T)$$

$$\text{Thermal conductivity} = K_X = f(P, T)$$

The Prandtl number is derived from the physical properties:

$$N_{PR} = \frac{C_p \mu}{K}$$

On the air side, density viscosity and thermal conductivity are calculated as functions of temperature only, as system pressure are close to ambient. Specific heat and Prandtl number are assumed constant at 0.25 Btu/lb \cdot °F and 0.70, respectively.

As was previously mentioned, a velocity of air is input to the third section of the heat exchanger to determine the cross-sectional dimensions:

$$\text{Mass velocity} = G = \rho(\text{velocity}) \text{ (G remains constant for all sections)}$$

$$\text{Width} = \text{height} = \sqrt{\frac{\dot{m}_{HX}}{G \sigma_o, HX}}$$

This assumes a square ended heat exchanger as shown in Figure B-4.

For the heat transfer characteristics of water, a general expression is used which was derived from Reference 17. The expression applies to tubes and is a function of NRE (Reynolds number) and NPR (Prandtl number):

$$\text{Number of tubes in a row} = N_{\text{row}} = \frac{\text{Width}}{T_{\text{HX}}}$$

(This calculation is only performed once in section 3 of the heat exchanger.)

$$V_x = \frac{4 \dot{m}_s}{\rho_x N_{\text{row}} \pi D_{i, \text{HX}}^2}$$

$$NRE_x = \frac{D_{i, \text{HX}} V_x \rho_x}{\mu_x}$$

$$NNU = f(NPR, NRE)$$

For the individual heat transfer coefficient on the water side in sections 1 and 3:

$$h_{i, x} = \frac{NNU_x K_x}{D_{i, \text{HX}}}$$

For section 2, $h_{i2} = 1,000 \text{ Btu/ft}^2\text{-hr-}^\circ\text{F}$ is assumed (this assumption is justified, since it does not have much effect on the overall coefficient).

The heat transfer characteristics of air are determined by the heat exchanger geometry. The constants used in the following equations are functions of the $T_{\text{HX}}/D_{o, \text{HX}}$ ratio:

$$\psi = (h/GC_p)(NPR)^{2/3} = a_1 NRE^{b_1}$$

The individual heat transfer coefficient is then:

$$h_{o, x} = \frac{\psi_x G_x C_{pa}}{NPR^{2/3}}$$

The overall heat transfer coefficient is of the standard form:

$$V_{ox} = \frac{1}{\frac{D_{o, \text{HX}}}{D_{i, \text{HX}} h_{ix}} + \frac{NWHX}{K_m} + \frac{D_{o, \text{MX}}}{DLHX} + \frac{1}{h_{ox}}}$$

where:

$$\bar{D}_{LHX} = \frac{D_{oHX} - D_{iHX}}{\ln(D_{oHX}/D_{iHX})}$$

$$x_{WHX} = \frac{D_{oHX} - D_{iHX}}{2}$$

and K_m = thermal conductivity of the tube material.

The heat transfer area and the exchanger length for the section are as follows:

$$A_{ox} = \frac{NTU_x C_{min x}}{U_{ox}}$$

$$L_x = \frac{A_{ox}}{a_{oHX} A_{frHX}}$$

When all three sections have been sized, the lengths and heat transfer areas are summed. Also done simultaneously is the pressure drop calculation for each section which will be discussed in paragraph B.1.1. A check is made to determine if the assumed pressure drop of water (of 5%) is close to the pressure drop calculated after finding the heat exchanger length. The difference must be less than 0.1% or the calculation is done again at the calculated pressure drop. For the air pressure drop, the difference must be large to change the overall heat exchanger dimensions (on the order of 10%). The water pressure drop controls the looping of the program due to the shift of the pinch point.

B.1.1 Heat Exchanger Pressure Drops – Water and Gas

The pressure drop through the heat exchanger is calculated after determining heat exchange dimensions from an assumed value of water pressure drop. For a water pressure drop, a friction factor (f) is calculated for each section of the exchanger. For a fluid inside of tubes:

$$f = 0.046 NRE^{-0.2} \text{ when } NRE > 2100$$

$$f = 16/NRE \text{ when } NRE < 2100$$

For each section of the heat exchanger, the ΔP is determined differently for the water side. For section 3:

$$\Delta P_{s3} = \frac{G_{s3}^2 V_1}{2 gc} \left[\left(1 + \sigma_{1, HX}^2 \right) \left(\frac{V_2}{V_1} - 1 \right) + f \frac{(\text{width})(NP_3) V_m}{V_{hs} V_1} \right]$$

ORIGINAL PAGE IS
OF POOR QUALITY

where:

$$NP_3 = \frac{L_3}{TSHX}$$

$$\sigma_{i, HX} = \frac{\pi D_{i, HX}^2}{4 TS^2_{HX}}$$

ORIGINAL PAGE IS
OF POOR QUALITY

$$\gamma_{hs} = \frac{D_{i, MX}}{4}$$

The section 2 pressure drop for the boiling water has been assumed to be the same as for section 3. This assumption yields a higher pressure drop value than what would actually occur in section 2.

The section 1 pressure drop is determined by:

$$\Delta P_{s1} = \frac{G_{s1}^2}{2 gc} v f \frac{(\text{width})(NP_1)}{\gamma_{hs}}$$

As can be seen, the pressure drop calculation must start with section 3 of the heat exchanger where the outlet pressure of water (steam) is an input.

The pressure drop for air is done for each section by the following equation:

$$\Delta P_x = \frac{G_x^2 V_1}{2 gc} \left[\left(1 + \sigma_{o, HX} \right) \left(\frac{V_2}{V_1} - 1 \right) + f \frac{A_{oX}}{ACHX} \frac{V_m}{V_1} \right]$$

The pressure drop of air is always small (less than 10%) and does not cause the heat exchanger calculation to loop for redetermination.

B.1.2 Heat Exchanger Cost

The heat exchanger cost is based on the overall heat transfer area for the gas side of the tubes. Reference 38 data was used to derive the following equation for 1970 base cost. This cost is for a floating head velocity type heat exchanger operating at 800 psig on the tube side. Shell pressure is low. The material is carbon steel.

$$1970 \$ = 405 (A_{oHX})^{0.67}$$

This cost is uninstalled. For installation, a multiplying factor of 1.86 is used. A higher factor is generally used to indicate piping hookups, but the cost of ductwork installation covers this factor.

An escalation index is entered into the program to bring up the cost to 1978 dollars. This factor is 1.6. The factor is based on an average 6% per year inflation rate.

B.2 PEAKING STORE SIZING

The peaking storage bed is sized in a simplified manner in the overall model. The diameter (D_B) is an input, and the length (L_B) is determined by one equation:

$$L_B = \left(\frac{\dot{m}_{\text{plant}}}{\rho_B} \right) \left(\frac{C_{pp}}{C_{pp}} \right) (\theta_C) \left(\frac{4}{\pi D_B^2} \right)$$

where:

- ρ_B = Bulk density of bed
- C_{pp} = Bulk heat capacity of bed
- θ_C = Charge time

The input of diameter has been specified equal to the length for the design model. This is a logical choice as a starting point, as the external surface area is kept near a minimum.

B.2.1 Peaking Store Pressure Drop

Pressure drops in the peaking store bed are calculated both for the charge and discharge modes in operating the system. In the charging mode, the plant gas flow rate is used in the discharge mode, the flow rate depends on the charge and discharge times. The discharging flow rate through the bed is determined from θ_C and θ_d :

$$\dot{m}_{\text{store}} = \left(\frac{\theta_C}{\theta_d} \right) \dot{m}_{\text{plant}}$$

The pressure drop is determined by the following sequence of equations:

$$V_D = \left(\frac{\dot{m}_D}{\rho_u} \right) \left(\frac{4}{\pi D_o^2} \right)$$

$$V_B = V_D \left(\frac{D_D^2}{D_B^2} \right)$$

$$NRE_p = \frac{(D_p)(\rho_u)(V_B)}{\mu_u (1 - E)}$$

$$f_B = \frac{150}{NRE_p} + 1.75$$

$$\Delta P_B = \left(\frac{f_B}{gc} \right) \left(\frac{2 L_B}{D_p} \right) \left(\frac{1 - \epsilon}{\epsilon^3} \right) \left(\frac{\rho_u V_B^2}{2} \right)$$

As can be seen by this series of equations, the void space in the bed has a considerable effect on ΔP . The particle diameter has a proportional effect.

B.2.2 Peaking Store Costs

The storage container in the design computer model is made of two layers of brick. One layer is an insulating layer of Kaolin insulating firebrick, and the other layer is a structural super-duty brick. Costs are derived from manufacturer's prices for large quantities of material for 1978 dollars. The installed cost of the container is based on the surface area of the container. The container cost is as follows:

$$1978 S = 23.474 \left(\pi D_B L_B + \frac{\pi}{2} D_B^2 \right)$$

This equation shows an installed cost of \$23.474 per square foot.

The cost of the installed storage material is fed in as an input of dollars per 100 pounds of material. From the volume of the bed and the bulk density, the material cost is calculated.

B.3 OPERATIONAL STORE SIZING

Sizing the operational store is fundamentally a transient analysis. As the design model is a steady-state model, it is assumed that the damping coefficient of the operational store is unity. Heat losses from the operational store are summed with those of the peaking store and approximated by a 200°F decrease in the mean source temperature. The pressure drop in the operational store is an identical calculation to that for the peaking store. The transient analysis of the storage beds is presented in Appendix C.

B.3.1 Operational Store Cost

The cost of the operational store follows the method of the peaking store presented in paragraph A.2.2.

B.4 TURBOGENERATOR AND ASSOCIATED EQUIPMENT

The turbine, generator, pump, and condenser form the major elements of the power generation system. The turbine and generator form a single item.

B.4.1 Turbogenerator Sizing

Once the steam flow rate has been determined from the energy balance in the heat exchanger (and the pinch point temperature checked), the power output of the turbine can be calculated. It is assumed that the discharge pressure is 3.0" Hg absolute.

Data obtained from Reference 30 was put into equation form to yield the following for electric power output in megawatts, MW_e :

$$MW_e = \left(\frac{\dot{m}_s}{1000a} \right)^{\frac{1}{1+b}}$$

The constant used (a and b) are derived from the inputs of temperature and pressure for the steam turbine. The constants are derived from Reference 30 data and when incorporated into the overall equation, can result in a negligible error of $\pm 2\%$. Conversion of megawatts to megawatt hours is accomplished by multiplying by the discharge time.

B.4.2 Turbogenerator Cost

The major variable influencing the cost of a turbogenerator is the design steam flow rate. Secondary effects of temperature and pressure exist but act more as limits; that is, the influence is very slight to a given value, then nearly prohibitive thereafter.

The equation for turbine cost was developed from tabular data received from Reference 30.

$$1978 \text{ turbogenerator cost} = 734 (\dot{m}_s)^{0.65}$$

The equation fits the tabular data to within $\pm 1\%$ over the turbine size range of interest.

Tabular data covered an inlet pressure range from 265 psia through 815 psia for "off-the-shelf" units. Higher inlet pressures would require special manufacture at considerably higher cost and were eliminated from further consideration.

Tabular data covered a range of inlet temperature from 500 through 750°F. Extrapolation of the data to 950°F is expected to decrease the equation accuracy to $\pm 6\%$; however, turbine design inlet temperatures in excess of 950°F will require exotic blade materials and a significant cost increase (Reference 30).

The factors recommended by References 30 and 38 to cover turbogenerator installation costs are at considerable variance. A value intermediate to the two recommendations, at 1.257, was the multiplier used.

B.4.3 Turbopump Sizing

Calculations involving the turbopump are as follows:

$$hp = \frac{\dot{m}_s P_1}{550 \rho_w}$$

With an efficiency of 60% and converting to megawatt hours for a parasitic power determination:

$$MW\text{-hrs} = \frac{hp}{0.60} \times 7.457 \times 10^{-4} \times \theta_D$$

The turbopump parasitic power is subtracted from the turbogenerator output along with the fan power usage to determine the overall power output of the system.

B.4.3.1 Turbopump Cost

The turbopump cost is derived from Reference 38. Costs are based on volumetric flow rate and developed head. The following expression is used for installed 1978 dollars:

$$\text{Installed 1978 Dollars} = 69.72 (\text{gpm} \times \text{psi})^{.453}$$

In this expression, an installation factor of 2.1 is used along with a 1.6 escalation index. The installed cost does not cover associated piping as the more costly condenser installation factor includes this factor.

B.4.4 Condenser Sizing

The condenser sizing calculation uses the same relationships as that of the main heat exchanger. A single heat transfer mechanism is in effect so that multiple section calculations are unnecessary, and the complexity associated with internal pinch points is avoided. The following calculation assumes that all the steam coming from the turbogenerator is saturated at 115°F, and the cooling water is entering at 60°F. The condenser geometry is based on a hexagonal pattern where only tube spacing, tube OD, and tube ID are needed as inputs to define the geometry. The geometry calculations for α_{oc} , σ_{oc} , and γ_{hoc} are as follows for the steam side:

$$\sigma_{oc} = \text{free flow area/frontal area} = 1 - 0.9069 \left(\frac{D_{oc}}{TS_c} \right)^2$$

$$\alpha_{oc} = \text{heat transfer area/volume} = 3.6276 \frac{D_{oc}}{(TS_c)^2}$$

$$\gamma_{hoc} = \text{hydraulic radius} = \frac{\sigma_{o,c}}{\alpha_{o,c}}$$

Flow in the condenser is true countercurrent flow along the tubes for the calculation. The NTU effectiveness method is used for the calculation of the overall condenser dimensions. The following series is followed in the computer model:

Flow rate of cooling water, \dot{m}_c :

$$\dot{m}_c = \frac{\lambda_c \dot{m}_s}{C_{ps} (T_{out, co} - T_{in, co})}$$

The ratio of $C_{min}/C_{max} = 0$, since there is a phase change. The effectiveness, E, and NTU values are found by:

$$E = \frac{T_{out, c} - T_{in, c}}{T_{in, h} - T_{in, c}}$$

$$NTU = \ln(1 - E)$$

The individual heat transfer coefficients are determined by relations given in Reference 12. The relations are:

$$h_{oc} = \frac{1225 + 3.15 (T_s + T_w)}{\sqrt{D_{oc}} (T_s + T_w)}$$

$$h_{ic} = 163 V_c^{0.85} (1 + 0.0104 TBC)$$

where $NRE > 3000$ for h_i .

The wall temperature is assumed to be the bulk temperature of the cooling water. The velocity for the cooling fluid is input so that the Reynolds number, NRE , is always greater than 3,000 (a velocity equal to 2 ft/sec gives a NRE about equal to 10,000).

The overall coefficient for the condenser is determined by a standard form equation of the type:

$$V_{oc} = \frac{1}{\frac{D_{oc}}{D_{ic} h_{ic}} + \frac{N_{wc}}{K_m} \frac{D_{oc}}{D_{ic}} + \frac{1}{h_{oc}}}$$

The steam side heat transfer area can then be determined by the following expression:

$$A_{oc} = \frac{(NTU_c) C_{min,c}}{V_{oc}}$$

where:

$$C_{min} = C_{pc} \dot{m}_c \text{ for the cold side cooling water.}$$

The overall dimensions of the condenser are determined from the input velocity of cooling water and the geometry variables:

$$ATC = \frac{\pi}{4} D_{ic}^2$$

$$\dot{m}_{ct} = \rho_w V_c ATC \times 3600$$

ORIGINAL PAGE IS
OF POOR QUALITY

$$N_c = \frac{\dot{m}_c}{m_{ct}}$$

$$VOL_c = \frac{A_{oc}}{a_{oc}}$$

$$A_{fvc} = 0.866 N_c (TS_c)^2$$

$$D_c = \sqrt{\frac{4}{\pi} A_{fvc}}$$

$$L_c = \frac{VOL_c}{A_{fvc}}$$

This calculation assumes a circular cross-sectional area of the condenser.

Since the pressure in the condenser is small, a pressure drop calculation is not performed in the condenser. A check on the incoming velocity of steam is performed to determine if this is reasonable.

$$V_{sc} = \frac{\dot{m}_s}{\rho_s a_{oc} A_{fv} \times 3600}$$

The current velocity of incoming steam is calculated at less than 100 ft/sec, so the pressure drop would be small. The turbopump calculation assumes the pressure at the exit of the condenser to be zero. There is negligible error, since the pressure is only a few psi in relation to 100's of psi going into the heat exchanger.

B.4.4.1 Condenser Costs

Condenser costs are based on the heat transfer area calculation shown in the above section. The relation is derived from Reference 38.

$$\text{Condenser cost} = 92.5 (A_{oc})^{0.67}$$

The equation yields condenser cost in 1970 dollars before installation. The basis is a shell and tube condenser operating at below atmospheric pressures in the shell and below 100 psig in the tubes. The material is carbon steel, and the exchanger is a U-tube type.

The installation factor used in 2.3. To bring the cost up to 1978 dollars, an escalation index of 1.6 is multiplied by the installed cost. With the high installation factor used in the model, associated steam and cooling water piping is included in the 1978 installed price.

B.5 DUCTWORK SIZING

Ductwork sizing parameters (length and diameter) are program input specifications.

B.5.1 Ductwork Pressure Drops

The pressure drop in the ductwork and the baghouse is all calculated on an equivalent length basis. The equivalent lengths are input to the computer program. The calculation repeats for each section of the ductwork:

$$V_a = \left(\frac{\dot{m}_a}{\rho_a} \right) \left(\frac{4}{\pi D_o^2} \right)$$

$$N_{RE} = \frac{\rho V D}{\mu}$$

$$f_D = \frac{0.316}{N_{RE}^{0.25}} \quad \text{if } N_{RE} > 2100$$

$$f_D = \frac{64}{N_{RE}} \quad \text{if } N_{RE} < 2100$$

$$\Delta P_D = \left(\frac{f_D}{g_c} \right) \left(\frac{L_D}{D_D} \right) \left(\frac{\rho_a V_a^2}{2} \right)$$

These calculations are performed for both the charge and discharge modes of operation in the system.

B.5.1.1 Ductwork Costs

Costs of ductwork are also manufacturer's derived costs. The computer model bases the cost on the equivalent length used in the pressure drop calculations. The equivalent length covers fittings used in the system such as elbows, tees, and valves. The diameter of the ductwork is also considered. Ductwork already present downstream of the system is not costed.

The expression to calculate installed cost is:

$$1978 \text{ dollars} = 76.8 (L_D)(D_D)$$

The cost assumes minor structural supports, and insulation is included in the price.

The material of the ductwork can either be a somewhat exotic metal or a Kaolin brick-lined arrangement. The costs do not differ significantly in these types of materials.

B.6 FAN SIZING

Fans are sized to deliver a desired flow rate at a given pressure drop. Each fan is designated to supply the required pressure drops that occur in a specific portion of the system. Table B-2 shows the designations for both charging and discharging modes. Figure B-5 shows the nomenclature of the schematic shown in Figure B-1. The individual pressure drops that are calculated are summed for the various fan horsepower determinations. Fan number 8 is oversized, since it is based on the entire peak storage flow rate and not just makeup air. In all probability, this fan would not exist in a real system; but since it is presently in the computer model, it is included here. The equation for the horsepower (hp) is as follows:

$$\text{hp} = 4.156 \times 10^{-7} \left(\frac{\Delta P_F}{P_{\text{op}}} \right) (460 + T_{\text{air}}) (\dot{m}_a)$$

The equation is a modified version of a general form equation found in Reference 40.

The next step in the calculation simply converts horsepower over to megawatts at a 37% efficiency for the fan motor. For a practical parasitic power consideration, the megawatts are multiplied by the respective charge or discharge time to obtain megawatt hours. The fan requirements in megawatt hours are summed and the total power usage subtracted from the turbine output (also in megawatt hours). When all parasitic power is considered, the total output of the system can be determined.

Table B-2
FAN ΔP DESIGNATIONS

Fan No.	Ductwork Lengths	Equipment
Charging		
2	1, 2	Peak store (Includes baghouse in equivalent length)
8	Inactive during charge	
9	4, 5	
11	6	
Discharging		
2	1, 3, 5	Heat exchanger Peak store (Includes baghouse in equivalent length)
8	7	
9	2, 4	
11	6	

B.6.1 Fan Costs

Fans are costed by Reference 38 at low pressure drops based on volumetric flow in CFM. The base equation is:

$$\text{Fan cost} = 9.0 (\text{CFM})^{0.68}$$

Units are 1970 dollars, uninstalled. Installation of a fan is assumed, from Reference 38, at 10%. To bring the cost up to 1978 dollars, the installed cost is multiplied by 1.6.

APPENDIX C THERMAL STORAGE BED COMPUTER PROGRAM

The following sections present a complete description of the thermal storage bed computer program. This program may be used for both types of storage devices in the system (operational and peaking), since it maps out the temperature of the bed and the gas with time. A sample computer output is presented at the end of the technical discussion.

C.1 PRESSURE DROP ACROSS THE PACKED BED

The pressure drop across the packed bed is calculated in a similar way to that across an empty tube. It is still based on the concept of the velocity head, i.e.:

$$\Delta P = (f) \left(\frac{L_D}{D_D} \right) \left(\frac{1}{2} \rho_a V_a^2 \right)$$

However, for flow through a packed bed, the pressure drop is mainly due to the friction between the fluid and the particle rather than that between the fluid and the tube wall. Thus, a modification must be made in the above equation to include terms for the effective cross-sectional area available to the flow passage and the hydraulic radius of the packing particle. Several equations have been proposed in the literature to calculate the pressure drop across the packed bed. Among them, the most widely accepted one, is the Ergun equation (Reference 32) which can be written in the following form:

$$\Delta P_B = (f_B) \left(\frac{2 L_B}{D_P} \right) \left(\frac{1 - \epsilon}{\epsilon^3} \right) \left(\frac{1}{2} \rho_a V_B^2 \right)$$

$$f_B = (150) \left(\frac{1 - \epsilon}{N_{RE, P}} \right) + 1.75$$

Here, $N_{RE, P}$ is defined as:

$$N_{RE, P} = \frac{\rho_a V_B D_P}{\mu_a}$$

In the above equations, V_B is based on the superficial cross-sectional area of the bed. The effect of the voidage on the flow resistance is accounted for by a separate term; the term $(1 - \epsilon)/\epsilon^3$ in the Ergun equation and the term $1 - \epsilon$ in the f_B equation.

C.2 SURFACE HEAT LOSS FROM STORAGE BEDS

The radial thermal conductivity losses are based on heat loss through the wall of the storage container. For the data presented here, no insulation is assumed and these conductivity losses are on the order of 1.0 to 2.0%, depending on bed size. Thermal conductivity losses are based on an average temperature of the bed and the double layer of brick forming the container. The average temperature is based on 1,100°F and the storage discharge temperature. The thermal conductivity of the wall, K_w , is 0.046 Btu/hr-ft-°F. The radial loss equation used is:

$$q_w = \frac{K_w A_w \Delta T_w}{t_w}$$

The heat loss rate, q , is converted into a percentage by dividing by the hourly heat input from the plant at 1,100°F, discharging at T_R for the various cases.

C.3 Bed Axial Effects

The heat transfer mechanisms in packed beds are very complicated (Reference 33), especially in those used for the energy storage. For one thing, the bed is a heterogeneous system with two different phases: gas and solid particles. Secondly, the heat transfer under study is a transient process. In order to undertake any theoretical analysis, certain assumptions must be made to simplify the system, but not at the expense of distorting the physical phenomenon occurring in the system. The following assumptions are made in the present analysis:

1. All the physical properties of air and solid particle are independent of temperature.
2. For axial heat transfer calculations, radial heat transfer efforts are ignored. Over a given cross-sectional area of the bed, the fluid has one temperature and the solid has another.
3. The temperature gradient within the particles is neglected. This is due to the fact that, compared to the transfer of heat from fluid to solid, the transfer of heat by conduction within the solid particle itself is much faster. This assumption is valid at least for small or high thermal conductivity packing particles. For large low conductivity particles, the nonuniform temperature within the particle then must be taken into the consideration experimentally.
4. The transfer of heat in the axial direction is restricted to the fluid phase. The transfer of heat through the solid can be neglected.

The last assumption needs some explanation. The heat transfer data in packed beds can generally be classified into two groups. The first group accounts for the local heat transfer between the fluid and the particle. The second group accounts for the heat transfer through the bed as a whole. The data of the second group assumes that the bed is a homogeneous

system; and an effective thermal conductivity, K_e , is used to lump together the various heat transfer mechanisms through the bed. K_e can be expressed in the form of:

$$K_e/K_a = K_e^0/K_a + a_3 NRE, P NPR$$

The first term on the right-hand side of the above equation is the static thermal conductivity of the bed when no fluid flows through the bed. It results from a complex thermal conduction network, including thermal conduction through solid, through the contact points between particles, through the fluid film near the contact surface between particles, and through the fluid in the void space of the packing (Reference 33). K_e^0 depends on the thermal conductivity of the packing particle. For steel balls, K_e^0/K_a is around 13 (Reference 34). The second term on the right-hand side of the equation is the heat transfer contributed by the fluid mixing. In the axial direction, " a_3 " assumes a value of 0.50 for gas, while in the radial direction, it takes a value of 0.10 (Reference 35). As the flow rate of the fluid increases, the mixing effect controls the heat flow in any packed bed. As an illustration, consider a packed bed of steel balls. At $NRE, P = 200$,

$$\frac{\text{heat transfer due to mixing}}{\text{total heat transfer rate}} = \frac{(a_3 \lambda)(NRE, P)(NPR)}{K_e^0/K_a + (a_3 \lambda)(NRE, P)(NPR)} = \frac{(0.5)(200)(0.68)}{13 + (0.5)(200)(0.68)} = 84\%$$

For the range of NRE, P greater than 200, which are the cases encountered in the present study, the contribution of the fluid mixing can be even greater. Therefore, it is a valid assumption to neglect the heat transfer through the solid particles and consider only the heat transfer through the void space of the packing.

Based on the above assumptions, the equations which govern the performance of a packed bed thermal storage system can be written as:

$$\rho_a C_{pa} \epsilon \frac{\partial T_a}{\partial \theta} + \rho_a C_{pa} V_B \frac{\partial T_a}{\partial z} = K_e \frac{\partial^2 T_a}{\partial z^2} + h_v (T_p - T_a) \quad (C-1)$$

$$\rho_p C_{pp} (1 - \epsilon) \frac{\partial T_p}{\partial \theta} = h_v (T_a - T_p) \quad (C-2)$$

The first equation above represents the thermal energy balance for the air fluid while the second represents the solid particles. Schumann has derived analytical solutions for T_a and T_p which are widely cited in the literature (Reference 22). However, there are several limitations on his solutions:

1. The inlet air temperature is held constant.
2. The initial temperature is uniform throughout the bed.
3. The axial thermal conduction is neglected.

C.4 STORAGE BED MODEL

To provide more general solutions to the above equations, two sets of boundary conditions are of interest; we refer to these cases as STORE 1 and STORE 2. In STORE 1, the inlet air temperature is allowed to vary with time, but the calculation is either for charge or discharge mode. In STORE 2, the inlet air temperature is fixed at one value during the charge mode and at the other during the discharge mode, but the calculation can be set up for cycles of charge and discharge modes. In either case, the initial temperatures are not necessarily uniform for the whole bed. The basic formulations of the algorithms are the same for either case. They are outlined below.

We must transform the equations which govern the performance of a packed bed thermal storage system into finite difference equations in order to solve them numerically with a computer. Two representations are usually used to transform a differential equation into a difference equation – the forward or explicit representation, and the backward or implicit representation (Reference 37). Which of these two representations should be chosen depends on the problem under investigation. For the packed bed heat transfer problem, the backward representation is preferred because it gives a more accurate solution with the same amount of the computation time than does the forward representation.

Now consider the nodal diagram for the packed bed (see Figure C-1). The bed is divided into "N" nodes. "N" must be an odd integer as the first node is for the inlet air and the remaining nodes are in pairs. Node 2 through Node (N+1)/2 are for the air fluid in the different sections of the bed, while Node (N+3)/2 through N are for the corresponding solid particles. Using the backward representation, we may write down the following finite difference equations:

Node 1

$$T_{i+1, 1} = \text{inlet air temperature} = T_{in}(\theta_{i+1})$$

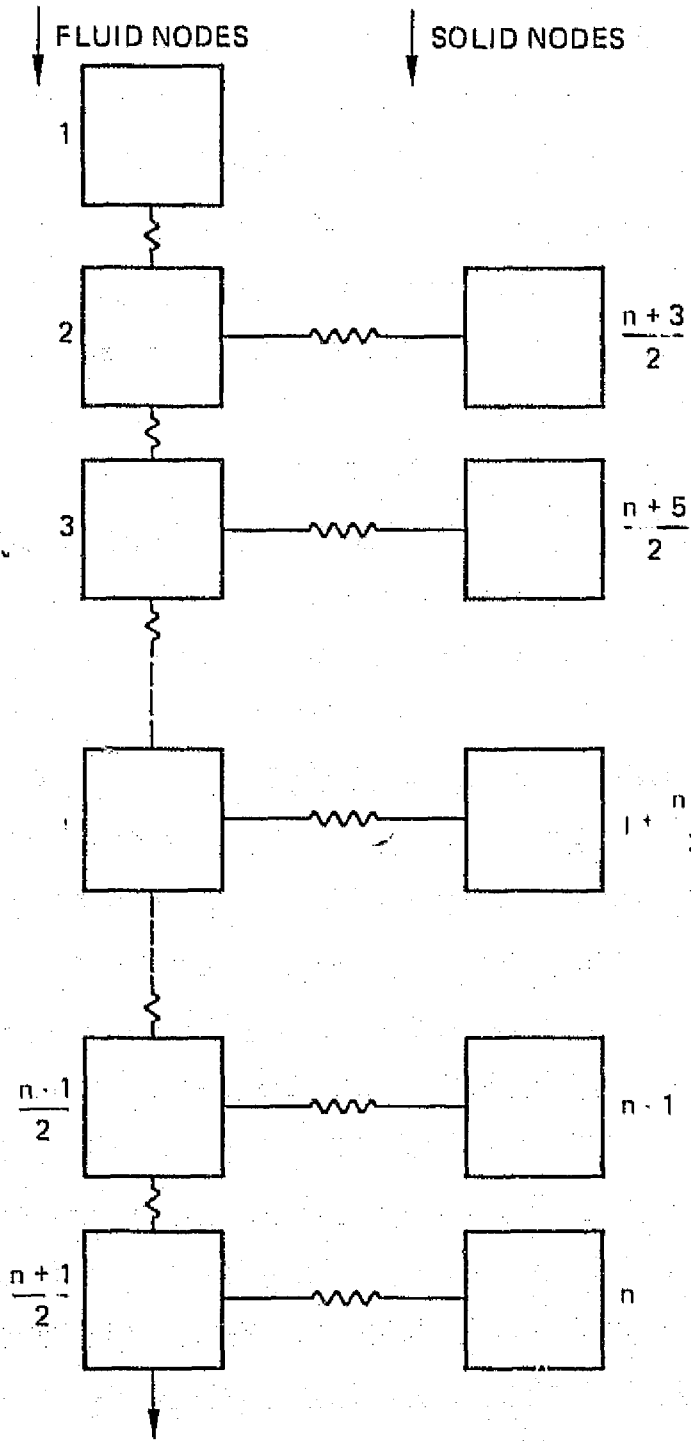
Node 2

$$(\rho_a C_{pa} \epsilon) \frac{T_{i+1, 2} - T_{i, 2}}{\Delta \theta} + (\rho_a C_{pa} V_B) \frac{T_{i+1, 2} - T_{i+1, 1}}{\Delta z} = (K_e) \frac{T_{i+1, 3} - T_{i+1, 2}}{(\Delta z)^2} + h_v \left(T_{i+1, \frac{N+3}{2}} - T_{i+1, 2} \right)$$

Node 3 through Node $\frac{N-1}{2}$

$$(\rho_a C_{pa} \epsilon) \frac{T_{i+1, j} - T_{i, j}}{\Delta \theta} + (\rho_a C_{pa} V_B) \frac{T_{i+1, j} - T_{i+1, j-1}}{\Delta z} = (K_e) \frac{T_{i+1, j+1} - 2T_{i+1, j} + T_{i+1, j-1}}{(\Delta z)^2} + (h_v) \left(T_{i+1, j + \frac{N-1}{2}} - T_{i+1, j} \right)$$

NODAL DIAGRAM FOR PACKED BED



Node $\frac{N+1}{2}$

$$(\rho_a C_{pa} \epsilon) \frac{T_{i+1, \frac{N+1}{2}} - T_{i, \frac{N}{2}}}{\Delta\theta} + (\rho_a C_{pa} V_B) \frac{T_{i+1, \frac{N+1}{2}} - T_{i+1, \frac{N-1}{2}}}{\Delta_z} =$$

$$- (K_e) \frac{T_{i+1, \frac{N+1}{2}} - T_{i+1, \frac{N-1}{2}}}{(\Delta_z)^2} + (h\nu) \left(T_{i+1, N} - T_{i+1, \frac{N+1}{2}} \right)$$

Node $\frac{N+3}{2}$ through N

$$(\rho_p C_{pp}) (1 - \epsilon) \frac{T_{i+1, j} - T_{i, j}}{\Delta\theta} = (h\nu) \left(T_{i+1, j} - \frac{N-1}{2} - T_{i+1, j} \right)$$

Rearranging the above equations, we then obtain:

Node 1

$$T_{i+1, 1} = T_{in} (\theta_{i+1})$$

Node 2

$$- \left(\frac{\rho_a C_{pa} V_B}{\Delta_z} \right) T_{i+1, 1} + \left[\frac{\rho_a C_{pa} \epsilon}{\Delta\theta} + \frac{\rho_a C_{pa} V_B}{\Delta_z} + \frac{K_e}{(\Delta_z)^2} + h\nu \right] T_{i+1, 2} - \frac{K_e}{(\Delta_z)^2} T_{i+1, 3}$$

$$- (h\nu) T_{i+1, \frac{N+3}{2}} = \left(\frac{\rho_a C_{pa} \epsilon}{\Delta\theta} \right) T_{i, 2}$$

Node 3 through Node $\frac{N-1}{2}$

$$- \left[\frac{\rho_a C_{pa} V_B}{\Delta_z} + \frac{K_e}{(\Delta_z)^2} \right] T_{i+1, j-1} + \left[\frac{\rho_a C_{pa} \epsilon}{\Delta\theta} + \frac{\rho_a C_{pa} V_B}{\Delta_z} + \frac{2 K_e}{(\Delta_z)^2} + h\nu \right] T_{i+1, j}$$

$$- \frac{K_e}{(\Delta_z)^2} T_{i+1, j+1} - (h\nu) T_{i+1, j} + \frac{N-1}{2} = \left(\frac{\rho_a C_{pa} \epsilon}{\Delta\theta} \right) T_{i, j}$$

Node $\frac{N+1}{2}$

$$-\left[\frac{\rho_a C_{pa} V_B}{\Delta z} + \frac{K_e}{(\Delta z)^2} \right] T_{i+1, \frac{N-1}{2}} + \left[\frac{\rho_a C_{pa} \epsilon}{\Delta \theta} + \frac{\rho_a C_{pa} V_B}{\Delta z} + \frac{K_e}{(\Delta z)^2} + h_v \right] T_{i+1, \frac{N+1}{2}} - (h_v) T_{i+1, N} = \left(\frac{\rho_a C_{pa} \epsilon}{\Delta \theta} \right) T_{i, \frac{N-1}{2}}$$

Node $\frac{N+3}{2}$ through N

$$-(h_v) T_{i+1, j} - \frac{N-1}{2} + \left[\frac{\rho_p C_{pp} (1-\epsilon)}{\Delta \theta} + h_v \right] T_{i+1, j} = \frac{\rho_p C_{pp} (1-\epsilon)}{\Delta \theta} T_{i, j}$$

In all the above equations, the terms on the left-hand side depend on the temperatures at $\theta = \theta_{i+1}$, while the terms on the right-hand side depend on the temperatures at $\theta = \theta_j$. Putting in a more compact form:

$$\bar{A} \bar{T}_{j+1} = \bar{B}_j \quad \text{or} \quad \bar{T}_{j+1} = \bar{A}^{-1} \bar{B}_j$$

where \bar{T}_{j+1} is the vector containing all the nodal temperatures at $\theta = \theta_{i+1}$. \bar{A} represents the characteristics of the thermal network, and \bar{B}_j depends on the nodal temperatures at $\theta = \theta_j$ and the inlet air temperature at $\theta = \theta_{i+1}$. With the inlet temperature being specified, it is a straightforward calculation to find the future temperature from the present temperature. It should be noted that since all the elements in matrix A do not depend on temperature and time, the matrix inversion of A^{-1} is performed only once throughout the calculation. The basic scheme of the flow charts for program STORE 1 and STORE 2 is shown in Figure C-2.

The axial thermal conductivity, K_e used in the above calculation is found from the equation shown in Section C.3. Assuming that the fluid mixing is dominant, then:

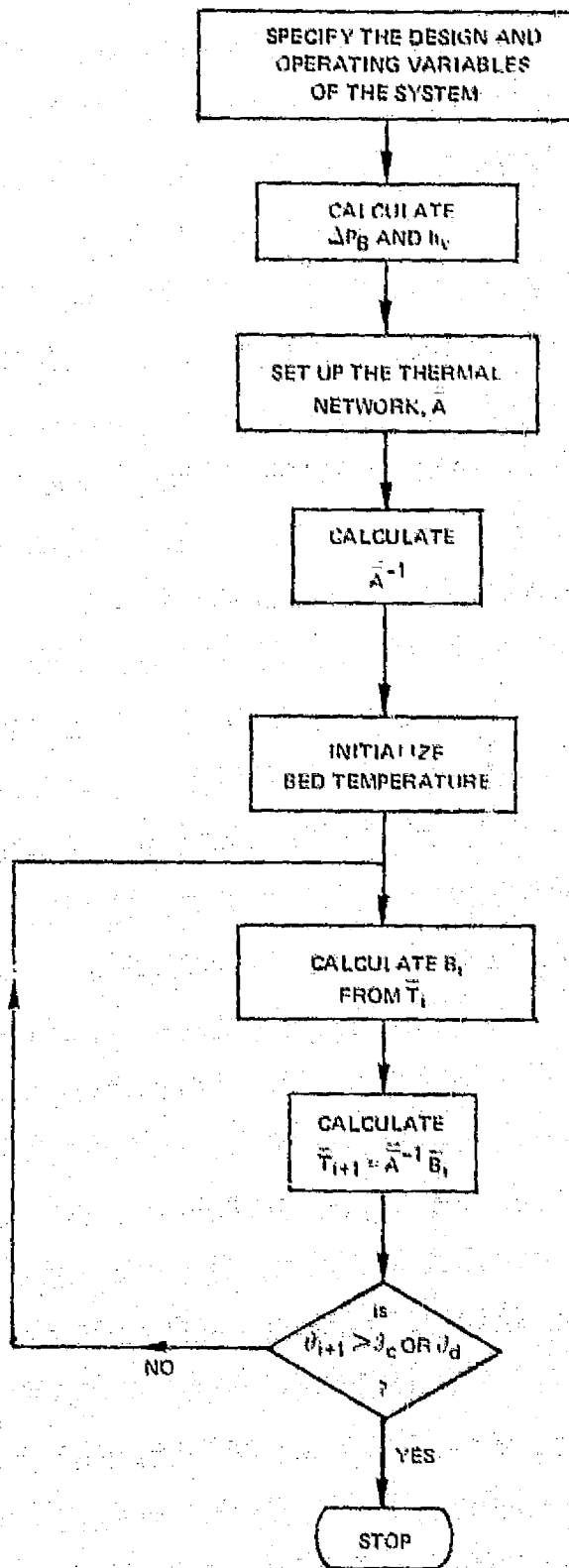
$$K_e/K_a \cong a_3 NRE, P NPR$$

The inverse of "a3" is usually referred as the Peclet number in the literature, which represents the relative significance of the heat transfer due to forced convection versus that due to mixing. "h_v" is calculated from the following correlations (Reference 36).

$$j_h = \left(\frac{h_a}{C_{pa} \rho_a V_B} \right) (NPR)^{2/3} = 0.91 NRE, A^{-0.51} \quad (NRE, A < 50)$$

$$= 0.61 NRE, A^{-0.41} \quad (NRE, A > 50)$$

BASIC SCHEME OF COMPUTER PROGRAM STORE 1 AND STORE 2



ORIGINAL PAGE IS
OF POOR QUALITY

and

ORIGINAL PAGE IS
OF POOR QUALITY

$$h_v = (S_e) (h_a)$$

where:

J_h = j - factor for heat transfer

S_e = external particle surface per unit volume of bed

$$NRE, A = \frac{\rho_a V B}{S_e \mu_a}$$

" h_a " is the heat transfer coefficient based on the surface of the packing. Multiplying " h_a " by " S_e " gives " h_v ".

C.5 TABLE C-1 DESCRIPTION

The first page of Table C-1 is self-explanatory listing the inputs to the program and some internal calculations. The mapping numbers shown in Table C-1 indicate a 41-node output system. Only one cycle is shown, but any number of cycles can be run. The charge mode is listed first followed by a fractional heat loss for the charge cycle. The discharge mode is then listed. In each set of 41 nodes, the top number is a gas input condition, excluding the initial bed temperature set. The next 2 rows are gas temperature then bed temperature. These are the temperatures at the time indicated at some cross-section in the bed. Essentially, the bed length is divided into 20 parts in this example. From this data, bed output temperature/time relationships are defined; and further analysis can be performed, eliminating steady-state assumptions used in the design model.

Table C-1

PARTICLE DENSITY(LB/CUBIC FT)=480.00 PARTICLE THERMAL CAPACITY(BTU/LB-F)= .09
 PARTICLE DIAMETER(FT)= .1250 BED DIAMETER(FT)= 18.84 BED LENGTH(FT)= 22.61
 NO. OF OPERATION CYCLES= 3
 HOT AIR TEMPERATURE(F)= 1300.00 REJECTED AIR TEMPERATURE(F)= 400.00

CHARGE TIME(HR)= 4.00
 NO. OF TIME NODES= 80 NO. OF SPACE NODES= 41
 TOTAL MASS FLOW RATE OF AIR(LB/HR)= 137000
 PRESSURE DROP(PHI)= .375 REP= 825.07
 HEAT TRANSFER COEFF(BTU/F-HR-CUBIC FT)= 294.84

DISCHARGE TIME(HR)=12.00
 NO. OF TIME NODES= 240 NO. OF SPACE NODES= 41
 TOTAL MASS FLOW RATE OF AIR(LB/HR)= 45667
 PRESSURE DROP(PHI)= .07 REP= 275.22
 HEAT TRANSFER COEFF(BTU/F-HR-CUBIC FT)= 154.20

Table C-1 (Continued)

CYCLE NO. 1

CHARGE MODE
INITIAL BED TEMPERATURE

400.00										
400.00	400.00	400.00	400.00	400.00	400.00	400.00	400.00	400.00	400.00	400.00
400.00	400.00	400.00	400.00	400.00	400.00	400.00	400.00	400.00	400.00	400.00
400.00	400.00	400.00	400.00	400.00	400.00	400.00	400.00	400.00	400.00	400.00
TIME (HR) = 1.00										
1300.00										
1252.38	1162.88	1043.13	913.09	789.72	683.44	598.51	534.43	488.76	456.56	
435.36	421.63	412.98	407.65	404.44	402.54	401.43	400.80	400.44	400.24	
1236.66	1130.51	999.21	865.03	743.91	643.90	566.77	510.44	471.10	444.63	
427.39	416.47	409.72	405.65	403.23	401.82	401.01	400.56	400.30	400.16	
TIME (HR) = 2.00										
1300.00										
1296.26	1284.66	1259.79	1218.07	1158.88	1084.69	1000.25	911.36	823.64	741.70	
668.69	606.28	554.83	513.78	481.97	457.96	440.27	427.52	418.53	412.44	
1295.12	1280.66	1250.96	1203.05	1137.37	1057.56	969.23	878.57	791.19	711.32	
641.57	583.06	535.66	498.46	470.08	448.98	433.65	422.75	415.15	410.07	
TIME (HR) = 3.00										
1300.00										
1299.67	1298.38	1294.76	1286.88	1272.42	1249.23	1215.76	1171.48	1117.04	1054.18	
985.43	913.74	842.12	773.22	709.20	651.62	601.03	557.98	522.17	493.95	
1299.38	1297.95	1293.92	1285.10	1267.27	1240.89	1203.64	1155.37	1097.15	1031.13	
960.15	887.33	815.67	747.74	685.47	630.12	582.27	541.96	508.82	482.98	
TIME (HR) = 4.00										
1300.00										
1299.97	1299.83	1299.36	1298.15	1295.50	1290.40	1281.62	1267.84	1247.78	1220.50	
1185.51	1142.88	1093.31	1038.01	978.62	916.99	855.04	794.54	737.14	686.07	
1299.96	1299.78	1299.21	1297.74	1294.57	1288.59	1278.49	1262.88	1240.54	1218.61	
1172.77	1127.31	1075.15	1017.71	956.78	894.29	832.17	772.19	715.86	666.21	
HEAT LOSS VS AVAILABLE HEAT = .0598										
DISCHARGE MODE										
INITIAL BED TEMPERATURE										
400.00										
686.07	737.14	794.54	855.04	916.99	978.62	1038.01	1093.31	1142.88	1185.51	
1220.50	1247.78	1267.84	1281.62	1290.40	1295.50	1298.15	1299.36	1299.83	1299.97	
666.21	715.86	772.19	822.17	874.29	926.78	984.29	1037.71	1075.15	1112.77	
1210.61	1240.54	1262.88	1278.49	1288.59	1294.57	1297.74	1299.21	1299.78	1299.96	
TIME (HR) = 1.00										
400.00										
475.42	562.70	643.28	719.59	787.91	853.00	916.09	977.10	1035.09	1088.75	
1136.84	1178.35	1212.77	1240.05	1260.65	1275.42	1285.43	1291.82	1295.65	1297.78	
492.01	583.26	664.78	737.08	804.00	868.21	930.94	991.47	1048.76	1101.43	
1148.22	1188.20	1220.95	1248.54	1269.57	1278.95	1287.83	1293.35	1296.57	1298.31	
TIME (HR) = 2.00										
400.00										
477.23	477.65	543.59	615.45	687.34	756.99	823.96	888.39	950.13	1008.61	
1062.95	1112.16	1155.40	1192.13	1222.19	1245.83	1263.66	1276.53	1285.42	1291.17	
432.98	489.29	559.01	632.32	704.26	773.37	839.73	903.56	964.68	1022.40	
1075.78	1123.80	1165.64	1200.84	1229.33	1251.46	1267.91	1279.61	1287.55	1292.59	
TIME (HR) = 3.00										
400.00										

ORIGINAL PAGE IS
OF POOR QUALITY

117

**APPENDIX D
OPERATIONAL DATA COLLECTION**

Operational data needed to design a system for energy conservation within the iron and steel industry was collected from the Bethlehem Recycling Plant in Seattle. This task also involved the measurement of physical properties for slag produced in the two electric arc furnaces at the Seattle plant.

D.1 SLAG PHYSICAL PROPERTY MEASUREMENT

In precontractual studies, the baseline system utilized a slag bed heat storage system. To properly estimate the performance of such a system, the physical properties of slag were measured. The determined properties were the density, specific heat, and the thermal conductivity.

D.1.1 Density and Specific Heat of Slag

Three specimens of slag were chosen for 1) high porosity, 2) low porosity, and 3) high steel content. These were subjected to specific heat measurement at two (relatively low) temperatures and to specific gravity measurement. Specific gravity was measured by immersion; hence, internal voids and small pores would not be filled with water. The results of these tests are presented in Table D-1. Measurement of specific heat at higher temperatures are not possible using existing equipment. An average specific heat of 0.11 Btu/lb-°F is cautiously inferred from this data. This value is low as most metallic oxides are of the order of 0.20. One of the expected advantages of slag was a relatively high specific heat, and it was felt this would compensate for the expected low thermal conductivity (compared to metals). On an overall properties basis, scrap steel with a specific heat of 0.10 Btu/lb-°F, a thermal conductivity of 10 Btu/lb-°F, and a density of between 250 and 420 lb/ft³ may well provide a more advantageous system, depending upon the scrap supply logistics. A scrap steel filled storage bed could be considered as a stockpile of reserve raw material; hence, a low first cost item.

Table D-1
DENSITY, SPECIFIC GRAVITY AND SPECIFIC HEAT OF SLAG SPECIMENS

	Specific Gravity	Density lb/ft ³	Specific Heat at 70°F	Specific Heat at 212°F
1 Porous	2.2	137	0.10	0.13
2 Nonporous	3.6	225	0.11	0.10
3 Magnetic (moderately porous)	2.8	175	0.12	0.10

D.1.2 Slag Thermal Conductivity Measurements

The measurements for thermal conductivity involved determining thermal conductivity of a packed bed as well as that of a single solid specimen. The data for these tests is presented in Table D-2. The packed bed test apparatus is shown in Figure D-1, and the solid specimen test apparatus is shown in Figure D-2.

Table D-2
SLAG THERMAL CONDUCTIVITY RESULTS

	Large Particle Bed	Small Particle Bed	Solid Sample
Void space — includes internal porosity of particle void space — excludes internal porosity of particle.	64% 41%	63% 40%	0 0
Number of particles	285	1,385	—
Average weight/particle	2.75 lb/ea	0.58 lb/ea	—
Thermal conductivity, Btu/ft ² F-hr	0.63	0.17	1.2 ± 15%
Density, lb/ft ³	137	137	225

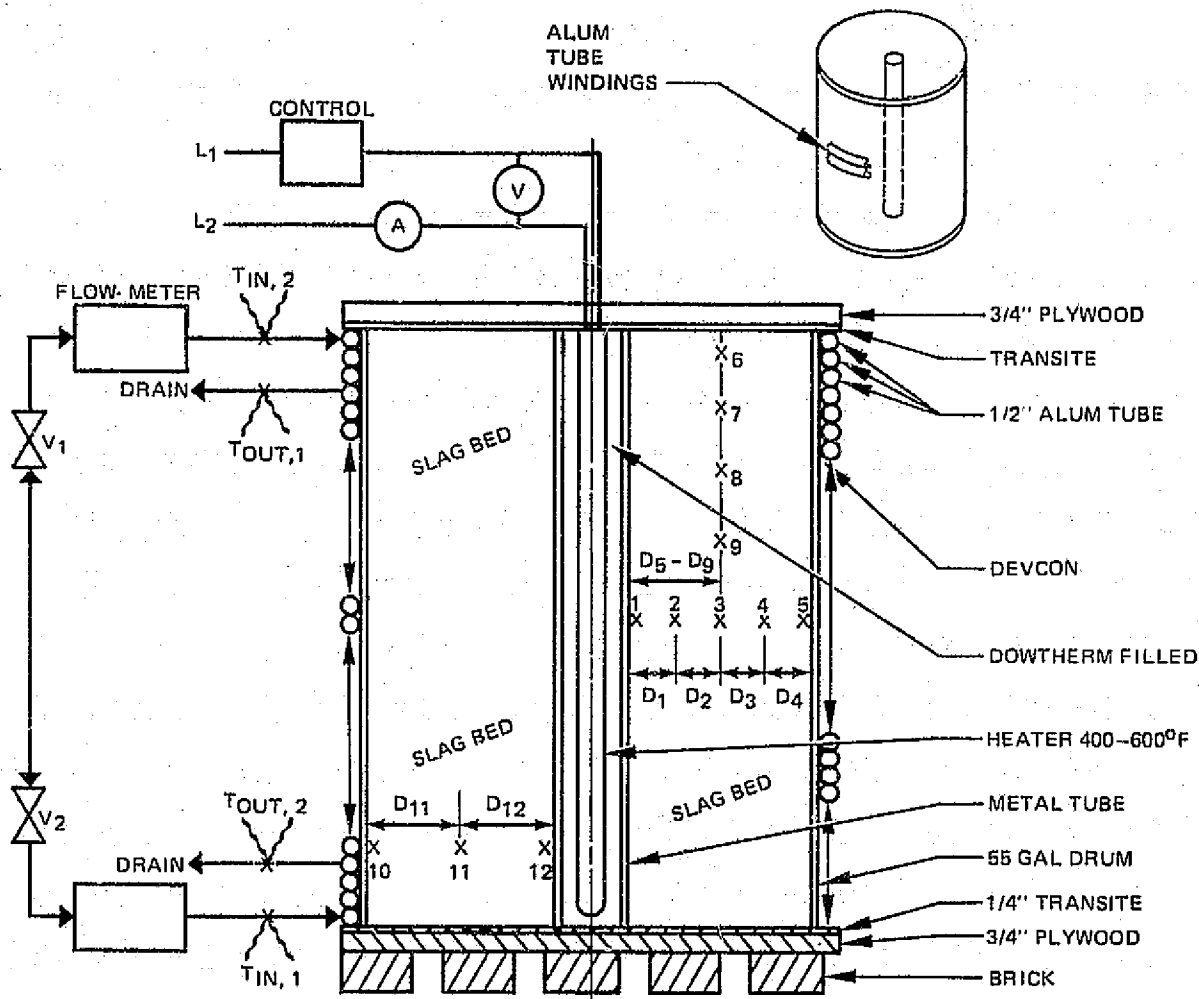
D.1.2.1 Slag Bed Thermal Conductivity Testing

The overall thermal conductivities for packed beds composed of two different size particles were obtained. Figure D-1 shows the location of thermocouple instrumentation. Overall bed thermal conductivity was calculated using overall heat transferred from the central core to the outer cylindrical surface and the temperature profile measured at the mid-plane. Some free convection effects were noted during the test as indicated by the deviation in the isothermal surfaces from the expected cylindrical form shown in Figure D-3. The overall results of bed testing are shown in Table D-2.

D.1.2.2 Solid Slag Thermal Conductivity Testing

Figure D-2 shows the apparatus arrangement used to determine the thermal conductivity of a single slag specimen. A relatively large mass of slag was selected at random and reduced to 1.0-inch thick slabs using commercial lapidary equipment. These slabs were prone to fracture as 1) the solidification process and subsequent handling induces considerable crazing and 2) the different sawing properties of slag matrix and steel inclusions causes

SLAG BED ARRANGEMENT

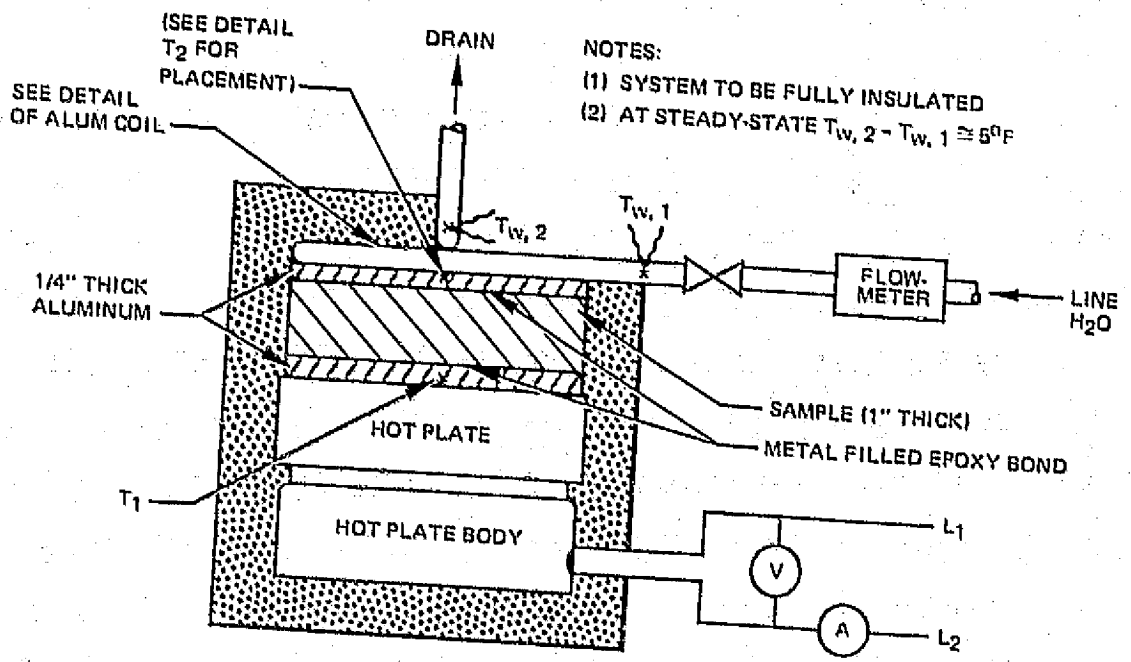


NOTES:

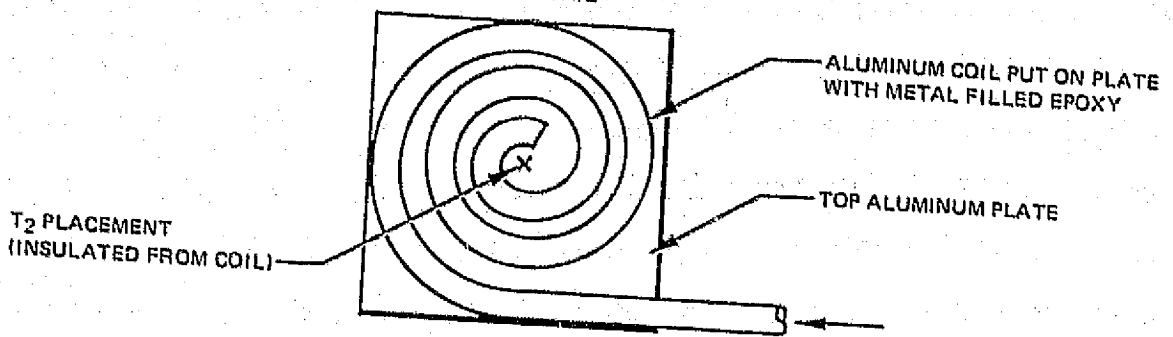
- (1) INSULATION TO BE INSTALLED AROUND ENTIRE TEST ARRANGEMENT.
- (2) TEMPERATURE PROBES IN BED (1 - 12) ARE PUT ON SLAG SURFACE.
- (3) ALUMINUM TUBE ON OUTSIDE OF BARREL IS SET UP FOR COUNTERCURRENT WATER FLOW (TWO SYSTEMS).
- (4) ALL PROBE DISTANCES ($D_1 - D_{12}$) ARE TO BE KNOWN.
- (5) HEATER MUST BE CENTERED IN BARREL AND MUST MAINTAIN A CONSTANT TEMP AT STEADY STATE.

*ORIGINAL PAGE IS
OF POOR QUALITY*

MAIN SET-UP



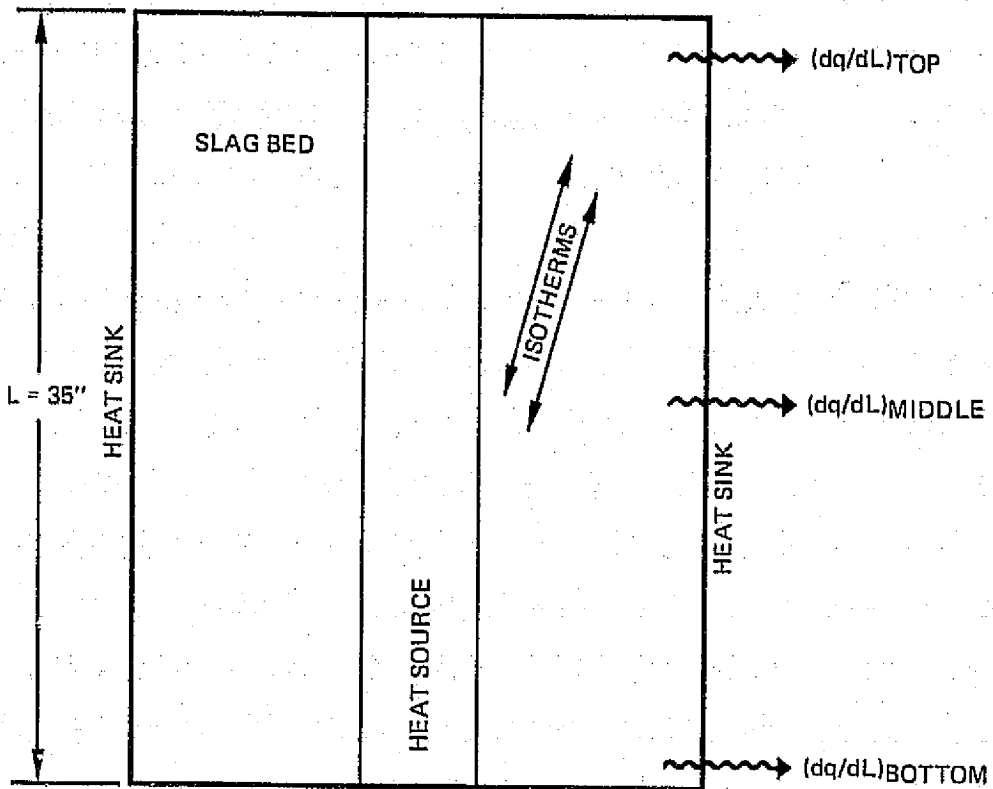
COIL DETAIL



- NOTES:
 (1) SAMPLE IS 1 INCH THICK
 (2) SAMPLE WILL HAVE AN IRREGULAR SHAPE (DRAWING SHOWS A SQUARE SAMPLE)

CONVECTION EFFECTS IN SLAG BED

NOTE: q_{TOTAL} IS THE HEAT PICKED UP BY THE WATER



$$(dq/dL)_{TOP} > (dq/dL)_{MIDDLE} > (dq/dL)_{BOTTOM}$$

$$(dq/dL)_{MIDDLE} = q_{TOTAL} / L_{BARREL}$$

ORIGINAL PAGE IS
OF POOR QUALITY

considerable chatter during the sawing process. The largest slab produced had sides nearly perpendicular to the sawn faces. This slab was tested with its "as-sawn" irregular perimeter rather than risking additional fracture in an attempt to create a simple geometric shape. The effective heat transfer area was calculated as the average of the areas of the two faces, as determined by a radial planimeter.

To demonstrate the reliability of this test, a sample with a known thermal conductivity (aluminum) was prepared with the same irregular shape to verify this test. The test was completed with some varying results. The measured thermal conductivity of aluminum was lower than the actual value by about 15%. Since aluminum has a very high thermal conductivity, heat pickup by the water coil would be more difficult than in the slag sample. The reported thermal conductivity of 1.2 Btu/ft-°F-hr for slag is felt to be accurate to within $\pm 15\%$.

APPENDIX E REFERENCES

1. American Iron and Steel Institute, "Energy Conservation in the Steel Industry". 84th General Meeting, May 26, 1976
2. Battelle Columbus Laboratories, "Potential for Energy Conservation in the Steel Industry", NTIS PB-244097, May 30, 1975
3. Booz-Allen and Hamilton, Incorporated, "The Impact of Energy Shortages on the Iron and Steel Industries", NTIS PB-238749, August 1974
4. Energy Research and Development Administration, "Priority Listing of Industrial Processes by Total Energy Consumption and Potential for Savings", Contract No. EC-77-X-01-5015, 1977
5. Sandia Laboratories, "Survey of High Temperature Thermal Energy Storage", SAND 75-8063, March 1976
6. Iron and Steel Engineer, "New Economics of Steel – More Steel With Less Capacity", December 1975
7. American Iron and Steel Institute, "Annual Statistical Report for 1976"
8. American Iron and Steel Institute, "Directory of Iron and Steel Works of the United States and Canada", 1974
9. Iron Age, "Profile of a Greenfield Steel Plant", September 12, 1977
10. American Iron and Steel Institute, "Reflections on Steel's Energy Maze", Steel 1977/2
11. McAdams, "Heat Transmission", 3rd Edition, McGraw Hill Book Co., NY, 1954
12. Potter, "Power Plant Theory and Design", Ronald Press Company, NY
13. Smith and VanNess, "Introduction to Chemical Engineering Thermodynamics", 2nd Edition, McGraw Hill, NY, 1959
14. McCabe and Smith, "Unit Operations of Chemical Engineering", 2nd Edition, McGraw Hill, NY, 1967

15. Perry, Chilton, Kirkpatrick, "Perry's Chemical Engineers' Handbook", 4th Edition, McGraw Hill, NY, 1969
16. Baasel, "Preliminary Chemical Engineering Plant Design", Elsevier, NY, 1976
17. Kays and London, "Compact Heat Exchangers", McGraw Hill, NY, 1964
18. Riaz, "High Temperature Energy Storage in Native Rocks", Solar Energy Conference, August 17, 1976
19. Furnas, "Heat Transfer From a Gas Stream to a Bed of Broken Solids", Trans. A. Inst. Chem. E., Vol. 24, 1930
20. Close, "Rock Pile Thermal Storage for Comfort Air Conditioning", Mechanical and Chemical Engineering Transactions of the Institute of Engineers, Australia, Vol. MCI, No. 1, May 1965
21. Hung and Nevins, "Unsteady-State Heat Transfer With a Flowing Fluid Through Porous Solids", ASME Publication, 65-HT-10, August 8-11, 1965
22. Schumann, T. E. W., "Heat Transfer: A Liquid Flowing Through a Porous Prism", Journal, Franklin Institute, Vol. 208, July-December 1929
23. Turner, G. A., "A Method of Finding Simultaneously the Values of the Heat Transfer Coefficient, the Dispersed Coefficient, and the Thermal Conductivity of the Packing in a Packed Bed of Spheres: Part I - Mathematical Analysis", AIChE Journal, July 1967, p. 678
24. Bell, J. C. and Katz, E. F., "A Method for Measuring Surface Heat Transfer Using Cyclic Temperature Variations", Paper Presented at Process Heat Transfer and Fluid Mechanics Institute, June 22-24, 1949, held at Berkeley, Ca., Published by ASME, 1949, p. 243
25. Löf, G. O. G. and Hawley, R. W., "Unsteady-State Heat Transfer Between Air and Loose Solids", I/EC, Ind. and Eng. Chemistry, Vol. 40, June 1948, pp. 1061-1070
26. Saunders, M. A. and Ford, H., "Heat Transfer in the Flow of Gas Through a Bed of Solid Particles", Iron and Steel Institute Journal, Vol. CSL.I, No. 1, 1940
27. Chukhanov, Z. F., "Heat and Mass Transfer Between Gas and Granular Material", Int. Four. Heat and Mass Transfer, Vol. 6, August 1963, pp. 691-701

28. Denton, J. C. and Afgan, N. H., "Future Energy Production Systems, Heat and Mass Transfer Processes, Vol. 1", Hemisphere Publishing Corp., Washington and London, 1976
29. Personal Communication, Interpace Refractories
30. Personal Communication, Turbodyne Corporation
31. Coughanower, D. R. and Koppel, L. B., "Process Systems Analysis and Control", McGraw Hill Book Co., NY, 1965, p. 212
32. Bird, R. B., Stewart, W. E., and Lightfoot, E. N., "Transport Phenomena", John Wiley & Sons, Inc., NY, 1960, p. 196
33. Yagi, S. and Kunii, D., "Studies on Effective Thermal Conductivities in Packed Beds", AIChE Journal, Vol. 3, No. 3, 373, 1957
34. Yagi, S., Kunii, D., and Wakao, N., "Studies on Axial Effective Thermal Conductivities in Packed Beds", AIChE Journal, Vol. 6, No. 4, 543, 1960
35. James J. Carheny, "Chemical and Catalytic Reaction Engineering", McGraw Hill Book Co., NY, 1976, p. 160
36. Bird, R. B., Stewart, W. E., and Lightfoot, E. N., "Transport Phenomena", John Wiley & Sons, Inc., NY, 1960, p. 411
37. Chapman, A. J., "Heat Transfer", The MacMillan Co., London, 1967, p. 186
38. Guthrie, Kenneth M., "Process Plant Estimating Evaluation and Control", Craftsman Book Co., Ca., 1974
39. Rase, Howard F. and Barrow, M. H., "Project Engineering of Process Plants", John Wiley & Sons, Inc., NY, 1966, p. 53
40. Hichs, Tyler G., "Standard Handbook of Engineering Calculations", McGraw Hill, 1972
41. United States Steel Corporation, "Steelmelting Furnaces", Steel Plant Design Series, 1956
42. Technical and Economic Assessment of Phase Change and Thermochemical Advanced Energy Storage, Interim Technical Report, EPRI, Palo Alto, Ca., July 1976

43. Glenn, D., Technical and Economic Feasibility of Thermal Energy Storage for Ceramic and Brick Industries, Proceedings for Information Exchange Meeting, NASA/Lewis, September 8-9, 1976
44. Turner, Robert H., Thermal Energy Storage Using Large Hollow Steel Ingots, International Solar Energy Society Proceedings, Vol. 8, August 15-21, 1976
45. Anon., "Off Peak Electrical Thermal Storage for Industrial Process Heating, The Engineer", Vol. 266, October 1968
46. Rice, Richard, Development of a Phase Change Thermal Storage Unit for the Sandia Solar Total Energy System Test Facility at Albuquerque, New Mexico, Proceedings from Information Exchange Meeting, NASA/Lewis, September 8-9, 1976
47. Bussard, R. W., "Economic Optimization Analysis of the Solar Total Energy System for Ft. Hood", Private Communication, May 11, 1976
48. Public Service Electric and Gas Company, "An Assessment of Energy Storage Systems Suitable for Use by Electric Utilities", Electrical Power Research Institute and Energy Research and Development Administration, Vol. II, July 1976